NOVEL PROCESS FOR OXIDATIVE DEHYDROGENATION OF LPG TO HIGH VALUE OLEFINS: Catalyst design and kinetic modelling

BY

GAZALI TANIMU

A Dissertation Presented to the

DEANSHIP OF GRADUATE STUDIES

KING FAHD UNIVERSITY OF PETROLEUM & MINERALS

DHAHRAN, SAUDI ARABIA

In Partial Fulfillment of the
Requirements for the Degree of

DOCTOR OF PHILOSOPHY

In

CHEMICAL ENGINEERING

APRIL-2019

KING FAHD UNIVERSITY OF PETROLEUM & MINERALS

DHAHRAN- 31261, SAUDI ARABIA

DEANSHIP OF GRADUATE STUDIES

This thesis, written by **GAZALI TANIMU** under the direction of his thesis advisor and approved by his thesis committee, has been presented and accepted by the Dean of Graduate Studies, in partial fulfillment of the requirements for the degree of **DOCTOR OF PHILOSOPHY IN CHEMICAL ENGINEERING.**

Dr. Sulaiman S. Al-Khattaf
(Advisor)

Dr. Mamdouh Al-Harthi
Department Chairman

Dr. Mohammed Ba-Shammakh
(Co-Advisor)

Dr. Salam A. Zummo
Dean of Graduate Studies

Dr. Mohammad M. Hossain
(Member)

9/5/19

Date

Dr. Shaikh Abdur Razzak
(Member)

Dr. Isam Al-Jundi
(Member)

This Dissertation is dedicated to the memory of my late sisters: Hauwa'u and Safiyyah Tanimu, may their souls continue to rest in perfect peace

ACKNOWLEDGMENTS

TABLE OF CONTENTS

CHAPTER 5 NEW MESOPOROUS CATALYST SYSTEM CONTAINING BI_2SIO_5 FOR N-BUTANE ODH

LIST OF TABLES

LIST OF FIGURES

LIST OF ABBREVIATIONS

ODH   :   Oxidative Dehydrogenation

DH   :   Dehydrogenation

BD   :   Butadiene

OC   :   Oxygenate and Cracking

PO   :   Partial Oxidation

BET   :   Brunaeur Emmett Teller

BJH   :   Barret Joyner Halenda

FID   :   Flame Ionization Detector

GC   :   Gas Chromatography

GHSV   :   Gas Hourly Space Velocity

JCPDS   :   Joint Committee on Powder Diffraction Standards

LSQCURVEFIT   :   Least Square Curve Fit

MATLAB   :   Matrix Laboratory

ODE   :   Ordinary Differential Equation

SS   :   Sum of Square Errors

TCD   :   Thermal Conductivity Detector

TPD   :   Temperature Programmed Desorption

TPR	:	Temperature programmed Reduction
WHSV	:	Weight hourly space velocity
XRD	:	X-ray Diffraction
TEOS	:	Tetraethyl orthosilicate
EQA	:	Equilibrium Adsorption
HN-HB	:	High Nickel High Bismuth loading
HN-LB	:	High Nickle Low Bismuth loading
MN-LB	:	Medium Nickel Low Bismuth loading
LN-LB	:	Low Nickel Low Bismuth loading

ABSTRACT

Full Name   : [GAZALI TANIMU]

Thesis Title   : [Novel process for oxidative dehydrogenation of LPG to high value olefins: catalyst design and kinetic modelling]

Major Field   : [CHEMICAL ENGINEERING]

Date of Degree : [April, 2019]

Catalytic oxidative dehydrogenation of alkanes is an alternative irreversible reaction used for the production of olefins (ethylene, propylene, and butenes) and diolefins (butadiene). It requires low operational cost and has a less environmental impact. It is an exothermic reaction that occurs at a lower temperature and the catalyst used can obtain oxygen directly from the feed stream without requiring additional re-oxidation. The presence of oxygen in this method reduces coking and extends catalyst lifetime. The formation of water as a byproduct of this process makes it possible to avoid the thermodynamic limitations associated with conventional methods.

This research intends to contribute towards enhancing the light olefins production. This was achieved through a novel system of catalyst design using hierarchical nano-consortium of multi-component metal oxides supported catalysts. The active metal oxides of the catalysts consist of Ni and Bi, in their best combination for an enhanced performance. All the catalysts were be synthesized using co-impregnation technique and calcined at two steps of 350 °C for 1 h and 590 °C for 2 h. The physical and chemical properties of the catalysts were examined using BET for surface area and pore structure determination, XRD for crystallinity, Transmission Electron Microscopy (TEM) for morphologies, XPS for

bonding states and binding energies, Temperature Programmed Reduction (TPR) for redox property and NH_3 and CO_2 Temperature Programmed Desorption (TPD) for acidic and basic property respectively. The effect of different supports; Al_2O_3, SiO_2, and ZrO_2 on the dispersion of active oxides, reducibility and acid-base properties was discussed. SiO_2 supported catalyst gave the highest dehydrogenation selectivity of 79.1 % due to its weak acidity compared to the other supports. Pore structure effect of catalyst obtained with mesoporous silica supports (SBA-15, silica foam, MCM-41) was investigated. Mesoporous SBA-15 supported catalyst showed a clear superiority in activity (n-butane conversion: 28.9 %) and selectivity (butadiene selectivity: 47.5 %) compared to the other supported catalysts. Butadiene yield was in the order SBA-15 > Silica foam > MCM-41. Varying active metal (Ni and Bi) loading on SBA-15 was investigated for an optimum combination. The reaction mechanism was elucidated using Delplots techniques. Delplots for experiments with n-butane, 1-butene, and 2-butene feeds were constructed. These analyses revealed that butadiene formed from both 1-butene and 2-butene. Kinetic studies using one of the catalysts was done using the Kinetic model editor (KME) to provide better understanding of the catalytic performance and to estimate the kinetic parameters (pre-exponential factors and activation energies).

ملخص الرسالة

الاسم الكامل: غزالي تنعيم

عنوان الرسالة: عملية جديدة لازالة الهيدروجين المؤكسد من غاز البترول المسال الى أوليفينات مرتفعة القيمة

التخصص: الهندسة الكيميائية

تاريخ الدرجة العلمية: أبريل 2019

يستخدم التفاعل الحفزي لإزالة الهيدروجين المؤكسد للألكانات كبديل لإنتاج الأوليفينات (الإيثيلين، البروبيلين، البوتين) وثنائي الأوليفينات (البيوتادبين). ويتطلب هذا التفاعل تكاليف تشغيل منخفضة وله تأثير بيئي أقل مقارنة بالطرق التقليدية. ويعتبر التفاعل طارداً للحرارة ويتم عند درجة حرارة منخفضة ويمكن للحفاز المستخدم أن يحصل على الأكسجين مباشرة من اللقيم دون الحاجة إلى إعادة الأكسدة الإضافية. ويقلل وجود الأكسجين في هذه الطريقة من ترسب الكربون ويطيل العمر الاستخدامي للحفاز. كما يتيح انتاج الماء كمنتج ثانوي لهذه العملية تجنب القيود الديناميكية الحرارية المرتبطة بالطرق التقليدية.

ويهدف هذا البحث إلى المساهمة في تعزيز إنتاج الأوليفينات الخفيفة. ولقد تم تحقيق ذلك من خلال تصميم نظام حفزي جديد باستخدام مجموعة نانوية هرمية من حفازات مدعمة من أكاسيد فلزية متعددة المكونات. وتتكون أكاسيد المعادن النشطة للعوامل الحفازة من Ni و Bi وذلك في أفضل مزيج بينهما لتحسين الأداء. ولقد تم تحضير جميع الحفازات باستخدام تقنية التشريب المشترك وتكلسها على خطوتين من 350 درجة مئوية لمدة ساعة واحدة و 590 درجة مئوية لمدة ساعتين. وتم تعيين الخواص الفيزيائية والكيميائية للحفازات باستخدام طريقة BET لتحديد المساحة السطحية والتركيب المسامي وحيود الأشعة السينية XRD للتبلر والمجهر الإلكتروني للإرسال (TEM) للتركيبات ومطيافية الاشعة السينية للاكترون الضوئي XPS لحالات الترابط وطاقات الربط والاختزال الحراري المبرمج (TPR) لخاصية الأكسدة وطريقة NH_3 و CO_2 والنضح الحراري المبرمج (TPD) للخواص الحمضية والقاعدية على التوالي. وتمت مناقشة نتائج تأثير المدعمات Al_2O_3 و SiO_2 و ZrO_2 على تشتت الأكاسيد النشطة وخواص قابلية الاختزال والخواص

الحمضية القاعدية. ولقد نتج عن الحفاز المدعم بـ SiO_2 أعلى انتقائية لإزالة الهيدروجين بنسبة 79.1 ٪ بسبب ضعف الحمضية مقارنة بالمدعمات الأخرى. وتم فحص تأثير التركيب المسامي للحفاز المدعم باستخدام السيليكا المتوسطة (15-SBA ، رغوة السيليكا ، 41-MCM). وأظهر الحفاز المدعم ذات المسامات الكبيرة 15-SBA تفوقاً واضحاً في النشاط الحفزي (تحويل البيوتان: 28.9٪) والانتقائية (انتقائية البوتادين: 47.5٪) مقارنة بالحفازات المدعمة الأخرى. وأظهرت النتائج أن إنتاج البوتادين كان بالترتيب 41-MCM < رغوة السيليكا < 15-SBA. وتم فحص تغيير تحميل المعادن النشطة (Ni و Bi) على 15-SBA للحصول على تركيبة حفزية مثالية. كما تم توضيح حركية التفاعل باستخدام تقنية Delplots. واستخدمت Delplots في التجارب باستخدام البيوتان ، 1-البيوتين ، و 2-البيوتين. وكشفت التحاليل أن البيوتادين يتشكل من 1-بيوتين و 2-بيوتين. وأجريت دراسات حركية التفاعل باستخدام أحد الحفازات والنموذج الحركي (KME) لتقديم تفسير أفضل للأداء الحفزي ومعرفة عوامل الحركية (الأس وطاقات التنشيط).

CHAPTER 1

INTRODUCTION

The demand of olefins and diolefins in most polymer and petrochemical industries especially in Saudi Arabia is on the increase. This motivated the interest towards the search for an on-purpose production techniques different from the conventional methods. Light alkanes (lower alkanes of C_2-C_4) are highly available, relatively less expensive compared to their corresponding alkenes leading to an economic advantage and are environmentally non-aggressive products, hence their usage as raw materials in most chemical industries [1],[2].

80% of ethylene is used worldwide in the production of a wide variety of commercially important chemicals such as polyethylene, polystyrene, ethylene dichloride straight chain, higher alkenes and so on. The market for ethylene has been growing at a rate of 2–5% per year. The global capacity of ethylene is around 150 million tons as of 2012, and it reached 160 million tons at the end of 2015 [3]. The demand of 1-butene in the world industries is about 1.3 million metric tons per year and that of butadiene is 10 million in 2006 and has reached 13 million tons at the end of 2015 with 3-4% annual increment [4]. Butadiene is used mainly as a monomer in the manufacture of polymers such as synthetic rubbers including styrene butadiene rubber (SBR), Polybutadiene rubber (PBR), Nitrile rubber which are tough and/or elastic and commonly used for the production of tires [5],[6].

The commercial (conventional) methods for olefins production includes: Steam cracking process which is a gaseous one phase homogeneous reaction occurring at temperatures greater than 800 $^{\circ}$C, it involves the decomposition of hydrocarbon feed stocks using steam producing different products like alkanes, alkenes and molecular hydrogen [7]. Catalytic cracking process is a process used for upgrading streams from the refinery (heavy and low-value). It uses mainly vacuum gas oil, residue and de-asphalted oil as feed stocks and convert them into light and higher value products like gasoline. Olefins are mainly obtained as co-products in this process in a low amount [7]. Catalytic dehydrogenation process is a reaction that involves the decomposition of alkanes (saturated) into olefins (unsaturated) and H_2 molecule. It is the reverse of hydrogenation reaction. All these processes produces high purity olefins but have major drawbacks as they both are endothermic reactions, leads to coke formation thereby deactivating the catalyst, they are thermodynamically limited reactions hence only produce acceptable yields at high temperatures. Selectivity is difficult to control at such temperatures and finally they are highly energy intensive [8], [9].

Dehydrogenation reaction is an endothermic process requiring high reaction temperature (600-700 $^{\circ}$C) for an economical conversion. Butane dehydrogenation requires higher temperature compared to butene for the same conversion. At these high temperatures, many side reactions including cracking and secondary reactions occur, hence the need for a selective catalyst and short residence time [10]. Dehydrogenation reactions unit available in the industries used mainly transition metals like platinum, tin, vanadium and chromium supported on alumina catalysts. Alumina as a support compared to other supports like silica, titania, zirconia etc has high thermal stability,

mechanical strength and strong catalyst regeneration capabilities. The major drawback of alumina is that it speeds up undesired side reactions like cracking and isomerization resulting from its acidic sites, this in turn lead to coke formation and deposition.

A common dehydrogenation process is the Houdry process (developed in 1993), it is a single step process of hydrogen abstraction from butane. It uses chromia-alumina catalyst which is usually regenerated after few minutes of usage using air to burn off the coke layer. Another dehydrogenation process is the Dow process which utilizes butenes in the presence of steam to produce butadiene. The catalyst used in this process is Ca-Ni phosphate stabilized with Cr_2O_3, the heat of dehydrogenation is provided by the superheated steam. The catalyst is also regenerated and the product is isolated from reaction mixture using extractive distillation. Shell and Phillips petroleum also developed paraffin dehydrogenation processes using Fe-Cr oxide catalysts with K_2O additive and Fe oxide bauxite catalyst respectively [11].

Oxidative dehydrogenation of alkanes is an alternative irreversible reaction used for the production of olefins and di-olefins. It is an exothermic reaction that occurs at lower temperature and the catalyst used can obtain oxygen directly from the feed stream without requiring additional re-oxidation. The presence of oxygen in this method reduces coking and extends catalyst life time [12-14]. The major challenge in oxidative dehydrogenation is selectivity control mainly due deep oxidation reactions to CO and CO_2, the correct co-feeding of oxygen can reduce this effect together with selectivity improvement by proper catalyst design (catalyst that ensures selective adsorption of intermediate and effective desorption of targeted product) [15],[16]. The catalytic performance for ODH is related to the surface acidity/basicity property and reduction-

oxidation (redox) property. The lattice oxygen of the catalyst is involved in oxidation process oxidizing hydrogen and olefins intermediates. After which the surface of the catalyst that has been reduced earlier is restored back to normal state by gas phase oxygen adsorption. The evolution of the lattice oxygen is promoted by the interaction between the metal oxides [17].

20wt% Ni and 30wt% Bi as metal weight to support weight supported on gamma-Al_2O_3 (hereafter 20Ni-30Bi-O/gamma-Al_2O_3) was obtained as an effective catalyst for the oxidative dehydrogenation of butane to butadiene [18]. The influence of calcination on the performance of Bi-Ni-O/gamma-Al_2O_3 catalyst for n-butane oxidative dehydrogenation to butadiene was also investigated [19]. The effect of substituting (partial/full) metal species active sites (nickel oxide) in 20Ni-30Bi-O/gamma-Al_2O_3 with Fe and Co oxides was also studied [20]. The metal oxides were considered because both Ni, Fe and Co have proximity in properties owing to their position in the periodic table and also their ability to switch their oxidation states (FeO_x, CoO_x, NiO_x) thereby showing an interesting redox character and acidic/basic properties suitable for oxidative dehydrogenation reactions. Mono main metal (Ni, Fe, Co), binary metal (Ni-Fe, Ni-Co and Fe-Co) and ternary metal (Ni-Fe-Co) effects on the catalyst activity and selectivity were discussed. This thesis work is a continuation of the above studies and the main objectives are discussed in the research objectives section.

1.1 Research Objectives

The main aim of the research is to enhance the production of light olefins (mainly butadiene) from n-butane via oxidative dehydrogenation. The detailed objectives are:

- Carrying out thermodynamics analyses to predict the oxidative dehydrogenation of n-butane equilibrium product compositions and thermodynamic favorable reaction pathway

- Synthesizing various metal oxides supported catalysts for the catalytic conversion of n-butane

- Characterizing the prepared catalysts using the state of the art techniques such as X-Ray diffraction (XRD), Temperature programmed desorption (TPD), Temperature programmed reduction (TPR), Transmission electron microscopy (TEM), X-ray photoelectron spectroscopy (XPS), Nitrogen adsorption-desorption isotherms

- Studying the relationship between molecular structures of the different catalyst samples and investigating metal oxides-support interaction and its effect on catalyst performance

- Optimizing the various reaction conditions ranging from temperature, feed ratio and contact time and elucidating the reaction mechanisms (network) using the Delplot techniques

- Developing a kinetic model that describes accurately the product gas composition during the catalytic reactions and to estimate the intrinsic kinetic parameters (Activation energies and pre-exponential factors) using KME.

1.2   Uniqueness of the Research

To the best knowledge of the investigator, the following aspects have not been duly studied in the reported literatures:

- The utilization of commercially available active metal oxides and supports, which are not noble element and toxic.

- The one step ODH process of n-butane to butadiene which ensures no butene separation at the intermediate step.

- The use of Delplot techniques and kinetic modelling editor (KME) which are new tools for reaction network elucidation and kinetics studies.

1.3   Scope and Outline of the Work

The scope of this research will be limited to the oxidative dehydrogenation process for converting n-butane to butadiene using metal oxides supported catalysts. This has been broken down in to the following chapters

Chapter two reported a detailed and up-to-date literature review on catalytic oxidative dehydrogenation of n-butane. Previous work done using various groups of catalysts, reported reaction mechanisms and kinetic studies available in the open literature. Thermodynamic analyses of the process was also discussed using in-built RGibbs reactor in Aspen Plus version 8.0 software.

Chapter three reported the effects of supports on the catalytic performance of n-butane to butadiene. The catalysts were synthesized with Ni and Bi supported on Al_2O_3, SiO_2 and

ZrO$_2$ supports. Only metal oxides of Ni and Bi were also tested to clarify the roles of the supports in the dispersion of active species, reducibility and acid-base properties.

Chapter four reported the pore structure effect of mesoporous silica supported catalyst on the oxidative dehydrogenation of n-butane to butadiene. The result from chapter three revealed that SiO$_2$ supported catalyst was more selective for the dehydrogenation pathway compared to Al$_2$O$_3$ and ZrO$_2$. Mesoporous silica (MCM-41, Silica foam and SBA-15) were then investigated with a view to improving the catalytic performance due to their special properties of high dispersion ability, thermal stability and highly ordered pore structure

Chapter five reported a continued study on the role of mesoporous silica supported catalyst in improving the selectivity to butadiene from n-butane. SBA-15 was loaded with varying amount of Ni and Bi in order to get an optimum combination with balanced suitable properties for a highly selective butane to butadiene reaction pathway.

Chapter six reported the utilization of Delplots techniques for the elucidation of the reaction network from n-butane to butadiene. Based on the network, possible reactions were proposed and utilized in the kinetic model editor (KME) to obtain the kinetic parameters for the ODH reaction.

Chapter seven provided the conclusions of the work presented in the thesis and some recommendations for future work.

CHAPTER 2

LITERATURE REVIEW

2.1   Butadiene

Butadiene is an unsaturated hydrocarbon produced as a secondary product from the dehydrogenation (hydrogen abstraction process) of a saturated hydrocarbon mainly butane. Normal butane is first dehydrogenated to form butylene (primary product) and finally butadiene is formed from the dehydrogenation of butylene [1]. Butadiene is a colorless, non-corrosive gas or liquid with a mild aromatic or gasoline-like odor at room temperature, it is highly reactive, toxic and flammable hence classified as a hazardous chemical [21]. Butadiene is mainly polymerized for the production of synthetic rubber. A homo polymer from butadiene (Polybutadiene) is a liquid material and very soft, while Acrylonitrile butadiene styrene (ABS), Styrene butadiene (SBR) and Acrylonitrile butadiene (NBR) produced as copolymers from butadiene and styrene are elastic and tough. Automobile tires producing companies mainly used SBR [8].

2.1.1   Uses of Butadiene

The major use of butadiene is in the production of polymers which have variety of usage domestically and industrially, they improve the performance and functionality of domestic products, safety and also reduces costs of the products. Butadiene-based polymers are used in construction materials, automobiles, Computer and telecommunication equipment, packaging and household articles [22],[23].

8

2.2 Direct Dehydrogenation vs Oxidative Dehydrogenation

The existing commercialized means of dehydrogenation of n-butane and n-butenes is through direct dehydrogenation. This process is usually carried out over Cr/Alumina catalysts at high temperatures (> 600°C) [24]. Due to the high temperatures involved, there is thermal cracking which leads to much coke deposition and catalyst deactivation. As a result, there is need for regular regeneration of the catalysts [25]. The drawbacks of the direct dehydrogenation process includes: the process is thermodynamically limited because the dehydrogenation is an equilibrium process between alkanes, alkene and hydrogen which thus limits the yield of olefins, the process cannot be operated at high pressures because there are more molecules on the products sides than the reactants, the process is endothermic, there is high coke formation and catalyst deactivation due to high reaction temperatures [26], [27]. The selectivity for alkenes obtained through ODH is low because of the faster oxidation of the alkenes produced to CO_2 than the alkane feedstocks since the latter process is thermodynamically favoured. [28].

Some researchers have also carried out both oxidative and non-oxidative dehydrogenations of iso-butanes in one reactor using silica-supported VO_x materials as catalysts. Using this method, the oxidation of isobutenes to CO_x at high temperatures (conversions) was suppressed because a low amount of oxygen was required for the process. Also, the small amount of oxygen helps in burning of coke deposits during the reaction and the catalyst stability increased as the reaction progresses because the active species were reoxidized [29].

Normally, in non-oxidative dehydrogenation, n-butane is dehydrogenated to butenes first, followed by the dehydrogenation of butenes to butadiene over Cr-Alumina catalysts. But

9

in ODH, there is no limitation of thermodynamic equilibrium and the precursors which lead to the formation of coke can be removed easily by the oxygen. The selective production to 1,3-butadiene from n-butane is difficult because under the severe reaction conditions for n-butane activation, the butenes and butadiene produced form carbon dioxide and water on quickly reacting with oxygen [30].

2.3   Oxidative Dehydrogenation of Alkanes

Oxidative dehydrogenation of alkanes is an alternative irreversible reaction used for the production of olefins and diolefins. It is an exothermic reaction in which the byproduct produced is water instead of hydrogen and occurs at lower temperature. The catalyst used can obtain oxygen directly from the feed stream without requiring additional re-oxidation. The presence of oxidant (like oxygen) in the method also reduces catalyst deactivation by coking due to the efficient removal of coke and its precursors thereby extending catalyst life time [17],[31].

The major challenge in oxidative dehydrogenation is selectivity control mainly due to parallel and consecutive reactions resulting from the combustion of reactant (partial oxidation) to CO and CO_2, the correct co-feeding of oxygen can reduce this effect together with selectivity improvement by proper catalyst design and formulation [20].

The activity and selectivity of a catalyst for ODH depends on its acidic/basic properties and reduction-oxidation (redox) characteristics. The catalyst is reduced by losing its lattice oxygen which is used in the reduction reaction with water as byproduct, it then adsorbs molecular oxygen from the feed to regain its earlier oxidation state. The interaction

10

between the metal components of the catalysts (active species and support) plays a great role in the availability or otherwise of the lattice oxygen for the reaction [32].

Several researchers reported vanadium oxide and chromium oxide as active species with different oxides as carriers (Alumina, Silica, Titania, Zirconia, Ceria etc) showing good results for the ODH of lower paraffins [33-35]. The catalytic performance relies on the type of carrier, catalyst loading and synthesis method [36]. Hakuli et al [37] investigated different chromia supported catalysts and concluded that alumina and silica-supported chromium oxides were the most effective for the production of lower olefins. Vanadia supported on basic supports not acidic or neutral oxides have been found to be the most selective catalysts for propane oxidative dehydrogenation as reported by Corma et al [38]. Volpe et al [39] concluded from his investigation on n-butane dehydrogenation using VOx supported on USY, NaY, γ-Al$_2$O$_3$ and α-Al$_2$O$_3$ that VOx/USY has the highest activity and selectivity due to VOx monolayer and its mild acidity. Investigation on the reactivity of vanadia on various supports was conducted by Arena et al [40] and the conclusion drawn was that vanadia was more reactive on amphoteric oxides with TiO$_2$ having the highest reactivity and that the dispersion and reducibility of the active phase is greatly influenced by the acidic/basic property for the support.

Chromia-Alumina is a dual functional catalyst due to its acidic function obtained from the support and dehydrogenation function due to chromium oxide. Vuurman et al [41] reported that the catalytic dehydrogenation properties of the Chromia-Alumina catalyst are due to surface chromium oxide species and not the bulk chromium oxide phases like CrO$_3$ or Cr$_2$O$_3$. De Rossi et al [42] investigated propane dehydrogenation on Chromia/Silica and Chromia/Alumina catalysts and concluded that, the active sites for the dehydrogenation are

11

Cr^{III} and not Cr^{II} species and that Chromia supported on zirconia has the highest activity compared to silica and alumina supports. This is because the proper coordination of chromium on the surface sites of zirconia is preserved and the oxygen ion necessary for reduction (H$_2$ abstraction) is more readily available.

Jibril et al [43] investigated the oxidative dehydrogenation of isobutane on chromium oxide-based catalyst, they tested different supports (Al$_2$O$_3$, TiO$_2$, MgO, and SiO$_2$), different chromium precursors and partially substituting the chromium with some metals (V, Ni, Co, Mo and Bi). They concluded that, chromia supported on alumina has the best performance with chromium nitrate as the best precursor and that partial substitution of chromium by the metals has little or no contribution on the catalyst performance with Nickel addition slightly increasing the selectivity with same conversion.

Ajayi et al [44] studied n-Butane dehydrogenation over mono and bimetallic MCM-41(highly dispersed Silica) catalyst under oxygen free atmosphere by varying the weight percent of the metals in the catalyst. They concluded that 1.2Cr2.8V/M-41 has the highest butane conversion and butene selectivity.

2.4   Catalyst Development for Lower Alkanes ODH

The catalyst systems studied by several researchers as obtained from literature for oxidative dehydrogenation of lower alkanes can be grouped into three.

- Catalyst based on alkali and alkali earth metals
- Catalyst based on noble metals
- Catalyst based on oxides of transition metal

2.4.1 Catalysts based on Alkali and Alkali Earth Metals

Catalysts based on Group 1 and 2 metals show good olefin selectivity for ethane and propane, of this catalyst systems the most prominent one is Li/MgO. Although Li/MgO combination shows reasonable activity [45], [46], the catalyst is usually promoted with halogens mainly chlorine. Hence, halides have high significance towards achievements of good yields resulting from their acidic properties that positively affects dehydrogenation reaction. These catalysts activate ethane at temperature above 600 °C to form ethyl radicals that react in the gas phase [47]. Addition of Tin oxide (SnO_2), Lanthanium oxide (La_2O_3), Neodymium oxide (Nd_2O_3), or Dysprosium oxide (Dy_2O_3) further improves the performance of Li/MgO. Ethene yield is up to 77% when Dy_2O_3 is used as a promoter and a remarkable selectivity is achieved when the reaction temperature gets closer to melting point of LiCl [48]. Propene is the best alkene produced through oxidative dehydrogenation of propane. Ethene can as well be synthesized in large quantity via catalytic dehydrogenation, chemical industries still maintain steam cracking for ethene production [10].

2.4.2 Catalysts based on Noble Metals

Catalysts in this group have active species that contains noble metals such as Platinum, Rhodium, Palladium, which are very efficient catalysts for combustion. Paraffins can be converted to alkenes using nobel metal catalysts under specific reaction conditions like reduced contact times and little oxygen supply [10]. At lower temperatures these noble metal catalysts are usually non-selective, however they can be used for selective oxidation at temperature around 1000°C, and non-oxidative same phase reactions greatly influence the formation of products. The selectivity is enhanced by high alkane-oxygen ratio as well

as a higher temperature. This leads to nearly complete conversion of oxygen in a way that non-oxidative conversion of paraffins results like steam reforming together with cracking. The catalyst mainly deactivates due to coking and sintering [49]. Enclosing the active noble metals in a passive support helps mitigate the deactivation. The over layer of support suppresses the oxidative dehydrogenation process and prevents sintering of metals with decrease in coke formation for high temperature reactions.

2.4.3 Transition Metal Oxides based Catalysts

This category of catalyst allows low temperature activation of alkanes relative to group I and II as well as noble metals. Hence the performance of catalysts for this group is usually better. The oxidative dehydrogenation reaction of lower paraffins using oxides of metals in the transition series on a support occurs via the mechanism of Mars Van Krevelen, in which lattice oxygen in the catalysts is used for oxidizing the paraffin as well as the reoxidation by the gas phase molecular oxygen [44],[50]. Some factors dictates the performance of the catalyst like the redox properties, chemical nature of the active oxygen species and the acid-base character, which in turn depend on the loading and dispersion of the transition metal and the kind of support used [36].

Transition metal oxides have reducible oxygen (surface lattice oxygen) that partake in oxidative dehydrogenation in the absence of gaseous oxygen. Even though, the active oxygen specie partake also in other non-selective routes of ODH resulting to CO_x. The two most important systems are the molybdenum-based catalytic system and the vanadia–based catalytic system although from literature the molybdenum systems are less active.

For ethane, the ethylene yield values shown are close to, and sometimes even better than the corresponding values obtained from steam cracking although for propane ODH the values are not too interesting from an industrial point of view. Conditions leading to best propylene yields also leads to production of remarkable amount of ethylene, hence finding a catalyst of industrially acceptable conversion to this olefin is still a major goal [51].

2.5   Properties of Catalysts used for Alkanes ODH

The catalysts used for oxidative dehydrogenation reaction have some basic characteristics that influenced the activity and the selectivity of the catalyst. They are discussed as follows;

2.5.1   Active Lattice Oxygen Species

Metal oxides used as active species for ODH of paraffins have lattice oxygen which participate in the reduction reaction process. The difference in the affinity of the active oxygen species to bind with paraffins is among the main factors that determines the performance (activity and selectivity) of most metal oxides supported catalysts [52]. A study by Weckhuysen and Keller [53] on vanadium oxide supported catalyst reported that 3 categories of lattice oxygen bonds are associated with the catalysts which are end V=O, intermediate V-O-V and V-O-Carrier bond each with different binding strength. They concluded that the lattice oxygen from the V-O-Support bond is the one that is involved in the catalytic reduction reaction.

2.5.2   Surface Coverage of Active Species

The dispersion of active metal oxides on the support plays a great role on the performance of the supported catalyst. The dispersion depends on the active metal loading and preparation method [54]. Bell et al [55] and Klose et al [56] investigated the effect of

amount of vanadia loading as the main factor leading to distinguished VO_X species on the surface of the carrier (support). They also investigated different type of supports (TiO_2, SiO_2, Al_2O_3 and ZrO_2) with emphasis on alumina-supported vanadia. The conclusions drawn was with little loading of vanadia, isolated VO_4 species which is highly dispersed is formed, isolated monovanadates changes to polymeric polyvanadates with increase in VO_X density which increases continuously until monolayer coverage is attained. Crystalline V_2O_5 nanoparticles forms at high loading of vanadium.

2.5.3 Support Effect

The physico-chemical properties (surface area and acid-base) of the carrier (support) used in metal supported catalysts significantly determines the selectivities of the olefins produced. This is related to the different interactions (dispersion and reducibility) of the active species on different types of support.

Acidic or basic property of the support controls the catalyst selectivity and reactivity due to their influence on reactants adsorption and product desorption. Catalyst with acidic support favor basic reactant adsorption and acidic product desorption, hence with controlled acidic character of support, a catalyst can be designed with higher selectivity in oxidative dehydrogenation reaction [57]. It was concluded in a work by Blasco and Lopez-Nieto [14] and also by Corma et al [38], that catalysts which are very selective are obtained with oxides of vanadium supported on basic oxide (MgO, La_2O_3) compared to oxides of acidic metals, this is as a result of the strong interaction between acidic V_2O_5 and the basic support leading to highly dispersed VOx species responsible for the higher selectivities to olefins and the opposite is true with acidic supports [14], [58].

16

2.5.4   Redox Properties of Supported Metal Catalysts

The reducibility of active metal oxides play a great role in their activities and selectivities as catalysts for ODH reactions. This property of the metal oxides is greatly influenced by the type of support used which determines the strength of the lattice oxygen used for the redox process.

Lopez-Nieto investigated the reducibility of vanadium oxide catalysts using temperature programmed reduction on different support oxides and concluded that acid-base property of the support strongly influenced the reducibility of the oxides with a negative effect on basic support oxides [1].

2.6   ODH of n-Butane to Butadiene

This is a reaction that involves series removal of molecule of hydrogen from normal butane forming 1,3-Butadiene in the presence of an oxidant (mainly oxygen) with water as a byproduct. Normal butane is a saturated and highly stable hydrocarbon hence requires high temperature for the activation process, it is slightly different from the ODH of ethylene and propylene because of the presence of two secondary atoms of carbon ($-CH_2-$) hence it has high chance of undergoing side reactions to yield other products.

2.7   Catalysts Development for n-Butane ODH

Most researchers focus more on the catalyst development for ethane and propane oxidative dehydrogenation with more emphasis on vanadia, molybdena and chromia supported catalysts. Some of the literatures reviewed for the catalyst development for butane ODH are discussed in this section.

Ariola and Nava investigated the ODH of n-butane using Iron-Zinc oxide catalyst. They employed XRD, TPR and Mossbauer spectroscopy to determine the catalytically active phase and concluded that zinc ferrites ($ZnFe_2O_4$) having spinel structure is the selective catalyst for ODH of n-butane to butenes which further produces butadiene in the presence of ZnO as a modifier. The ZnO interacts with the iron from the zinc ferrite modifying the electron density of the iron which is responsible for the selectivity to butadiene [59].

Armendariz et al studied ODH of n-butane on zinc-chromium-ferrite catalyst. The catalyst was characterized using XRD and Mossbauer spectroscopy. The chromium was added as a promoter that substitutes Fe^{3+} in the octahedral sites which increases the basicity of the lattice oxygen thereby enhancing the selectivities to butadiene and CO_2 [60]

Vasil'ev and Galich reported that the method of active components deposition on the support strongly determines the performance of cobalt-molybdenum and magnesium-molybdenum catalyst used in the ODH of normal butane. Catalyst activity increases proportionally to the number of active components which are cobalt, magnesium and molybdenum especially with a support of low surface area [8].

Xu et al investigated the dehydrogenation of n-butane over vanadia supported on silica gel catalyst using impregnation method of preparation and characterized using XRD, UV-Vis, FTIR, Raman and BET measurements. The influence of VO_x loading and reaction temperature were studied and they concluded that at low VO_x loading and temperature of 590~600°C, n-butane conversion and olefin yield of highest value was obtained [61].

McGregor et al studied the effect of vanadia species in VO_x/Al_2O_3 for n-butane dehydrogenation by varying the vanadium loadings. The catalysts were characterized using

FTIR and solid state NMR and concluded from their findings that a strong relationship exist between the surface species of VO_x and the performance of the catalyst with high activity and low selectivity for isolated VO_x species and polymeric VO_x species having greater selectivity to the targeted olefins [62].

Malaika et al investigated the ODH of n-butane to butadiene using chemically modified activated carbon as catalyst. The conclusion was that at low temperature only oxidation takes place leading to the formation of CO_2 but with increase in temperature up to 300^oC and above, 1,3-butadiene and 1-butenes are formed as the major products [12].

Lee et al investigated oxygen mobility influence together with oxygen capacity of $Mg_3(VO_4)_2$ supported with different oxides (Al_2O_3, ZrO_2, MgO, CeO_2) for ODH of n-butane. Their experimental findings shows that at the initial stage of the reaction $Mg_3(VO_4)_2$/MgO is the most active catalyst and $Mg_3(VO_4)_2$/ Al_2O_3 the least active. The activity decreases with time for the MgO catalyst while $Mg_3(VO_4)_2$/ZrO_2 showed stable catalytic activity, hence the conclusion that oxygen mobility and oxygen capacity directly affects the stability of the catalyst activity and the initial catalytic activity respectively [63].

Kwon Lee et al in a similar study investigated the ODH of normal butane to normal butene and 1,3-butadiene over $Mg_3(VO_4)_2$/MgO-ZrO_2 catalyst with varying Mg:Zr in the support. The support was prepared using gel-oxalate co-precipitation method and the catalyst by wet impregnation method and was characterized using XRD, XPS and ICP-AES techniques. They concluded that the catalyst with Mg:Zr of 4:1 has the highest activity and selectivity due to its highest oxygen capacity and acidity as confirmed by TPRO and TPD respectively [64].

Xu et al investigated the catalytic ODH of n-butane over V_2O_5/MO-Al_2O_3 (M= Alkaline earth metals: Mg, Ca, Ba, Sr) with varying V_2O_5 loading. The catalyst were characterized by BET, XRD, FTIR, H_2-TPR and Raman spectra and the results showed that only MgO modified Alumina produce a catalyst with high activity and selectivity while that of Ca, Ba and Sr showed low activity due to the formation of orthovanadate phase which seldom undergoes reduction. The high activity of the MgO modified Alumina is due to the good dispersion of VOx species due to increased surface area of the support and the existence of crystalline phase of MgO [65].

Furukawa et al also examined the performance of bifunctional catalysts (Palladium-based intermetallic compounds) supported on silica in n-butane ODH. They used a variety of metals in addition to Pd; these metals are Bi, Fe, Ge, In, Sn and Zn. The use of Pd-Bi, Pd-In and Pd_3Fe catalysts instead of only Pd catalyst led to dramatic increase in butenes and butadiene selectivities and yields because the second metal effectively stops the undesired n-butane combustion and also the oxygen conversion was approximately 100% [66].

Jermy et al investigated the catalytic ODH of normal butane to butadiene using Bi-Ni-O/γ-Alumina and reported from their experimental findings that the support itself is selective for the ODH of n-butane to butenes and partial oxidation to CO, the dispersion of NiO on the support reduces the partial oxidation selectivity and enhanced butadiene selectivity. Addition of bismuth to the catalyst was confirmed to give more selectivity to butadiene due to improved NiO dispersion and the redox property of the resulting catalyst [18].

Vanadia catalysts supported on TiO_2 are also effective catalysts for n-butane ODH. Their performance was studied by Le Minh et al [67]. The main reaction product obtained was

1-butene. They also examined the effect on La doping on the activity and selectivity of the vanadia catalyst. Doping of the catalyst with La led to increased selectivity to butenes and butadiene but because of the V_2O_5 clusters which reduced the ODH sites, there was an overall loss in activity. The combined effect of these is a decrease in butenes yield on doping with La, this means that La-doping for vanadia catalysts used for n-butane ODH is not worthwhile [67].

2.8   Catalytic Properties of NiO Supported Catalysts in Alkanes ODH

The important properties of active metals that influence their performance as active and selective catalyst for oxidative dehydrogenation reaction are redox property and acid/base character. These properties can be enhanced by doping promoters and modifiers to the active metal components and the support as investigated by many researchers, some of which were discussed in the previous section.

Nickel oxide is a relatively less expensive oxide that has been reported to activate short chain alkanes (C_2-C_4) in the presence of molecular oxygen with resulting high activity and at low reaction temperatures. The products obtained however are mainly oxidation products (CO and CO_2) with little dehydrogenation products. NiO has been reported to have improved performance in its activity and selectivity when supported or promoted on metal oxides. This promotion reduces the selectivity of oxidation products and enhanced that of dehydrogenation [68].

The nature of Ni species and the acidity/basicity of the catalyst are the two factors that influence its performance as a catalyst. The nature of the Ni species are influenced by the valence of the promoters with high valency reducing the concentration of the non-selective

non-stoichiometric oxygen in Ni^{3+} species leading to higher selectivity [69]. Lopez-Nieto et al [68] studied the effect of promoted NiO catalysts for the ODH of ethane and concluded from XPS findings that non-stoichiometric Nickel sites Ni^{3+} are involved in the non-selective catalytic processes resulting from the stabilization of electrophilic oxygen species and the removal of these species improves ethylene selectivity. Jermy et al [19] reported that NiO when promoted with Bismuth oxide results in an improved performance, this is due to the participation of Bi_2O_3 as oxygen mobile oxides which is critical in the formation of electrically active grain boundaries in the NiO. The redox system by the Ni species is better stabilized with bismuth oxide (which act as controlled O_2- supplier) as hierarchical nanoparticle cohabitation hence making the system highly efficient.

Mesoporous silicas (MCM-41, SBA-15, and foam) have been used as support to prepare well-dispersed tungsten oxide catalyst [70-72]. Oxidative dehydrogenation of n-butane was reported using vanadium nanoparticles impregnated over mesoporous silica support [73]. Mesoporous silica support showed an enhanced performance by stabilization of nanoparticles due to their ordered structure and well-defined pore sizes.

Titanosilicates which contain materials such as vanadium have also been studied extensively for n-butane ODH. Cun et al studied the performance of titanosilicates and SBA-15 catalysts which contain vanadium in the ODH of n-butane to butenes and butadiene at low temperature and low vanadia content. Increased loading of TiO_2 catalysts lead to greater conversions because the presence of oxygen in the lattice structure leads to greater catalyst reducibility but due to oxidation of the ODH products, there is a steep drop in selectivity to C_4 alkenes. In comparison to SBA-15 catalysts which contain vanadium,

V-containing titanosilicates showed greater catalytic activity. SBA-15 catalysts showed a very low conversion (1.5%) under the same reactions as the titanosilicates [25].

Titanosilicates are commonly used as catalyst supports for n-butane ODH. Setnicka et al [27] examined the effect of titanium loading on silica support for vanadium containing mesoporous silica and titanosilicate materials in n-butane ODH at a reaction temperature of 460°C and 5% conversion. Catalysts in which titanium had been incorporated (V-Ti-HMS) were four times as active as catalysts with no titanium (V-HMS) even though VO_x species were distributed at the same rate for both catalysts. Although the former catalyst shows a higher activity, it gives the same selectivity to butenes and butadiene as the latter catalyst under the same reaction conditions. The C_4-ODH selectivity was approximately 45% for the catalysts with butadiene as the main product. The main advantage of the V-Ti-HMS catalyst is that it can achieve the same yield and butenes selectivity as the V-HMS catalyst at a temperature 100°C lower [27].

Liu et al [74] investigated n-butane ODH using VO_x/SBA-15 catalysts having different loading of VO_x (2.24-28.0 wt% V content) at a reaction temperature of 520 °C. The catalysts were prepared by incipient wetness impregnation method and characterized by N_2 adsorption, XRD, HRTEM, H_2-TPR, NH_3-TPD and EPR techniques. At loading of 8.96V-SBA-15, an improved n-butane conversion and butene selectivity compared to 8.96 V-SiO_2, was obtained. This is due to an increased dispersion of V species, presence of V^{4+} species and the well-defined pore structure of the mesoporous SBA-15 support [74]. In another work by the same authors, MgO-modified VO_x/SBA-15 was compared to VO_x/SBA-15 and the former was found to exhibit higher C4 olefins selectivity and yield mainly due to the increase in VO_x reducibility and relatively lower acidity [75].

2.9   ODH of Paraffins Reaction Mechanism

The mechanism of oxidative dehydrogenation rely mostly on the paraffin and the catalyst used, but the basic steps involved in a typical reaction are:

- Alkane interaction with the surface of the catalyst (physisorption)

- Breakage of C-H bond forming alkyl species

- Alkyl species react with nearby surface oxygen (β-elimination) to form olefins

- Reoxidation of the catalyst by molecular oxygen.

2.9.1   Kinetic Models for ODH of Light Alkanes

Light alkanes are gases and their ODH involves solid catalyst, hence forming heterogeneous system. The catalytic reaction proceeds via the following steps:

- Reactants (Alkanes) diffusion to the catalyst surface

- Reactants adsorption on the catalyst surface

- Surface reaction

- Products desorption from the surface of the catalyst

- Products of reaction diffuse from the surface of the catalyst

Based on this reaction steps, the models used for ODH reactions are Eley Rideal model, Langmuir Hinshelwood model, Rake model, Mars Van Krevelen model (Redox model) and power law model.

For ODH reactions using transition metal oxide catalyst, most literatures reported the kinetics following Mars Van Krevelen model (Mechanism of reduction-oxidation) where the active species oxygen participates in the ODH reaction by removing molecule of

hydrogen from the paraffin thereby forming water as a byproduct which is removed by surface dehydration. The reduced catalyst is re-oxidized by the gas phase molecular oxygen [10], [76].

For the ODH of n-butane, based on the acidic/basic property of the catalyst, two reaction networks are proposed by several researchers, for a catalyst with basic character alkenes are formed directly from normal butane while 1,3-butadiene as a consecutive reaction product while for catalyst with acidic character, olefins and diolefins are produced firstly from normal butane with CO_x as products of series reaction. Hydrogen removal from normal butane determines the reaction rate while second hydrogen removal/desorption of olefinic intermediate determines the selectivity. Olefinic intermediate desorption rate from catalysts with basic character is higher than that of catalyst with acidic character [77].

2.9.2 Kinetics of n-Butane ODH

Few kinetic studies have been reported regarding the ODH of n-butane and in fact the most studied catalyst for the investigations is a vanadium oxide active species catalyst. This is due to its high activity and selectivity relative to other mixed oxides or supported catalysts. Chaar et al applied a power law model using V-Mg-O catalyst and with a parallel-series reaction scheme to describe n-butane ODH. They concluded that, a similar mechanism exist for both propane and n-butane ODH and also the reaction rate was zero order in oxygen and 0.85 order in n-butane.

Tellez et al [78] studied the kinetics of n-butane ODH using VO_x/MgO catalyst. The conclusion was that, the selectivity to each mono-olefin (1-butene, cis- and trans-2-butene) decreases as conversion increases which is typical of an intermediate product. The

selectivity to CO_x products increased with space time (a behavior of secondary products) and that of butadiene increased also with conversion and was not equal to zero at zero space time which means it is both a primary and secondary product. Power law model was utilized and it revealed that the reaction order for oxygen in olefin and di-olefins production was smaller than that for CO_x formation which clearly indicates that higher selectivity to olefins is favored by low oxygen partial pressure.

Rubio et al [79] studied the kinetics of n-butane dehydrogenation under anaerobic conditions using the Mars Van Krevelen mechanism. It was concluded that the mechanism has a single type active site with a lattice oxygen and a weakly adsorbed oxygen. Olefins production is from the lattice oxygen while the adsorbed oxygen gives CO_x in an unselective reaction pathway.

The kinetics of n-butane ODH was studied by A. Dejoz et al [80] using a hydrotalcite of Mg/Al as support with vanadia as active species. Two types of LH models were proposed by the authors which are a model where both n-butane and oxygen are competitively adsorbed (CAM) and another model where the adsorption of the two reactants is non-competitive (NCAM). The model was develop assuming that the reaction controlling step is the combination of the adsorbed reactants and the uncompetitive oxygen adsorption. They considered two types of oxygen adsorption which are dissociative for selective products formation and non-dissociative for total combustion products formation. They concluded that two different mechanisms operated on the catalyst which are connected with the vanadium species redox functions and the vanadium-free sites of the support. Formation of a butyl radical through the breakage of the C-H bond is the initiation of the mechanism occurring on the redox sites. The radical formed interacts with the vanadium

species producing adsorbed alkenic intermediate. This mechanism led to the formation of CO_x products from n-butane and butenes by a parallel reaction at low conversions and a series reaction at high conversions respectively.

Lemonidou [81] studied also the kinetics of n-butane ODH on VMgO catalyst (30 wt. % V_2O_5). The influence of reaction temperature on the catalyst selectivities to olefins and diolefins and also the effect of intermediates (CO, butenes, and butadiene) addition on product distribution and conversion was investigated. This is to obtain the necessary information on the primary and secondary reaction rates. A kinetic reaction network having parallel and series steps was proposed based on the experimental data analysis. The reaction rate for each step was calculated by the intermediate reaction products combination method. Butadiene and CO_x were shown to be produced both in parallel from n-butane with butenes and also as products of series dehydrogenation and complete oxidation of butenes respectively. The rate of butane consumption was not affected by the partial pressure increase of butenes, butadiene and CO_x. This shows that the butane adsorption sites are not the same with that of the products.

Madeira et al [82] utilized cesium-doped nickel molybdate to study the kinetics and mechanism of n-butane ODH reaction. Under the reaction conditions, the products observed were only dehydrogenation products and CO_x. They proposed a redox mechanism having two different intermediates to describe the effects of the feeds partial pressure on the rates of products formation. The mechanism showed that butadiene is formed only from 1-butene while CO_x is obtained from all the hydrocarbon species. In a similar work by the same authors, a power law model was proposed for two different catalysts which are Cs-doped $NiMoO_4$ and un-promoted $NiMoO_4$. The influence of Cs addition resulted in an

increased activation energies, increased order of reaction for butane with respect to C_4 products and with a decrease in the order for CO_x but without any effect on the order related to oxygen. The difficulty in the reduction of Cs promoted $NiMoO_4$ resulted in the higher activation energies for all the products as well as n-butane. This also buttresses the fact that ODH of n-butane on this catalyst occurs via the Mars Van Krevelen mechanism.

2.10   Thermodynamic Analyses

Thermodynamic analysis for the oxidative dehydrogenation (ODH) reactions of n-butane and oxygen was conducted using the RGibbs in-built reactor contained in the Aspen Plus V8.0 software. RGibbs reactor performs rigorous reactions and multiphase equilibrium based on Gibbs free energy minimization algorithm. Peng Robinson equation of state was utilized and the binary interaction parameters were predicted for all the components by the software. The compositions at equilibrium for the ODH reactions were computed from 573 K to 873 K at 1 atm with varying O_2/n-C_4H_{10} inlet molar ratios (1.0, 2.0, and 4.0 mol/mol). The equilibrium n-butane conversions over the temperature ranges are presented in Figure 2.1. The conversion depended on the molar ratio of O_2/n-C_4H_{10} especially at lower temperatures. For direct dehydrogenation reaction, n-butane equilibrium conversion was very low at the initial temperatures and it increased at higher temperatures. This indicated that an oxidant is needed for good conversions at low reaction temperature. For the ODH reactions, n-butane conversion increased with increase in the molar ratio and reaction temperatures. An almost 100 % n-butane equilibrium conversion was observed for O_2/n-C_4H_{10} = 4.0 mol/mol at 700 K.
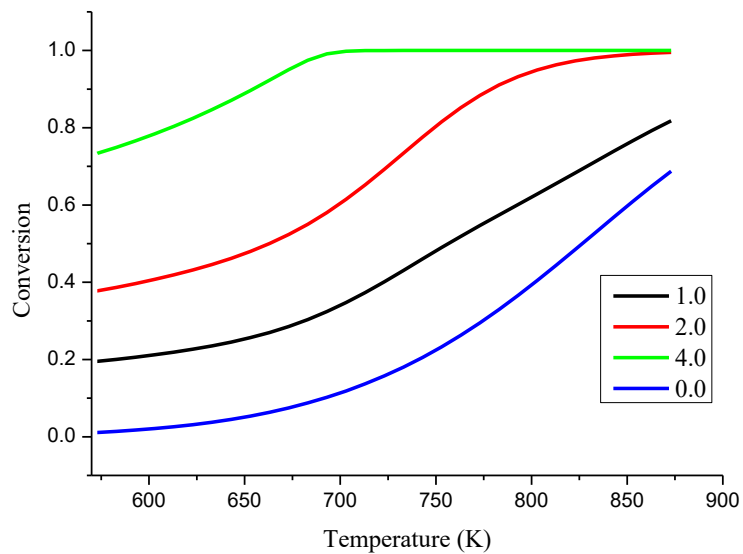
Figure 2.1 n-butane conversion at different O2/n-C4H10 molar ratios

The equilibrium compositions for direct dehydrogenation reaction are presented in Figure 2.2. The formation of butenes and butadiene increased at a very low rate compared to hydrogen with increase in temperature. It is an indication that hydrogen is the most favorable product at equilibrium.
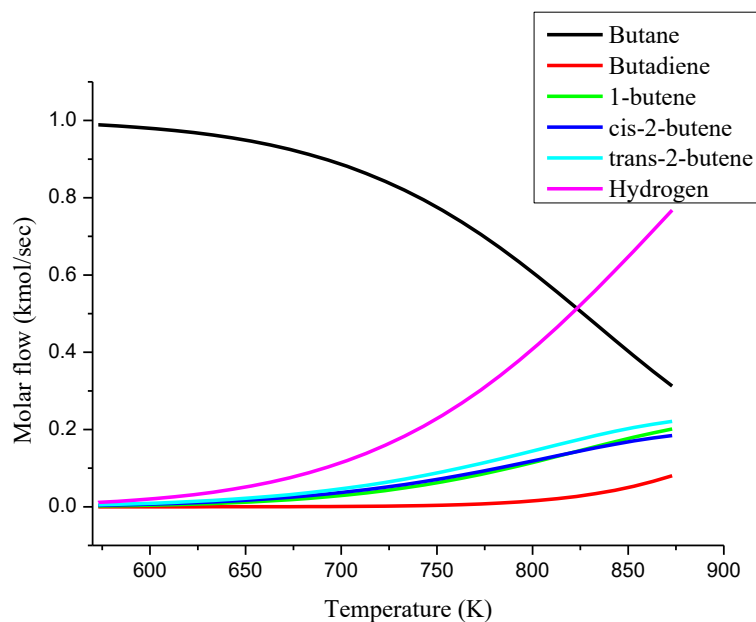
Figure 2.2 Equilibrium compositions for dehydrogenation at O_2/n-C_4H_{10} = 0.0 mol/mol.

The equilibrium compositions for the ODH of n-butane to butenes and butadiene together with other possible reaction pathway products (CO, CO_2, H_2, and H_2O) are presented in Figures 2.3, 2.4, and 2.5 for O_2/n-C_4H_{10} = 1.0, 2.0 and 4.0 mol/mol respectively. For O_2 and butane molar ratio of 1.0 mol/mol, butenes are the main dehydrogenation products with only a small amount of butadiene produced at higher temperatures. At O_2/n-C_4H_{10} = 2.0 and 4.0 mol/mol, the equilibrium amount of butenes first increases and then decreases while that of butadiene increases continuously. This supports the reaction scheme that butadiene is obtained as a secondary product in a series reaction from butane to butenes then to butadiene.
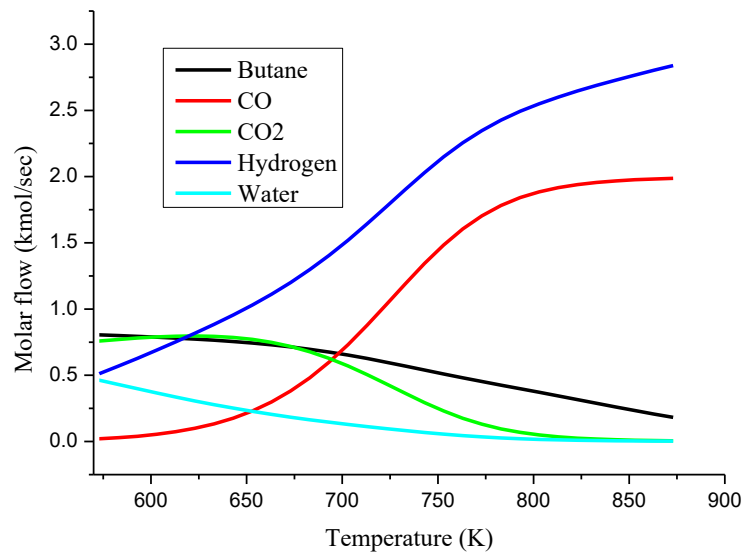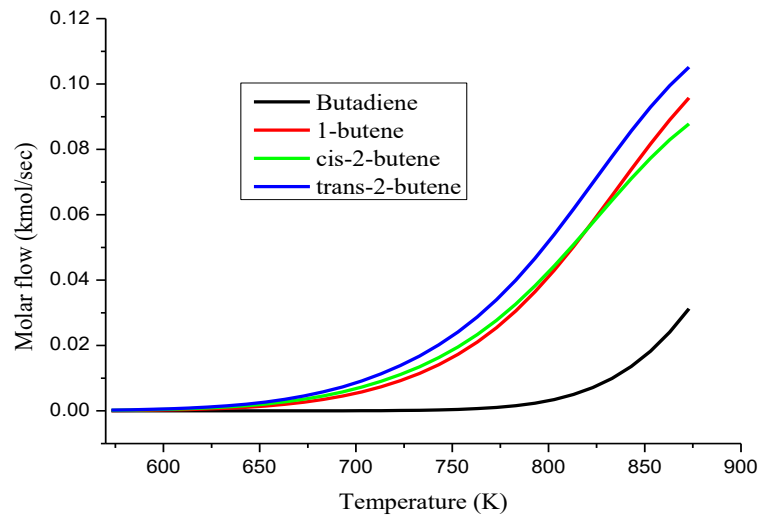
Figure 2.3 Equilibrium compositions at $O_2/n\text{-}C_4H_{10} = 1.0$ mol/mol
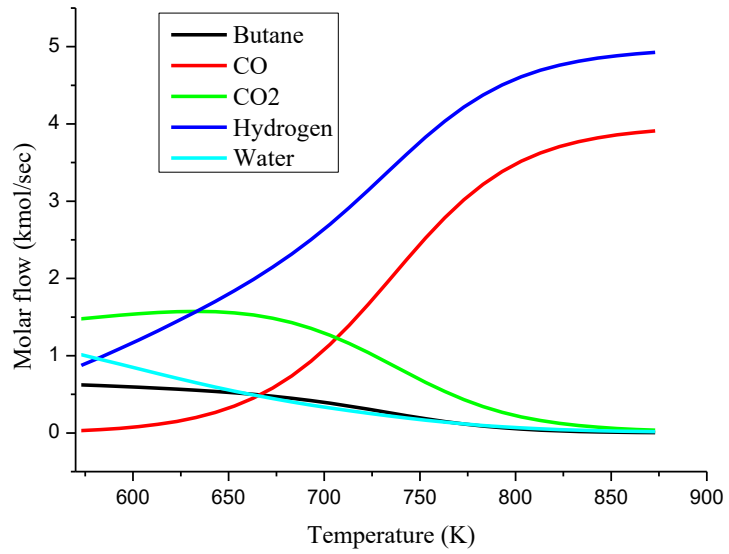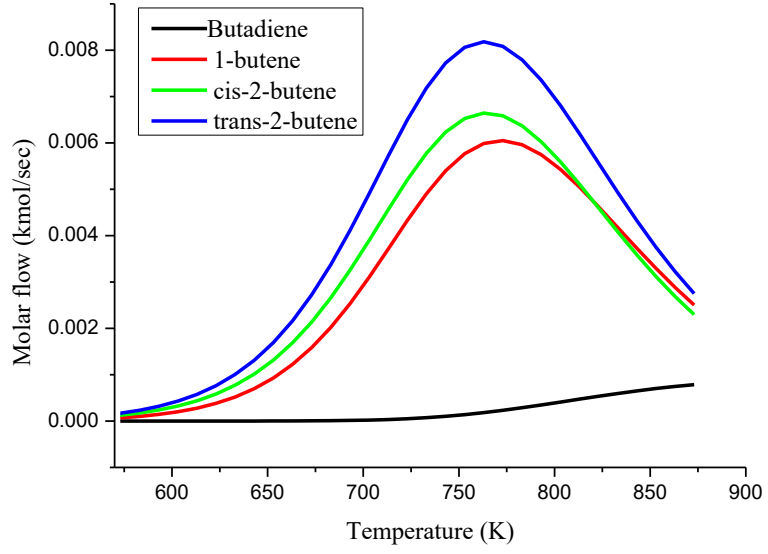
Figure 2.4 Equilibrium compositions at $O_2/n-C_4H_{10} = 2.0$ mol/mol
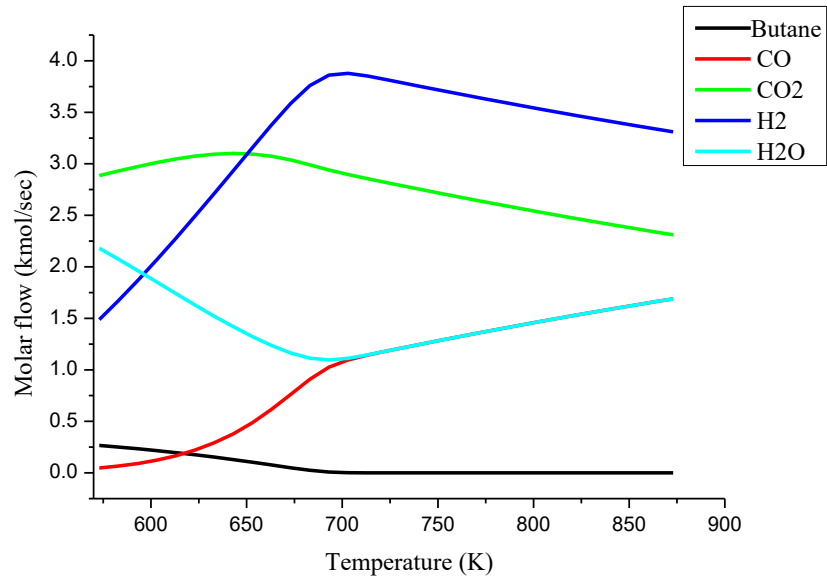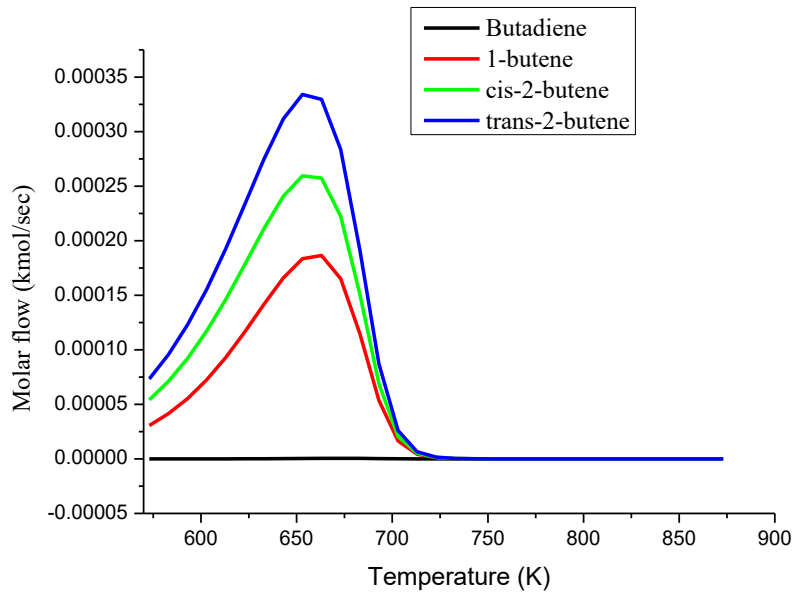
Figure 2.5 Equilibrium compositions at $O_2/n\text{-}C_4H_{10}$ = 4.0 mol/mol.

For all the $O_2/n\text{-}C_4H_{10}$ ratios, dry reforming products (CO and H_2) are the main reaction products at equilibrium. This clearly indicate that n-butane dry reforming is a more thermodynamically favorable reaction pathway than ODH of n-butane at the same

condition. Hence it is very vital to design catalysts that can promote the ODH reaction pathway kinetically for effective production of dehydrogenation products.

References

[1]   J. L. Nieto, Top. Catal. 41, 3–15, 2006.

[2]   C. Téllez, M. Abon, J. A. Dalmon, C. Mirodatos, and J. Santamaría, J. Catal. 195, 113–124, 2000.

[3]   A. Qiao, V. N. Kalevaru, J. Radnik, A. Srihari Kumar, N. Lingaiah, P. S. Sai Prasad, and A. Martin, Catal. Commun. 30, 45–50, 2013.

[4]   W. Yan, Q. Y. Kouk, J. Luo, Y. Liu, and A. Borgna, Catal. Commun. 46, 208–212, 2014.

[5]   A. N. Vasil'ev and P. N. Galich, Chem. Technol. Fuels Oils 33, 185–192, 1997.

[6]   S. Veldurthi, C.-H. Shin, O.-S. Joo, and K.-D. Jung, Catal. Today 185, 88–93, 2012.

[7]   S. A. Al-Ghamdi, "Thesis: Oxygen-Free Propane Oxidative Dehydrogenation Over Vanadium Oxide Catalysts: Reactivity and Kinetic Modelling," no. December, 2013.

[8]   L. Rodriguez, D. Romero, D. Rodriguez, J. Sanchez, F. Dominguez, and G. Arteaga, Appl. Catal. A Gen. 373, 66–70, 2010.

[9]   E. A. Mamedov and V. Cortis Corberan, Appl. Catal. A, Gen. 127, 1–40, 1995.

[10]   M. Bender, Chem Bio Eng Rev. 1, 136–147, 2014.

[11]   B. V. Vora, Top. Catal. 55, 1297-1308, 2012.

[12]   A. Malaika, K. Wower, and M. Kozlowski, Acta Phys. Pol. A 118, 459–464, 2010.

[13]   N. Ikenaga and S. Onishi, High Tech Res Cent, 1-7, 2013

[14]   I. C. Marcu, I. Sandulescu, Y. Schuurman, and J. M. M. Millet, Appl. Catal. A Gen. 334, 207–216, 2008.

[15]   I. Rossetti, G. F. Mancini, P. Ghigna, M. Scavini, M. Piumetti, B. Bonelli, F. Cavani, and A. Comite, J. Phys. Chem. C 116, 22386–22398, 2012.

[16]   M. Setnička, R. Bulánek, L. Čapek, and P. Čičmanec, J. Mol. Catal. A Chem. 344, 1–10, 2011.

[17]   B. P. Ajayi, B. R. Jermy, K. E. Ogunronbi, B. A. Abussaud, and S. Al-Khattaf, Catal. Today, 204, 189–196, 2013.

[18]   B. R. Jermy, B. P. Ajayi, B. A. Abussaud, S. Asaoka, and S. Al-Khattaf, J. Mol. Catal. A Chem. 400, 121–131, 2015.

[19]   B. R. Jermy, S. Asaoka, and S. Al-Khattaf, Catal. Sci. Technol. 5, 4622–4635, 2015.

[20]   G. Tanimu, B. R. Jermy, S. Asaoka, S. Al-Khattaf, J. Ind. Eng. Chem., 45, 111-120, 2017.

[21]   W. C. White, Chem. Biol. Interact.166, 10–14, 2007.

[22]   M. L. Pacheco, J. Soler, A. Dejoz, J. M. L. Nieto, J. Herguido, M. Menéndez, and J. Santamar, Catal. Today 61, 101–107, 2000.

[23]   J. Herguido, M. Menez, and J. Santamarı, Ind. Eng. Chem. Res. 38, 90–97, 1999.

[24]   B. R. Jermy, S. Asaoka and S. Al-Khattaf, Catal. Sci. Technol. 5, 4622–4635, 2015.

[25]   C. Wang, J. Chen, T. Xing, Z. Liu, Z. Liu, J. Jiang, and J. Lu, Ind. Eng. Chem. Res. 54 (14), 3602-3610, 2015.

[26]   O. Ovsitser and E. V Kondratenko, Chem. Commun. 46, 4974–4976, 2010.

[27]   M. Setnicka, P. Cicmanec, R. Bulánek, A. Zukal and J. Pastva, Catal. Today 204, 132–139, 2013.

[28]   L. M. Cam, N. D. Huyen, and N. N. Ha, J. Chem., 1-9, 2013.

[29]   M. Setnicka, P. Cicmanec, E. Tvaruzkova and R. Bulanek, Top. Catal. 56, 662–671, 2013.

[30]   D. Bhattacharyya, S. K. Bej, and M. S. Rao, Appl. Catal. A: Gen 87, 29–43, 1992.

[31]   F. Urlan, I. C. Marcu, and I. Sandulescu, Catal. Commun. 9, 2403–2406, 2008.

[32]   B. R. Jermy, B. P. Ajayi, B. A. Abussaud, S. Asaoka, and S. Al-Khattaf, J. Mol. Catal. A Chem. 400, 121–131, 2015.

[33]   M. A. Botavina, G. Martra, Y. A. Agafonov, N. A. Gaidai, N. V. Nekrasov, D. V. Trushin, S. Coluccia, and A. L. Lapidus, Appl. Catal. A Gen. 347, 126–132, 2008.

[34]   P. Michorczyk, J. Ogonowski, P. Kutrowski, and L. Chmielarz, Appl. Catal. A Gen.

349, 62–69, 2008.

[35]   T. V. Malleswara Rao, E. Vico-Ruiz, M. A. Bañares, and G. Deo, J. Catal. 258, 324–333, 2008.

[36]   E. Heracleous, M. Machli, A. A. Lemonidou, and I. A. Vasalos, J. Mol. Catal. A Chem. 232, 29–39, 2005.

[37]   A. Hakuli, M. E. Harlin, L. B. Backman, and A O. I. Krause, J. Catal. 184, 349–356, 1999.

[38]   A. Corma, J. M. L. Nieto, and N. Paredes, Appl. Catal. A Gen. 104, 161–174, 1993.

[39]   N. Ballarini, F. Cavani, A. Cericola, C. Cortelli, M. Ferrari, F. Trifirò, G. Capannelli, A. Comite, R. Catani, and U. Cornaro, Catal. Today, 91–92, 99–104, 2004.

[40]   F. Arena, F. Frusteri, A. Parmaliana, G. Martra, and S. Coluccia, Stud. Surf. Sci. Catal. 119, 665-670, 1998.

[41]   M. A. Vuurman, F. D. Hardcastle, and I. E. Wachs, J. Mol. Catal. 84, 193–205, 1993.

[42]   S. Derossi, G. Ferraris, S. Fremiotti, E. Garrone, G. Ghiotti, M. C. Campa, and V. Indovina, J. Catal. 148, 36–46, 1994.

[43]   B. Y. Jibril, N. O. Elbashir, S. M. Al-Zahrani, and A. E. Abasaeed, Chem. Eng. Process. Process Intensif. 44, 835–840, 2005.

[44]   B. P. Ajayi, B. R. Jermy, K. E. Ogunronbi, B. A. Abussaud, and S. Al-Khattaf, Catal. Today 204, 189–196, 2013.

[45]   B. Tope, Y. Zhu, and J. A. Lercher, Catal. Today 123, 113–121, 2007.

[46]   M. V. Martínez-Huerta, X. Gao, H. Tian, I. E. Wachs, J. L. G. Fierro, and M. A. Bañares, Catal. Today 118, 279–287, 2006.

[47]   F. Cavani and F. Trifiri, Catal. Today 24, 307–313, 1995.

[48]   S. Gaab, M. Machli, J. Find, R. K. Grasselli, and J. A. Lercher, Top. Catal. 23, 151–158, 2003.

[49]   B. Fu, J. Lu, P. C. Stair, G. Xiao, M. C. Kung, and H. H. Kung, J. Catal. 297, 289–295, 2013.

[50]   B. P. Ajayi, B. Rabindran Jermy, B. A. Abussaud, and S. Al-Khattaf, J. Porous

Mater. 20, 1257–1270, 2013.

[51]   F. Cavani, N. Ballarini, and A. Cericola, Catal. Today 127, 113–131, 2007.

[52]   V. Murgia, E. Sham, J. C. Gottifredi, and E. M. F. Torres, Lat. Am. Appl. Res. 34, 75–82, 2004.

[53]   B. M. Weckhuysen and D. E. Keller, Catal. Today 78, 25–46, 2003.

[54]   S. A. Karakoulia, K. S. Triantafyllidis, G. Tsilomelekis, S. Boghosian, and A. A. Lemonidou, Catal. Today 141, 245–253, 2009.

[55]   K. Chen, S. Xie, A. T. Bell, and E. Iglesia, J. Catal. 198, 232–242, 2001.

[56]   F. Klose, T. Wolff, H. Lorenz, A. Seidel-Morgenstern, Y. Suchorski, M. Pirkowska, and H. Weiss, J. Catal. 247, 176–193, 2007.

[57]   H. H. Kung and M. C. Kung, Appl. Catal. A Gen.157, 105–116, 1997.

[58]   T. Blasco, J. Catal.157, 271–282, 1995.

[59]   H. Armendariz, G. Aguilar-Raos, P. Salas, M. A. Valenzuela, I. Schifter, H. Arriola, and N. Nava, Appl. Catal. A, Gen. 92, 29–38, 1992.

[60]   H. Armendariz, J. A. Toledo, G. Aguilar-Rios, M. A. Valenzuela, P. Salas, A. Cabral, H. Jimenez, and I. Schifter, J. Mol. Catal. 92, 325–332, 1994.

[61]   Y. Xu, J. Lu, M. Zhong, and J. Wang, J. Nat. Gas Chem. 18, 88–93, 2009.

[62]   J. McGregor, Z. Huang, G. Shiko, L. F. Gladden, R. S. Stein, M. J. Duer, Z. Wu, P. C. Stair, S. Rugmini, and S. D. Jackson, Catal. Today 142, 143–151, 2009.

[63]   H. Lee, J. K. Lee, U. G. Hong, Y. Yoo, Y. J. Cho, J. Lee, H. S. Jang, J. C. Jung, and I. K. Song, J. Ind. Eng. Chem. 18, 808–813, 2012.

[64]   J. K. Lee, H. Lee, U. G. Hong, J. Lee, Y. J. Cho, Y. Yoo, H. S. Jang, and I. K. Song, J. Ind. Eng. Chem.18, 1096–1101, 2012.

[65]   B. Xu, X. Zhu, Z. Cao, L. Yang, and W. Yang, Chinese J. Catal. 36, 1060–1067, 2015.

[66]   S. Furukawa, M. Endo, and T. Komatsu, ACS Catal. 4 (10), 3533-3542, 2014.

[67]   J. M. L. Nieto, B. Solsona, R. K. Grasselli, and P. Concepcion, *Top. Catal.* 57, 1248–1255, 2014.

[68]   E. Heracleous and A. A. Lemonidou, Catal. Today 112, 23–27, 2006.

[69]   T. Bhuiyan, P. Arudra, M. Akhtar, A. Aitani, R. Abudawoud, M. Al-Yami, S. Al-Khattaf, Appl. Catal. A: Gen 467, 1025, 2013.

[70]   T. Bhuiyan, P. Arudra, M. Akhtar, A. Aitani, R. Abudawoud, M. Al-Yami, S. Al-Khattaf, Can. J. Chem. Eng. 92, 1271, 2014.

[71]   M. A. Ibrahim, M. N. Akhtar, J. Cejka, E. Montanari, H. Balcar, M. Kubu, S. Al-Khattaf, J. Ind. Eng. Chem. 53, 119, 2017.

[72]   R. Bulanek, A. Kaluzova, M. Setnicka, A. Zukal, P. Cicmanec , J. Mayerova, Catal. Today 179, 149, 2012.

[73]   W. Liu, S. Y. Lai, H. Dai, S. Wang, H. Sun and C. T. Au, Catal. Lett. 113, 147-154, 2007.

[74]   W. Liu, S. Y. Lai, H. Dai, S. Wang, H. Sun and C. T. Au, Catal. Today. 131, 450-456, 2008.

[75]   S. A. Al-Ghamdi, M. M. Hossain, and H. I. De Lasa, Ind. Eng. Chem. Res. 52, 5235–5244, 2013.

[76]   R. Grabowski, Catal. Rev.48, 199–268, 2006.

[77]   R. Grabowski, Catal. Rev. 48, 199–268, 2006.

[78]   C. Tellez, M. Menendez and J. Santamaria, J. Catal. 183, 210, 1999.

[79]   O. Rubio, J. Herguido and M. Menendez, Chem. Eng. Sci. 58, 4619, 2003.

[80]   A. Dejoz, J.M. Lopez Nieto, F. Melo and I. Vazquez, Ind. Eng. Chem. Res. 36, 2588, 1997

[81]   A. A. Lemonidou, Appl. Catal. A: Gen. 135, 137, 2001.

[82]   L.M. Madeira, F. J Maldonado-Hodar, M.F. Portela, F. Freira, R.M. Martin-Aranda, M. Oliveira, Appl. Catal. A: Gen 135, 137-153, 1996.

CHAPTER 3

Effect of Support in Ni-Bi-O/support Catalyst on Butane ODH
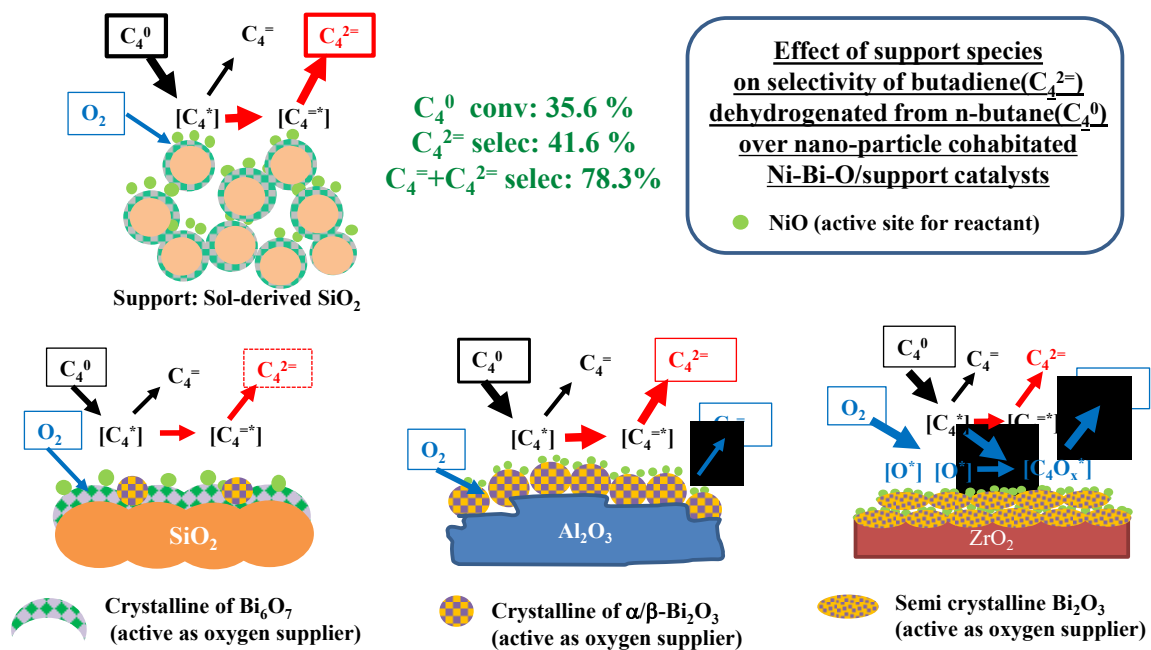
C_4^0 conv: 35.6 %
$C_4^{2=}$ selec: 41.6 %
$C_4^=+C_4^{2=}$ selec: 78.3%

Effect of support species on selectivity of butadiene($C_4^{2=}$) dehydrogenated from n-butane(C_4^0) over nano-particle cohabitated Ni-Bi-O/support catalysts

● NiO (active site for reactant)

Support: Sol-derived SiO_2

SiO_2

Crystalline of Bi_6O_7 (active as oxygen supplier)

Al_2O_3

Crystalline of α/β-Bi_2O_3 (active as oxygen supplier)

ZrO_2

Semi crystalline Bi_2O_3 (active as oxygen supplier)

Published as:

Abstract

NiO-Bi$_2$O$_3$/different support catalysts, containing 20 wt% Ni and 30 wt% Bi as metal weight to support weight (hereafter 20wt%Ni-30wt%Bi-O/support) have been studied for oxidative dehydrogenation of n-butane to butadiene. Al$_2$O$_3$, SiO$_2$, ZrO$_2$ and none (: without support) were used as gel and sol type supports. The activity and selectivity of oxidative dehydrogenation of n-butane to butadiene over the Ni-Bi-O/support catalyst strongly depended on the supports. The order of the butadiene selectivity for the gel-type support was Al$_2$O$_3$ > SiO$_2$ > ZrO$_2$ >> none, while SiO$_2$ showed the highest butadiene selectivity with 1-butene feedstock. The gel-type support effect as a hierarchical nano-particle cohabitation was also studied by using equilibrium adsorption method for the Ni-Bi-O impregnation. In the sol-type support case, the order is SiO$_2$ > Al$_2$O$_3$ > ZrO$_2$, where the SiO$_2$ sol shows not only superiority to gel-type, but also the best performance (n-butane conversion: 35.6 %, selectivity: dehydrogenation 78.3 %, butadiene 41.6 %) among support types and species. The sol-type SiO$_2$ hold balanced acid and base sites cooperating to improve butadiene selectivity, with suppressed oxygenate products, as a result of accelerating redox system with non-hierarchical nano-particle cohabitation of NiO, Bi$_6$O$_7$ and support SiO$_2$.

***Keywords*:** Oxidative dehydrogenation; *n*-butane; butadiene; nano-particle; support; silica sol.

3.1 Introduction

Butadiene is used mainly in the petrochemical and polymer industries as a raw material especially in the production of synthetic rubbers and automobile tires. It is mainly obtained as a byproduct from naphtha crackers (ethylene plants) with the main products being ethylene and propylene. The change of feedstocks from heavy into lighter (ethane and propane) has led to a decrease in butadiene supply as against the ever-increasing demand. This has led to a worldwide search for an on-purpose butadiene production technology.

Direct dehydrogenation using mainly chromium oxide supported on alumina catalyst was first investigated for producing butadiene, but it requires very high temperature [1-3]. At such high-temperature operation, frequent catalyst regeneration is required due to coke deposition. Though improved processes using butenes in the presence of steam to produce butadiene were reported, they are highly energy intensive [4,5] On the other hand, oxidative dehydrogenation with oxygen is not limited by thermodynamic equilibrium, it can be carried out at relatively lower reaction temperature and the catalyst deactivation is reduced due to the presence of oxygen [6-8]. However, controlling the product selectivity in ODH is a major challenge, considering the higher reactivity (than n-butane) of olefin products (i.e. butenes and butadiene) with oxidant forming unstable oxygenates and combustion products [9].

The performance of a catalyst in oxidative dehydrogenation is related to the acid-base surface character and its redox property. Many researchers have investigated different types of catalysts for the purpose of lower alkane oxidative dehydrogenation, some of which include V_2O_5/supports (Al_2O_3, SiO_2, TiO_2, ZrO_2) [10], Cr_2O_3/SiO_2 [11], Zn-Cr-FeO [12], Fe-Zn-O [13], $Mg_3(VO_4)_2$/supports (Al_2O_3, ZrO_2, MgO, CeO_2) [14],

Mg$_3$(VO$_4$)$_2$/MgO-ZrO$_2$ [15], V$_2$O$_5$/MO-Al$_2$O$_3$ (M=Mg, Ca, Ba, Sr) [16], V$_2$O$_5$/silica gel [17], VO$_x$/supports (USY, NaY, γ-Al$_2$O$_3$, α-Al$_2$O$_3$) [18], VO$_x$/Ti-HMS [19], VO$_x$/SBA-15 [20], MoO$_3$/MgO [21], V/supports (HMS, SBA-16, SBA-15, MCM-48) [22], V/TiO$_2$-SiO$_2$ [23]. Most of these catalysts have one problem with either activity or selectivity to butadiene and in most cases, the first step dehydrogenation products (1-butene and 2-butenes) dominate with little percentage of butadiene and some cracking products [8].

In our recent study, Ni-Bi-O/Al$_2$O$_3$ catalysts were shown to be effective for n-butane oxidative dehydrogenation. In particular, 20 wt% Ni-30 wt% Bi-O/Al$_2$O$_3$ catalyst subdued oxygenate production and showed high n-butane conversion and butadiene selectivity. The addition of Bi$_2$O$_3$ to NiO was found to introduce moderate basicity and improve redox character [24]. We also reported that the catalyst calcination through two steps of appropriate temperatures positively results in the highest dehydrogenation and butadiene selectivity. The cohabitation as 'hierarchical nano-particles' consisting of NiO, Bi$_2$O$_3$ and Al$_2$O$_3$ obtained at the preferable calcination condition, resulted in the redox and acid/base system of the combined oxides which is active and selective to the butadiene formation [25]. Furthermore, the composition effect of main metal species (Ni, Fe, Co) was also studied and improved catalyst performance was obtained on the ternary main metal system (Ni-Fe-Co) due to double improvements by Fe and Co respectively [26].

The roles of supports in catalysis cannot be ignored as the support plays a significant role in metal oxide species dispersion and also contribute to the overall acidic/basic property of the catalysts. The oxidative dehydrogenation of propane using V$_2$O$_5$/supports (Al$_2$O$_3$, SiO$_2$, TiO$_2$, ZrO$_2$) was studied and it was found that V$_2$O$_5$ over SiO$_2$ support are more selective for propene formation mainly due to less subsequent

reaction to CO and CO_2 compared to acidic supports such as Al_2O_3 and TiO_2 [10]. In our previous reports, the same Al_2O_3 support was used for the catalysts, hence there is a need to investigate the effect of different support species on dispersing Ni-Bi-O.

This manuscript tends to study the effect of support using Al_2O_3, SiO_2, ZrO_2 as shaped/calcined gel-type and un-calcined sol-type on the oxidative dehydrogenation of n-butane to butadiene. The important role of the supports was substantiated by testing the Ni-Bi-O metal oxide without a support. The states of nano-particle cohabitation with supports were examined by using equilibrium adsorption with or without enforced deposition by drying for the Ni-Bi-O impregnation. The catalytic performances with different supports were finally evaluated considering the textural characteristics with BET surface area, porosity, XRD, TEM, and TPR/TPD for redox and acid-base property.

3.2   Experimental

3.2.1 Catalyst Synthesis

The nano-sized porous Al_2O_3 with a pore diameter of 9.8 nm and a pore volume of 0.83 ml/g was prepared using a pH-controlled precipitation method [27-29]. For preparation, the boehmite precursors such as aluminum nitrate and sodium aluminate along with acid-base pair as precipitating reagents were used. The SiO_2 support was obtained from the market as CARIACT supplied by Fuji Silysia Chemical Ltd. The ZrO_2 support was prepared by calcination at 550 ^{o}C for 3 h from hydrated amorphous zirconia JRC-ZRO-2 with a surface area of 254 m^2/g as the Reference Catalyst supplied by Catalysis Society of Japan.

The Bi-Ni-O/support catalysts were prepared as standard (STD) samples by co-impregnation methods of equilibrium adsorption and enforced deposition. In order to clarify the state of metal oxide species, stopping impregnation at equilibrium adsorption (EQA) step was applied to prepare EQA catalysts. Nickel nitrate hexahydrate $Ni(NO_3)_2 \cdot 6H_2O$ (99 %, Fisher Scientific) was used as nickel source, while bismuth nitrate pentahydrate $Bi(NO_3)_3 \cdot 5H_2O$ (98 %, Fluka-Garantie) was used as bismuth source. For the preparation of 20 wt% Ni-30 wt% Bi-O/Al_2O_3 catalyst, 0.99 g of $Ni(NO_3)_2 \cdot 6H_2O$ was added to 80 ml of distilled water. After complete dissolution, 0.70 g of $Bi(NO_3)_3 \cdot 5H_2O$ was added and stirred. 1.0 g of dried support was added for impregnation and left overnight for aging. The sample was dried at 120 °C for 3 h and termed as-prepared catalyst. The EQA as-prepared catalysts were obtained by removal of the liquid part after aging before drying. The calcination of the as-prepared catalyst was done in two steps. In the first step, the temperature was raised to 350 °C at the rate of 10 °C/min and kept for 1 h. In the second step, the temperature was raised again at the rate of 15 °C/min to 590 °C and kept for 2 h for complete activation and stabilization.

3.2.2 Catalyst Characterization

The elemental analyses for equilibrium adsorbed Ni-Bi-O/support catalysts were obtained using the ICP instrument: ULTIMA 2 (HORIBA Scientific). The textural characteristics such as surface area and pore structure were analyzed on Micromeritics ASAP 2020 instrument (Norcross, GA), the pore surface area, pore volume, and pore diameter were measured using BJH adsorption method. X-ray diffraction of calcined samples was analyzed from (2θ) range of 5 ° to 80 ° using Rigaku Miniflex II desktop X-

ray diffractometer having Cu Kα radiation (wavelength λ=1.5406 Å) and 30 mA and 40 kV as operating parameters, a step size of 0.02° and a speed of 2 °/min.

The catalyst morphologies were analyzed using a high-resolution transmission electron microscope (HRTEM-model JEM-2100F) with an acceleration voltage of 200 kV. The redox character and acid-base property were analyzed using Temperature programmed reduction (TPR) and temperature programmed desorption (TPD) using BEL-CAT-A-200 chemisorption instrument. It is made up of a quartz sample holder having a furnace (suitable for high temperature), a mass spectrometer and a thermal conductivity detector (TCD). Injection of gas pulses with standard volume in helium background flow establishes the linearity of the TCD response. The redox property measurement was done using a gas mixture of Ar/H_2 (95/5 vol%) having a total flow rate of 50 cm^3/min. 100 mg of the calcined catalyst was preheated for 3 h at 300 °C in inert He after which it is cooled to room temperature. It was then heated at the rate of 20 °C/min up to 900 °C. H_2 intake was recorded with a TCD and CuO was used as a reference for calibrating the consumption of H_2. Ammonia and carbon dioxide temperature programmed desorption (NH_3 and CO_2 TPD) were carried out using the same equipment (BELCAT system) for acidity and basicity measurements respectively. 100 mg of the calcined catalyst sample was pretreated for 1 h at 500 °C using inert He (50 ml/min). It was then exposed to He/NH_3 mixture (He/CO_2 mixture for CO_2 TPD) in a volume ratio of 95/5 vol% for 30 mins at 100 °C. Gaseous NH_3 (CO_2) was removed by purging using He for 1 h and then TPD was performed using the same flow of He at a rate of 10 °C/min up to 600 °C and the desorbed gas (NH_3 or CO_2) was monitored using mass spectroscopy or TCD detector.

3.2.3 Catalyst Testing

The oxidative dehydrogenation reaction was carried out in an automated fixed bed reactor purchased from BELCAT, Japan. The as-synthesized catalyst (300 mg) was loaded into the reactor and calcined under air atmosphere. After calcination, the reaction started under a nitrogen atmosphere. The feed n-butane contact time was maintained at 0.42 h · g/mol. The total feed flow rate was maintained at 31.2 ml/min. The effect of three different temperatures (400, 450 and 500 ^{o}C) and various oxygen to n-butane ratio molar ratio (O_2/n-C_4H_{10} = 1.0, 2.0 and 4.0 mol/mol) were investigated. The products were analyzed through an online GC system, (Agilent, 7890N). The hydrocarbons and oxygenates were analyzed using FID and GC-Gas Pro capillary column (L: 60 m and ID: 0.32 mm), while gases, N_2, O_2, CO and CO_2, and H_2, respectively were detected using TCD and Shin Carbon 80/100 mesh SS column (He carrier) and MS5A 60/80 mesh SS column (Ar carrier). The products were confirmed by comparing with standard samples. The n-butane conversion, products selectivity were measured using the balance of carbon. As O_2 conversion is very important for selectivity in this experiment (n-butane oxidative dehydrogenation), it was also measured.

3.3   Results and Discussion

3.3.1 Catalyst Testing

3.3.1.1 Effect of support and the species

The effects of support and the species on the activity (n-butane conversion) and the selectivity in the standard (set up in our previous report [24]) reaction condition: 450 ^{o}C, O_2/n-C_4H_{10} = 2.0 are shown in Table 3.1. The O_2 conversion measured is also shown in

Table 3.1. The dehydrogenation products (DH: 1-butene, t-2-butene, cis-2-butene, and 1,3-butadiene; BD: 1,3-butadiene), oxygenate and cracked products (OC: carboxylic acids, C_2H_4, C_3H_6 and CO_2) and partial oxidation (PO: CO and H_2). The other gases CH_4, C_2H_6, and C_3H_8 were also detected in negligible quantities. All the supported catalyst showed superior performance compared to the unsupported catalyst (containing only metal species NiO and Bi_2O_3) and the selectivities to the various products depends on the type of support used. The related product route map from n-butane to butadiene with by-product formation is shown in Figure 3.1, corresponding to Table 3.1. The map in Figure 3.1 includes indirectly related reaction routes, DDH: direct dehydrogenation, and CB: combustion, out of broken line square.

Table 3.1 Comparison of catalytic performance for support species in Ni-Bi-O catalyst

Catalyst support	SiO$_2$	Al$_2$O$_3$	ZrO$_2$	none
n-C$_4$H$_{10}$ conversion [%]	17.6	24.0	23.7	4.8
(O$_2$ conversion)	(25)	(38)	(61)	(15)
Selectivity*[1] [C%] DH	79.1	75.1	48.5	31.5
2-C$_4$H$_8$	21.7	23.0	10.9	10.7
1-C$_4$H$_8$	25.5	15.7	17.5	17.7
BD	31.9	36.4	20.1	3.1
OC	17.5	23.7	51.5	64.7
PO	3.4	1.2	0.0	3.8
BD/DH %	40.4	48.5	41.5	9.8
(1-C$_4$H$_8$ + BD)/DH %*[2]	72.6	69.4	77.5	66.0
BD/(1-C$_4$H$_8$ + BD) %*[3]	55.6	69.8	53.5	14.9
BD yield	5.6	8.7	4.8	0.1

*[1] DH: dehydrogenation, BD: butadiene, OC: oxygenate and the cracked, PO: partial oxidation. *[2] selectivities at 1st step dehydrogenation, *[3] selectivities at 2nd step dehydrogenation

The butadiene selectivity for the catalyst support is in the order Al$_2$O$_3$ > SiO$_2$ > ZrO$_2$ >> none (only Ni-Bi-O), while n-butane conversion is Al$_2$O$_3$ = ZrO$_2$ > SiO$_2$ > none. For the main reaction selectivity, DH selectivity is SiO$_2$ > Al$_2$O$_3$ > ZrO$_2$ > none, and OC selectivity is reversely: none > ZrO$_2$ > Al$_2$O$_3$ > SiO$_2$ which clearly shows a trade-off relationship. PO selectivity is almost negligible in all the supports and it follows the order

as: none > SiO_2 > Al_2O_3 > ZrO_2. The Ni-Bi-O metal oxides without support (none) showed only very small activity (4.8 %) and negligible butadiene selectivity (3.1 C%) which clearly indicate that the effective catalytic performance in oxidative dehydrogenation reactions needs suitable support. Among the supports, 20wt% Ni 30wt% Bi on Al_2O_3 showed the highest butadiene selectivity (36.4 C%) at the highest n-butane conversion (24.0 %) followed by SiO_2 and ZrO_2. In particular, SiO_2 and Al_2O_3 support catalysts showed comparatively fewer tendencies toward large OC and PO selectivities. Contrarily ZrO_2 support catalyst has a strong tendency toward OC (51.5 C%) probably due to its interaction with Bi_2O_3 that generates more acidic sites.
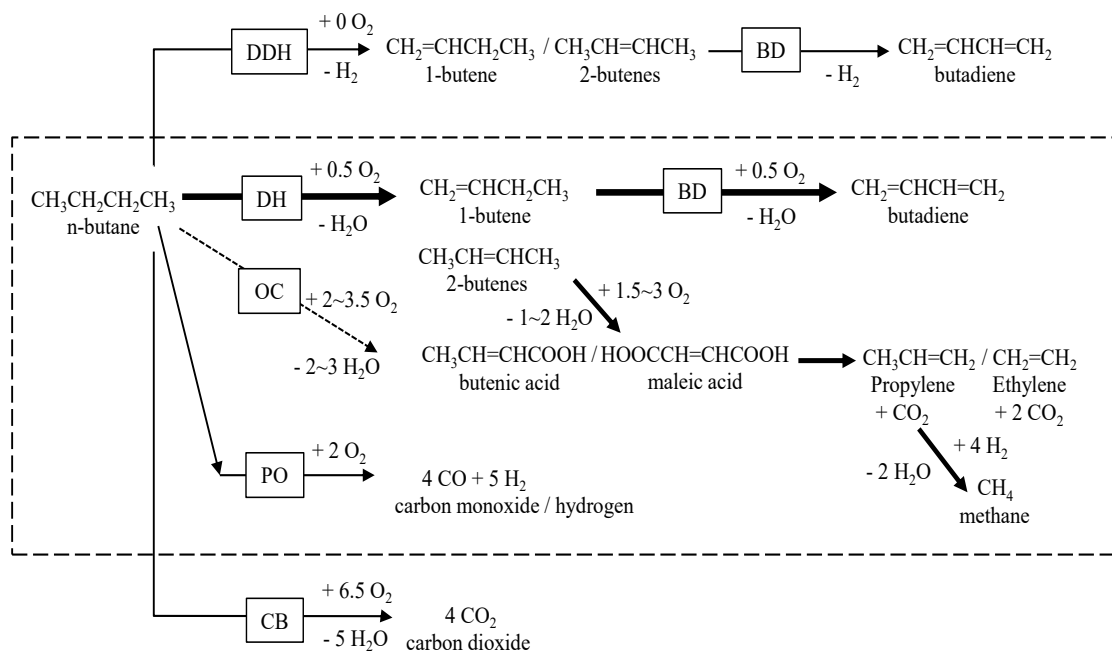
Figure 3.1 Route map from n-butane to butadiene including by-product formation

In Table 3.1, selectivity parameters for inside dehydrogenation from n-butane to butadiene through 1-butene intermediate are also shown as (1-C_4H_8 + BD)/DH: selectivity at 1st step dehydrogenation, BD/(1-C_4H_8 + BD): selectivity at 2nd step dehydrogenation, and BD/DH:

two- step total selectivity = [(1-C$_4$H$_8$ + BD)/DH] x [BD/(1-C$_4$H$_8$ + BD)], based on the concept for selective conversion from n-butane to butadiene as shown in Figure 3.1 from n-butane through 1-butene intermediate to butadiene. The values of the parameters in Table 3.1 shows that, for the support system, the values of the selectivity at 1st step dehydrogenation: (1-C$_4$H$_8$ + BD)/DH are similar, around 70 % even though for ZrO$_2$ support is close to 80 %, while the values of the selectivity at 2nd step dehydrogenation: BD/(1-C$_4$H$_8$ + BD) varied from 70 % to 15 % in the order of the support: Al$_2$O$_3$ > SiO$_2$ > ZrO$_2$ > none. Al$_2$O$_3$ shows the highest value of the two-step total selectivity: BD/DH (48.5 %). The strong point of Al$_2$O$_3$ support is that the catalyst showed high selectivity at both 1st and 2nd step dehydrogenation, which probably originates from the supporting state of NiO and Bi$_2$O$_3$ nano-particle cohabitation.

3.3.1.2 Equilibrium adsorbed metal oxide catalysts (EQA)

In order to further investigate and clarify the interaction effect of Bi$_2$O$_3$/support with a small amount of Ni species on the catalyst performance, equilibrium adsorption (EQA) catalysts and catalyst prepared under standard impregnation condition (STD) of EQA with enforced deposition were compared as presented in Table 3.2. The case of EQA catalyst contains only 20-25 % Ni and 70-90 % Bi compared to the amounts in the catalyst prepared with standard impregnation method respectively. This means the STD catalyst includes main Ni species almost on the Bi$_2$O$_3$ species dispersed over the support.

In the case of EQA NiO-Bi$_2$O$_3$ metal oxide over Al$_2$O$_3$ catalyst, the result shows that less amount but highly dispersed NiO species exist which are very active for oxygenate production. The presence of Bi$_2$O$_3$ as oxygen supplier with highly dispersed Ni species work to activate the active site for oxygenate production which consequently reduces the

dehydrogenation selectivity of the catalyst. The addition of NiO species in the 2nd layer for the case of standard impregnation suppressed the OC production. In the case of ZrO_2 support, a reverse trend was observed. The equilibrium adsorption catalyst showed high dehydrogenation and butadiene selectivity. The fact suggests that the active species for OC formation are made from excessively impregnated Ni on highly dispersed Bi_2O_3 over ZrO_2 support due to Bi species affinity against the support. However, in the case of EQA Ni-Bi-O/SiO_2, the oxygenate formation remains similar, which indicates the very less adsorption capability of the oxygen species on the Ni species over SiO_2 support and also a low metal supporting capacity compared to Al_2O_3 support.

Table 3.2 Comparison of EQA supporting step catalysts in Ni-Bi-O/support catalysts

Catalyst support	SiO$_2$	Al$_2$O$_3$	ZrO$_2$
Step	EQA (STD)	EQA (STD)	EQA (STD)
Ni/Bi wt%	4/22 (20/30)	5/24 (20/30)	4/27 (20/30)
n-C$_4$H$_{10}$ conversion [%]	14.1 (17.6)	29.1 (24.0)	29.4 (23.7)
O$_2$ conversion	19 (25)	66 (38)	63 (61)
Selectivity*[1] [C%]			
DH	79.7 (79.1)	56.9 (75.1)	61.5 (48.5)
2-C$_4$H$_8$	24.6 (21.7)	20.8 (23.0)	13.9 (10.9)
1-C$_4$H$_8$	31.7 (25.5)	10.6 (15.7)	10.9 (17.5)
BD	23.4 (31.9)	25.5 (36.4)	36.7 (20.1)
OC	17.5 (17.5)	40.2 (23.7)	38.3 (51.5)
PO	2.8 (3.4)	3.0 (1.2)	0.2 (0.0)
BD/DH %	29.4 (40.4)	44.8 (48.5)	59.7 (41.5)
(1-C$_4$H$_8$ + BD)/DH %*[2]	69.1 (72.6)	63.4 (69.4)	77.4 (77.5)
BD/(1-C$_4$H$_8$ + BD) %*[3]	42.5 (55.6)	70.6 (69.8)	77.1 (53.5)
BD yield	3.3 (5.6)	7.4 (8.7)	10.8 (4.8)

*[1] DH: dehydrogenation, BD: butadiene, OC: oxygenate and the cracked, PO: partial oxidation.
*[2] selectivities at 1st step dehydrogenation, *[3] selectivities at 2nd step dehydrogenation

Comparing the EQA and STD catalysts for the different supports, for the case of Al$_2$O$_3$, it showed that more NiO amount is required for DH (BD) selective catalyst with suppressed OC selectivity. This is possibly because, the acidic support interacts with the metal oxide species having the required basic character to moderate the acidic/basic

property of the resulting catalyst. This is required for hydrogen abstraction and 1-butene intermediate adsorption. Low amount of NiO in the 1st layer with high concentration of bismuth oxide species has active oxygen species that increases OC formation. Conversely, EQA ZrO_2 supported catalyst has basic sites as well as acidic sites leading to high DH (BD) selectivity and high OC selectivity. While such basic character is covered by enforced deposition and subsequently making it less basic, activity and BD selectivity wise, ZrO_2 is good as catalyst support but the oxygenate product is too high. Both ZrO_2 and Bi_2O_3 are typical basic oxides. The mixture of basic oxides sometimes shows acidity. Bi^{3+} in Zr^{4+}-O-Zr^{4+} network may generate acid site due to valency unbalance like in zeolite network. The interaction of ZrO_2 and Bi_2O_3 is considered strong enough to generate acid sites. Based on this, a mixture of NiO and Bi_2O_3 may show suppressed basicity of Bi_2O_3. This fact also buttresses the importance of basic character in DH. SiO_2 has weak adsorption and dispersion strength and hence it catalyst showed similar DH and OC selectivities for both EQA and STD catalysts. Even though conversion and BD selectivity increase for the STD catalyst probably due to the increase in 1-butene intermediate adsorption as well as basic sites that activates terminal methyl group, as can be observed in the decrease of 1-butene selectivity value from 31.7 C% to 25.5 C% for EQA and STD catalysts respectively.

3.3.1.3 Support effect on 1-butene feedstock reaction

In order to confirm the 2nd step reaction selectivity dependence on the supports, 1-butene was used as a feedstock and the result at standard reaction condition is shown in Table 3.3.

Table 3.3 Comparison of support species using 1-butene as feedstock in Ni-Bi-O catalyst

Catalyst support	SiO$_2$	Al$_2$O$_3$	ZrO$_2$
Feedstock	1-C$_4$H$_8$$^=$ (n-C$_4$H$_{10}$)	1-C$_4$H$_8$$^=$ (n-C$_4$H$_{10}$)	1-C$_4$H$_8$$^=$ (n-C$_4$H$_{10}$)
1-C$_4$H$_8$$^=$ (n-C$_4$H$_{10}$) conv	46.8 (17.6)	74.3 (24.0)	53.6 (23.7)
Selectivity [C%]			
BD	78.3 (31.9)	41.3 (36.4)	48.0 (20.1)
2-C$_4$H$_8$$^=$	18.1 (25.5)	52.1 (15.7)	49.1 (17.5)
DH$^+$	96.4 (79.1)	93.4 (75.1)	97.1 (48.5)
OC	1.2 (17.5)	4.3 (23.7)	2.6 (51.5)
PO	2.4 (3.4)	2.3 (1.2)	0.3 (0.0)
BD/DH$^+$	81.2 (40.4)	44.2 (48.5)	49.4 (41.5)
BD yield	36.7 (5.6)	30.6 (8.7)	25.7 (4.8)

*[1] DH$^+$: dehydrogenation and isomerization, BD: butadiene, OC: oxygenate and the cracked, PO: partial oxidation. *[2] selectivities at 1st step dehydrogenation, *[3] selectivities at 2nd step dehydrogenation

The case of n-butane feedstock comparison among the supports has already been discussed in Table 3.1. But comparing with 1-butene feedstock, all the supports showed superior performance because of the ease of activation and abstraction of the terminal H atom. Even though there is isomerization to 2-butenes, which are mostly desorbed into the gas phase without being converted into oxygenate and cracking (large OC) products especially for Al$_2$O$_3$ and ZrO$_2$ supports. Among the supports, using 1-butene feedstock, the conversion is in the order: Al$_2$O$_3$ > ZrO$_2$ > SiO$_2$ because it combines both dehydrogenation and isomerization degree (which is high among Al$_2$O$_3$ and ZrO$_2$) while SiO$_2$ has the least 2-butenes and hence OC selectivity. SiO$_2$ support showed a very high BD selectivity (78.3 C%) which is an indication of its superiority toward terminal methyl

H-abstraction (beta-position). The interaction of Bi_2O_3 with Al_2O_3 and ZrO_2 generates more strong acidic sites that facilitate the isomerization to 2-butenes with a resulting decrease in BD selectivity. SiO_2 support maintains the relatively weak acid sites and strong/moderate basic sites even after the metal oxide species impregnation.

3.3.1.3 Sol-derived support catalyst

In order to further utilize the superiority of SiO_2 support especially in terms of DH selectivity and to further investigate the possibility of improving its conversion, different type supports (sol-type) for Al_2O_3, ZrO_2 and SiO_2 were tested comparing with standard type supports (gel-type) studied above. The main aim is to enhance the dispersion of catalyst species as the sol-type supports present no restriction in terms of pore volume dispersing ability. The result is presented in Table 3.4.

Table 3.4 Comparison of sol-type supports in Ni-Bi-O/support catalysts

Catalyst support	SiO$_2$	Al$_2$O$_3$	ZrO$_2$
Support type	Sol (gel)	Sol (gel)	Sol (gel)
n-C$_4$H$_{10}$ conversion [%]	35.6 (17.6)	16.9 (24.0)	18.3 (23.7)
O$_2$ conversion	54 (25)	24 (38)	59 (61)
Selectivity*[1] [C%]			
DH	78.3 (79.1)	80.2 (75.1)	29.9 (48.5)
2-C$_4$H$_8$	18.6 (21.7)	27.2 (23.0)	8.4 (10.9)
1-C$_4$H$_8$	18.1 (25.5)	16.9 (15.7)	15.2 (17.5)
BD	41.6 (31.9)	36.1 (36.4)	6.3 (20.1)
OC	20.5 (17.5)	14.7 (23.7)	70.1 (51.5)
PO	1.1 (3.4)	5.0 (1.2)	0.0 (0.0)
BD/DH %	53.1 (40.4)	45.0 (48.5)	21.2 (41.5)
(1-C$_4$H$_8$ + BD)/DH %*[2]	76.2 (72.6)	66.1 (69.4)	72.0 (77.5)
BD/(1-C$_4$H$_8$ + BD) %*[3]	69.7 (55.6)	68.1 (69.8)	29.4 (53.5)
BD yield [C%]	14.8 (5.6)	6.1 (8.7)	1.2 (4.8)

*[1] DH: dehydrogenation, BD: butadiene, OC: oxygenate and the cracked, PO: partial oxidation. *[2] selectivities at 1st step dehydrogenation, *[3] selectivities at 2nd step dehydrogenation

For the Al$_2$O$_3$ supported catalysts, the gel type showed superior performance compared to the sol type in terms of conversion, the DH and OC shows trade-off relationship with the sol type slightly better in DH and also low OC which probably is due to its low interaction with Bi$_2$O$_3$ that reduces the acid sites generation but showed same

BD selectivity. ZrO_2 support case shows a complete negative trend in terms of both conversion and DH (BD) selectivity with a very high OC selectivity. This can be due to the fact that Bi_2O_3 interaction with the ZrO_2 sol allows for high oxygen concentration at the catalyst surface suitable for oxygenate and cracked products formation due to strong adsorption and this is similar to the case of equilibrium adsorbed catalyst discussed above. SiO_2 sol type support showed a very interesting performance as it improves both n-butane conversion from 17.6 % to 35.6 % and also BD selectivity from 31.9 C% to 41.6 C% thereby greatly improving BD yield almost 3 times from 5.6 C% to 14.8 C%. This is probably due to the high dispersion of silica sol in the active metal species, the maintenance of the Bi_2O_3/SiO_2 connection and also the presence of controlled acid and basic sites suitable for high DH (BD) selectivity.

3.3.2 Catalyst Characterization

3.3.2.1 Surface area and pore structure

The properties of the catalyst were analyzed using various physicochemical techniques. The main aim is to determine the nature of active sites and their interaction/dispersion with different supports. In the case of Al_2O_3 support, the fractal surface is important for cohabitating both Ni and Bi species [24,25]. The BET surface area and pore structure including pore surface area, pore volume and average pore diameter of various supports Al_2O_3, SiO_2, ZrO_2 and none (without support) are presented in Table 3.5. The catalyst without support (none), showed the BET surface area of 16 m^2/g (25 m^2/g-support: equivalent to catalyst with support). All catalysts exhibited lower BET surface area based on catalyst weight compared with the supports. Pore surface area and pore volume based on catalyst weight also reduced similarly to BET surface area. Since all the

supports were impregnated with 20 wt% Ni and 30 wt% Bi, the comparison between

support and catalyst about before-and-after changes in the BET surface area and pore

structures (pore surface area, pore volume and pore diameter) was performed using the

values based on weight of support i.e. the support values are based on its weight, while

catalysts are based on the support part weight as shown in Table 3.5.

Table 3.5 Physical properties of catalysts and supports.

Catalyst: (Support)	BET surface area		Pore surface area		Pore volume		Average pore diameter
	$[m^2/g\text{-}catalyst]^a$	$[m^2/g\text{-}support]^b$	$[m^2/g\text{-}catalyst]^c$	$[m^2/g\text{-}support]^d$	$[cm^3/g\text{-}catalyst]^e$	$[cm^3/g\text{-}support]^f$	$[nm]^g$
SiO_2	147	233 (242)	156	248 (263)	0.66	1.05 (1.22)	16.9 (18.6)
Al_2O_3	166	263 (276)	193	306 (338)	0.51	0.81 (0.83)	10.6 (9.8)
ZrO_2	26	41 (54)	28	44 (63)	0.12	0.19 (0.16)	17.1 (10.2)
none	16	25	14	22	0.22	0.35	62.9
SiO_2 sol	91	144	87	138	0.64	1.02	29.1
Al_2O_3 sol	185	294	205	326	0.16	0.25	3.1
ZrO_2 sol	102	162	108	171	0.13	0.21	5.0

[a]BET surface area, [c,e,g]Surface area, pore volume, and average pore diameter measured using BJH isotherm, [b,d,f] Surface area and pore volume calculated to support weight base by using the equation: SA or PV×[Σ(MO$_x$/M)+100]/100, where M = metal wt%; MO$_x$= metal oxide wt%; SA = surface area; PV = pore volume.

The catalysts with Al_2O_3 support showed a well-known trend with high BET and pore surface area values of 263 and 306 m^2/g-Al_2O_3 compared to only Al_2O_3 support, 276 and 338 m^2/g respectively. The catalyst with SiO_2 support showed slightly lower values, 233 and 248 m^2/g-SiO_2 of BET and pore surface area relative to SiO_2 support 242 and 263 m^2/g, respectively. The Al_2O_3 catalyst also showed high pore volume values of 0.81 ml/g-Al_2O_3 equivalent to the support value of 0.83 ml/g while the SiO_2 catalyst gave a lesser pore volume of 1.05 ml/g-SiO_2 compared to the support value 1.22 ml/g.

The ZrO_2 catalyst showed a lower surface area than Al_2O_3 and SiO_2 catalysts. The values 41 and 44 m^2/g-ZrO_2 for BET and pore surface area also reduced relative to ZrO_2 support values of 54 and 63 m^2/g respectively. The catalysts without any support showed lower values of surface area compared to the other catalysts with support. Furthermore, the comparison among the different support species should be based on values corrected with specific gravity SiO_2: 2.2, Al_2O_3: 3.3 and ZrO_2: 5.7. After the correction, Al_2O_3 showed nearly 2 times of SiO_2 catalyst surface area and ZrO_2 showed nearly half of SiO_2 catalyst surface area and pore volume respectively, while Al_2O_3 showed 1.2 times of SiO_2 catalyst pore volume

The catalyst having silica sol as support showed decreased but still large values of BET and pore surface area compared to the silica gel-type support catalyst. On the contrary, an increased pore diameter was obtained due to a pore volume which is equivalent to the gel-type support catalyst. This probably suggests the dispersion of the silica sol in the active species thereby increasing the metal species-support interaction. The catalyst having Al_2O_3 sol and ZrO_2 sol as support showed increased and larger values of BET and pore surface area compared to the gel-types supports respectively.

The physical properties of catalysts shown in Table 3.5 are not enough to explain the catalytic performance, especially activity in terms of n-butane conversion. The catalytic performances depend not only on the physical properties but also on chemical characteristics.

3.3.2.2 X-ray Diffraction

The X-ray diffraction (XRD) pattern for catalysts of 20 wt% Ni-30 wt% Bi-O metal oxides over different supports, species: Al_2O_3, SiO_2, ZrO_2 and none (without support) is shown in Figure 3.2. The main diffraction peaks in Figures 3.2 and 3.3 were indicated by several marks and the 2 theta range was expanded for NiO peaks identification.
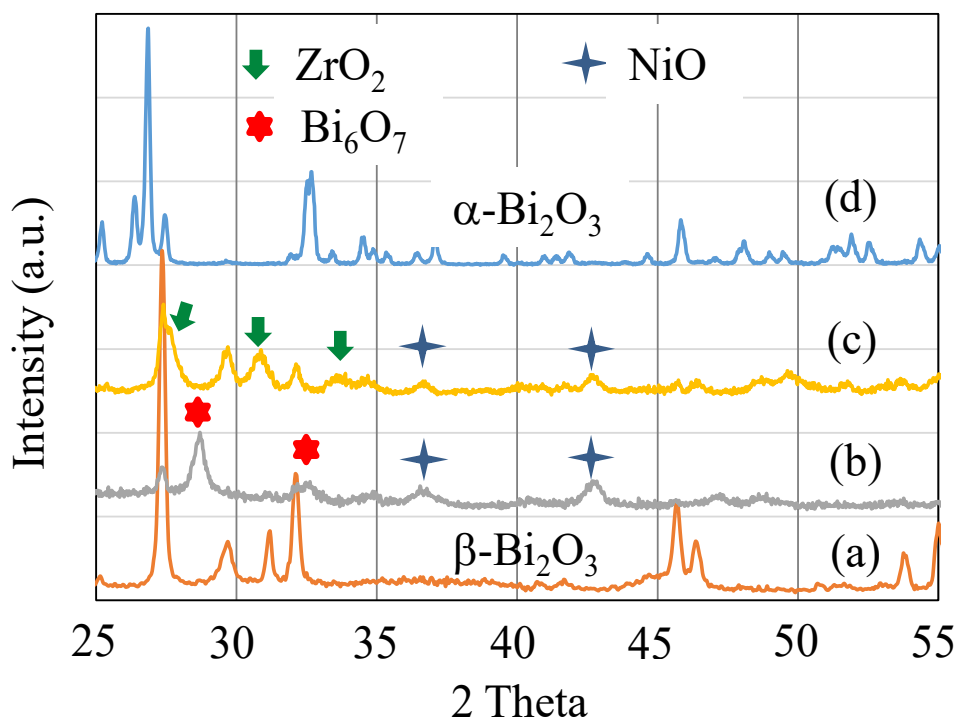
Figure 3.2 XRD patterns for catalysts of 20 wt% Ni-30 wt% Bi-O over different supports: (a) Al_2O_3 (b) SiO_2 (c) ZrO_2 and (d) none.

As reported in our previous work with Al_2O_3 supported catalyst [24], the NiO species were not detected by XRD for Al_2O_3 supported and non-supported catalysts. Therefore, the NiO species are expected to be as nanoparticles (less than 3 nm) or amorphous, which are below the detection limit of XRD. The XRD patterns of bismuth oxide over different supports show monoclinic alpha-Bi_2O_3, tetragonal beta-Bi_2O_3, Bi_6O_7 and amorphous (semi-crystalline) peaks. The crystallinity (determined by peak height) and crystal size (reverse of half-height width) of beta-Bi_2O_3 in the Al_2O_3 catalyst was significantly higher than the other catalysts. In our previous study [25], we showed that the Al_2O_3 catalysts contain partially Bi_2O_3 as alpha-phase, and the main phase as beta-phase with a main peak at $2\theta = 27.38°$ which is highly dispersed crystalline, and also active for butadiene formation. In the SiO_2 catalyst case, beta-Bi_2O_3 is not as clear crystalline but rather near the amorphous. Instead, another main peak around $2\theta = 28-29°$ which is a new phase of bismuth oxide was observed. NiO/Al_2O_3 and NiO/SiO_2 show XRD peaks of fine and large particles, 3 nm and 10 nm, respectively. The sizes of NiO particles in NiO/Al_2O_3 and NiO/SiO_2 were also confirmed with TEM. Though $NiO-Bi_2O_3/Al_2O_3$ catalyst did not show clear diffraction peaks of NiO, porosity showed fine particles formation as particle void after 2nd step deposition mainly consisting of NiO. $NiO-Bi_2O_3/SiO_2$ catalyst showed assignable diffraction peaks of 3 nm NiO fine particles. The formation of bismuth oxide Bi_6O_7 phase claimed in both of BiO_x/SiO_2 and $NiO-BiO_x/SiO_2$ catalyst was shown as an appearance of the new broad diffraction peak at narrower d spacing position instead of Bi_2O_3 main peak. XRD of SiO_2 supported catalyst shows no alpha-Bi_2O_3 hence the low selectivity to OC products. In the bismuth oxide structure, O_2 are stabilized to be less active for oxygenate production. Furthermore, the larger NiO with Bi_6O_7 phase in the SiO_2

catalyst is less active but highly selective for dehydrogenation. The ZrO_2 support catalyst showed more broadening and nearly amorphous, except ZrO_2 support peaks around $2\theta = 28$, 31 and 34° which agreed with the reported patterns [30]. NiO species are highly dispersed on probably alpha-Bi_2O_3 phase as nanoparticles, which are more active for oxygenate production. For the unsupported case, a highly crystalline alpha-Bi_2O_3 was observed around $2\theta = 27.1°$ and 32.9° which is less active and selective but does not show beta phase. NiO peaks were observed around $2\theta = 37°$ and 43° in the SiO_2 and ZrO_2 catalyst. These results clearly indicate that the metal oxides combination is not effective as independent large crystallites of both were observed and that also contributed to the low surface area. They do not form nano-consortium of metal oxides as well as mixed oxide interface [31] and hence their resulting less activity and selectivity to butadiene. This shows the importance of support for bismuth oxide phase building as well as mixed oxide interface to increase interaction among metal oxides. The activity and selectivity study shows that both Al_2O_3 and SiO_2 are able to stabilize Ni and Bi species as hierarchical cohabiting nanoparticles with highly dispersed bismuth oxide species as 2nd layer on the 1st layer of support and NiO dispersed as 3rd layer on bismuth oxide species with a high surface area. On the contrary, ZrO_2 has more strongly and highly dispersed Bi_2O_3 and NiO which caused large OC active species at the surface. A highly crystalline beta-Bi_2O_3 is dispersed on silica support similar to alumina support at the stage of EQA as shown in Figure 3.3 (a), the excess amount of bismuth oxide species and Ni impregnation at 2nd stage cooperate to ease the formation of Bi_6O_7 with fine NiO particles in the standard catalyst shown in Figure 3.3 (b).

XRD pattern of 20 wt% Ni-30 wt% Bi-O/silica sol catalyst is shown in Figure 3.3 represented as letter (c) compared with (b) the silica gel catalyst. The silica sol catalyst showed clear peaks with broad widths around $2\theta = 29$ and $32.5°$, 37 and $43°$ which are assigned to Bi_6O_7 phase and NiO, respectively. This nano-particle cohabitation of Bi_6O_7 and NiO was obtained mainly due to the less amount of beta-Bi_2O_3 satisfying the surface area of the sol-derived SiO_2 apart from the gel-type SiO_2. This cohabitation is also obtained as highly dispersed nanoparticles by sol-type SiO_2 nanoparticles preventing separated crystallization of alpha-Bi_2O_3 and NiO like the catalyst without support. The nanoparticles of this phase work either as active and selective sites or as active oxygen supplier for active 1st and 2nd step dehydrogenations thereby greatly enhancing activity and butadiene selectivity.
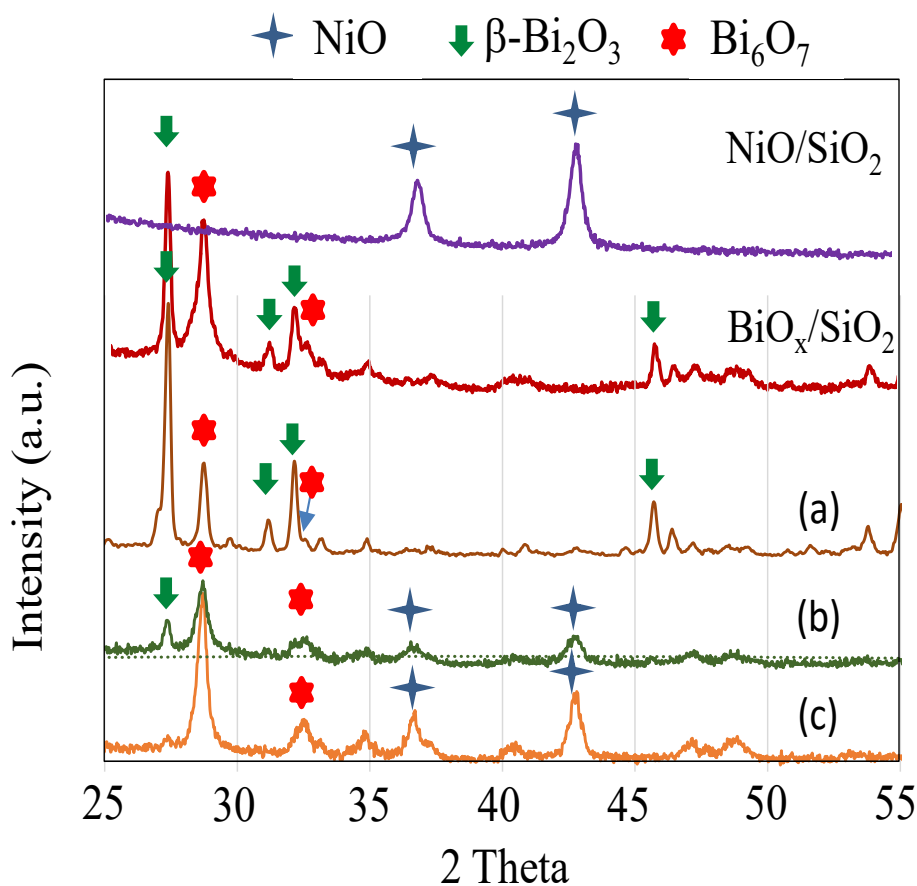
Figure 3.3 Comparison of X-ray diffraction pattern for supporting stage and support species in Ni-Bi-O catalyst (a) EQA SiO_2 gel (b) SiO_2 gel and (c) SiO_2 sol

3.3.2.3 TEM observation

The TEM images of 20 wt% Ni-30 wt% Bi-O metal oxides over different supports of Al_2O_3, SiO_2 and ZrO_2 are shown in Figure 3.4 a) - c). Detailed TEM observation for 20 wt% Ni-30 wt% Bi-O over Al_2O_3 have been explained in our previous report [25]. It clearly shows the hierarchical nanoparticle cohabitation of NiO at the upper layer (sub-nanometer), Bi_2O_3 (middle as ca. 10 nm) and Al_2O_3 at the ground level. The crystals of bismuth oxide over SiO_2 and ZrO_2 are too small to be observed by TEM. Preparation of reference samples NiO/SiO_2 and BiO_x/SiO_2 (apart from catalysts) followed by a

comparison of the XRD results proved that NiO-Bi_2O_3 solid solution does not exist. SiO_2 supported Bi_6O_7 (= $Bi_2O_{2.33}$) species similar to 2:1 mixed phase of Bi_2O_2 and Bi_2O_3 were assigned. NiO/Bi_2O_3 mixed oxide phase was not proved from Figure 3.4 (b) but suggested experimentally with HRTEM. Non-hierarchical amorphous particles consisting of ca. 10 nm NiO on fine (much less than NiO size) bismuth oxide nanoparticles were observed. In our previous paper for Al_2O_3 gel supported catalyst [24], a hierarchical nanoparticle cohabitation was clearly proved experimentally with HRTEM. Supporting the result with XRD measurement in this paper for the Al_2O_3 gel supported catalyst, the hierarchical structure was also shown using the preparation procedure including the stepwise depositions.
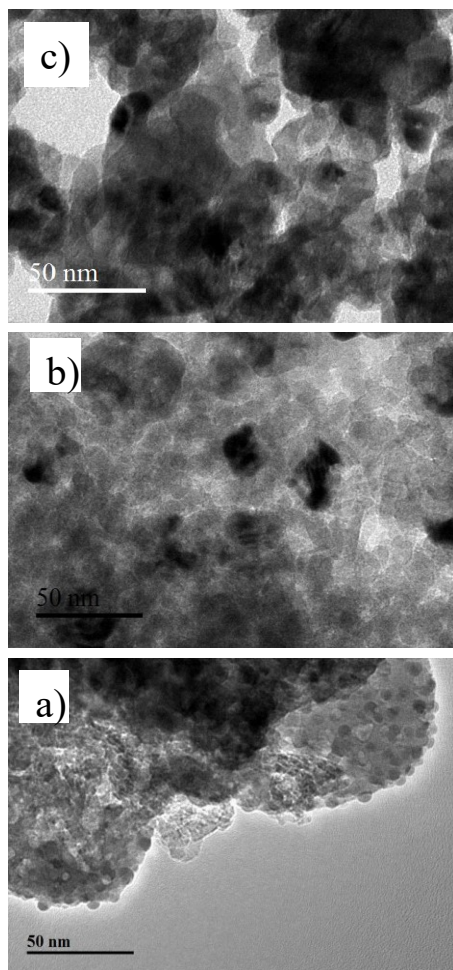
Figure 3.4 TEM image of 20 wt% Ni-30 wt% Bi-O/support: (a) Al_2O_3 (b) SiO_2 and (c) ZrO_2

3.3.2.4 Temperature programmed reduction

In oxidative dehydrogenation reactions, the redox character is an important factor considered for selective catalytic activity. Temperature programmed reduction (TPR) is used to measure the extent of reducibility of active species. Increased reducibility of active species accelerates the redox cycle thereby enhancing the catalyst activity. Figure 3.5 shows the H_2-TPR analyses of Ni-Bi-O supported on (a) Al_2O_3 (b) SiO_2 (c) ZrO_2 and (d) none (without support). TPR profiles of each single oxides of NiO/SiO_2 and BiO_x/SiO_2 as reference helped in better understanding to enforce the discussion on the TPR results shown

66

in Figure 3.5. NiO/Al_2O_3 and Bi_2O_3/Al_2O_3 were already shown in the previous paper [24]. Starting temperature of TPR is specific for each material and important for the material function, but peak temperature is more important as the catalyst and is dependent on redox catalysis, as shown in Figure 3.5. Since, TPR peak temperature is dependent on the mass of sample and reaction speed, TPR data was measured at the same condition, the same mass of the sample, the same H_2 flow rate and the same temperature programming. In this case, TPR data can be discussed not based on the starting temperature but on peak temperature with peak area after peak deconvolution (similar to NH_3-TPD). According to our previous study [25], Ni-Bi-O/Al_2O_3 showed two reduction peaks (500-650 ^oC) that are attributed to the reduction of NiO species, while the third reduction peak (700 ^oC) is ascribed to the reduction of Ni and Bi oxide species. The NiO species of such sample was reported to remain steady as an active one. The presence of such reduction peaks showed high selectivity to butadiene and low selectivity to oxygenate and cracked (OC) products.
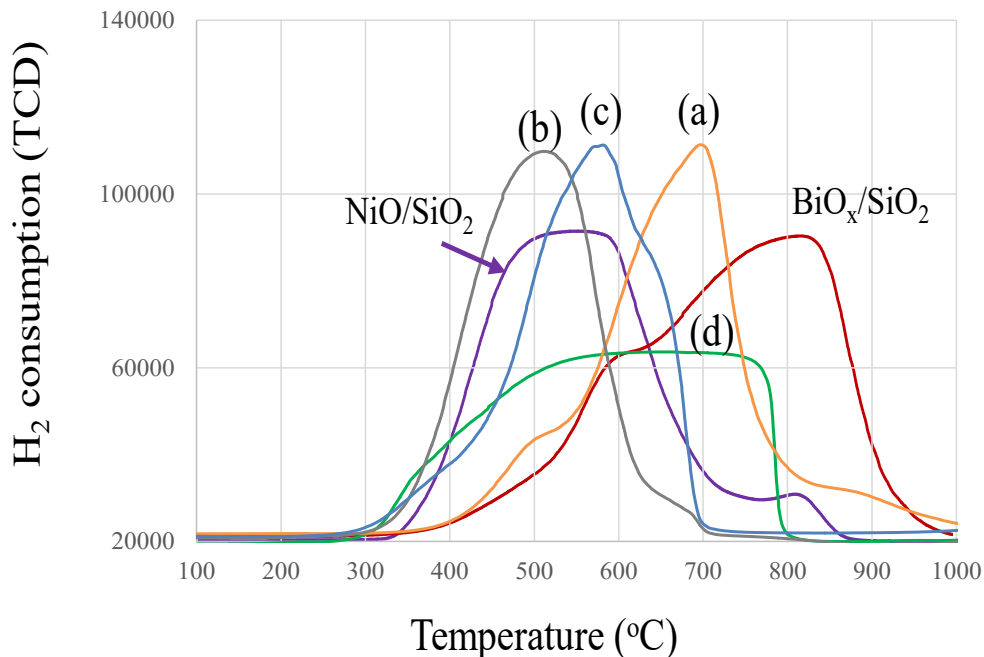
Figure 3.5 H$_2$-TPR study for catalysts of 20 wt% Ni-30 wt% Bi-O over different supports: (a) Al$_2$O$_3$ (b) SiO$_2$ (c) ZrO$_2$ and (d) none

The TPR profile of Ni-Bi-O supported on SiO$_2$ showed an intense reduction peak at 500 ºC larger than Al$_2$O$_3$ support and a small reduction peak from 625 ºC and extends up to 700 ºC. The particle size effect can be seen over SiO$_2$ support. The easy reduction of Ni-Bi-O metal oxide species at 500 ºC shows the presence of larger particle not firmly interacting with the support. These changes of reducibility over SiO$_2$ is considered to relate to the different state of NiO and Bi$_2$O$_3$ coordination between each other and the support. This low reduction temperature of SiO$_2$ is suitable for high BD selectivity. In order to simplify for discussion, the TPR profiles were divided into three regions: i) easily reducible (350-550ºC) ii) moderately reducible (550-650ºC) and iii) difficult reducible (650-850ºC) with the total as shown in Table 3.6.

The case of silica sol is also similar to the gel-type silica even though the H_2 consumption slightly increases as presented in Table 3.6. The shifting of reduction peak to higher temperatures clearly shows the formation of smaller particle of Bi_2O_3 interacting strongly with support. In the case of Al_2O_3 support, the maximum consumption of H_2 occurs at 700 ºC, indicating the presence of less reducible species. In the case of Ni-Bi-O supported on ZrO_2, a shift in the reduction towards high temperatures occurs. The onset of reduction starts at 350 ºC and second reduction peak maximum at 570 ºC, while third reduction peak starts at 625 ºC and extends up to 700 ºC. Compared to Al_2O_3, the reduction peak at 575 ºC for ZrO_2 is ascribed to the reduction of Ni and Bi species strongly coordinated each other over the support. This peak at 575 ºC plays a big role in ZrO_2 support for more formation of high oxygenate and cracking products. The H_2-TPR profile of unsupported bulk Ni-Bi-O metal oxides showed a broad reduction from 300-800 ºC. The reducibility of the bulk metal oxides showed early onset of reduction from 300 ºC and extends up to 800 ºC.

Table 3.6 H$_2$ consumption in TPR of 20 wt% Ni-30 wt% Bi-O/support catalysts.

Catalyst support	TPR H$_2$ consumption [m mol/g]			
Reduction temperature range	I (350-550 ºC)	II (550-650 ºC)	III (650-850 ºC)	total
SiO$_2$	3.74	1.12	0.13	4.99
(SiO$_2$ sol)	(3.75)	(1.10)	(0.38)	(5.23)
Al$_2$O$_3$	0.77	1.50	2.63	4.90
ZrO$_2$	2.65	2.61	0.66	5.92
none	1.47	1.00	1.31	3.78

The relationship between butadiene selectivity BD and OC (oxygenate and cracked) selectivity in ODH is shown in Figure 3.6. The oxygen mobility as monitored by H$_2$ reduction from TPR shows that butadiene selectivity is nearly inversely proportional to OC production. The butadiene shows valley type relation over four different supports and volcano type for large OC production with TPR peak temperature. Among the supports, the Ni and Bi species on ZrO$_2$ are highly dispersed and works for high oxygenate formation. The metal oxide site increased to activate oxygen species at the surface for oxygenate formation. This is unlike Al$_2$O$_3$ support where the nanoparticle sizes were observed as rather largely uniform and rigidly placed from TPR reduction profile and TEM analysis. In the case of SiO$_2$, the Ni-Bi-O species as seen from TPR are easily reducible and rather free from support in spite of the high porous character as seen from BET analysis. The species are preferable to butadiene selectivity. In SiO$_2$ case, the metal species are weakly dispersed

and hence do not activate oxygen species for oxygenate formation at the reaction condition. Even though, the species are easily reduced with SiO_2 (both gel and sol-type) case and difficult to reduce in Al_2O_3, both produce high selectivity to butadiene with suppressed oxygenate formation. Decisively, for selective butadiene formation, feed n-butane and intermediate butene reduce NiO species, which is re-oxidized by gas phase oxygen without supplying oxygen species for oxygenate formation.
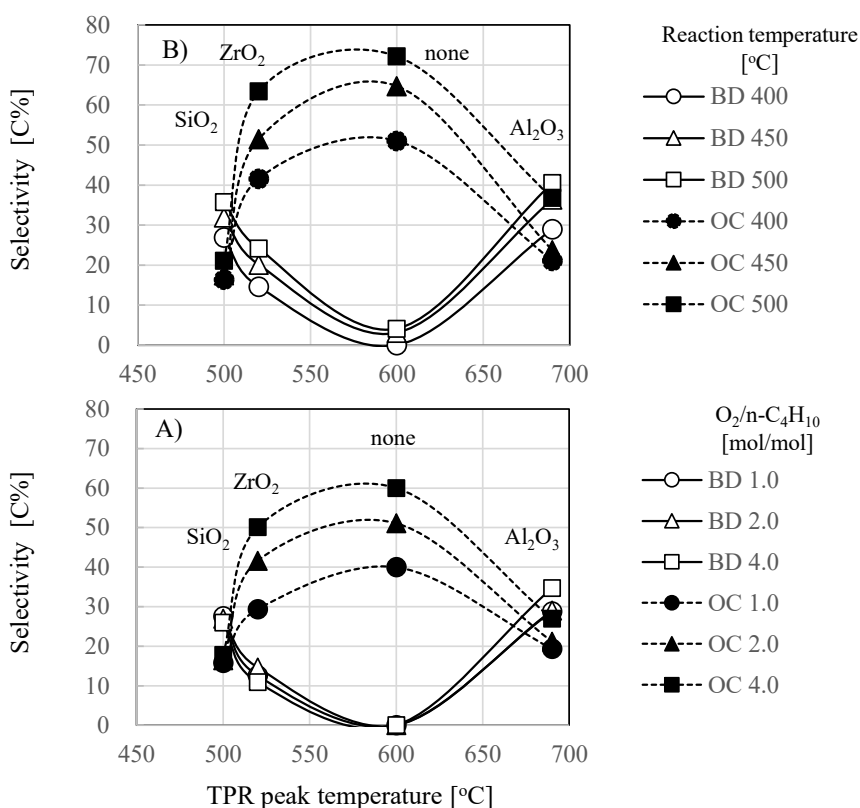
Figure 3.6 Correlation between TPR peak position and reaction selectivity: BD and OC, parameter: A) O_2/n-C_4H_{10}, B) reaction temperature.

The dependency on nickel redox system is further substantiated by measuring the spent catalyst. In DH, there was no carbon deposition observed, while a large amount of coke

formation occurred in the absence of oxygen. This shows that, in the absence of oxygen, the redox cycle is not effective and leads to excessive coke formation.

3.3.2.4 Temperature programmed desorption (CO_2/NH_3)

The basicity and acidity of the catalysts were measured using CO_2- and NH_3-temperature programmed desorption technique (CO_2- and NH_3-TPD) respectively. The results for catalysts of 20 wt% Ni-30 wt% Bi-O metal oxides over different supports, species: Al_2O_3, SiO_2 (gel and sol type), ZrO_2 and none (without support) are shown in Table 3.7. CO_2-TPD profiles are decomposed into three peaks centered at ca. 170 ^{o}C, ca. 300 ^{o}C and ca. 400 ^{o}C, named as I, II and III with referring to weak base, moderate base, and strong base, respectively. Similarly, NH_3-TPD profiles were decomposed into three peaks in the range of 100-250 ^{o}C, 250-400 ^{o}C and 400 ^{o}C <. The three peaks are named as I, II and III corresponding to weak acid, moderate acid, and strong acid sites, respectively.

Among the support species, all the four catalysts showed both basic and acidic sites. The basic sites are required for terminal H abstraction from n-butane and 1-butene intermediate while the acidic sites are necessary for 1-butene intermediate adsorption. The quantitative orders of total basicity is: Al_2O_3 > ZrO_2 > SiO_2 > none, and acidity for both total, weak and moderate is: Al_2O_3 > SiO_2 > ZrO_2 > none. The balance of acidity to basicity (ratio of acidic to basic sites) is in the order: SiO_2 > Al_2O_3 > ZrO_2 > none. This order is the same as DH selectivity and reverse of OC selectivity. Consideration of TPR peak temperature also revealed that butadiene selectivity had a reverse trend of OC selectivity.

Table 3.7 Temperature programmed desorption analysis (CO_2- and NH_3-TPD) of 20 wt% Ni-30 wt% Bi-O/support catalysts.

Catalyst (support)	Base amount with CO_2-TPD [mmol/g]*1				Acid amount with NH_3-TPD [mmol/g]*2			
	I	II	III	Total	I	II	III	Total
SiO_2 (SiO_2 sol)	0.031 (0.012)	0.002 (0.010)	- (0.010)	0.033 (0.032)	0.039 (0.049)	0.014 (0.013)	0.001 (-)	0.054 (0.062)
Al_2O_3	0.073	-	0.173	0.246	0.115	0.169	0.097	0.381
ZrO_2	0.027	0.039	-	0.066	0.018	0.011	0.005	0.034
none	0.019	0.01	-	0.020	0.002	-	-	0.002

*1: I (170°C peak): weak base, II (300°C peak): moderate base, III (400°C peak): strong base
*2: I (100-250°C): weak acid, II (250-400°C): moderate acid, III (>400°C): strong acid

Therefore, for all the data in Table 3.7, total basicity/total acidity ratio was calculated to be related to A) butadiene and OC selectivity; B) 1st step, 2nd step and total dehydrogenation inside. As shown in Figure 3.7, the result suggests that butadiene and OC selectivity positively and negatively depends on the total basicity/total acidity ratio respectively. The total basicity/total acidity ratio effect on the selectivity of dehydrogenation inside is slightly negative against 1st step dehydrogenation which is strongly positive while 2nd step dehydrogenation is almost neutral at high value. Although excess acidity disturbs 1-butene production on basic site at the 1st step, the acidity reversely works as promoter to accelerate the 2nd step, where weak acidic sites combine with strong/moderate basic sites for selective dehydrogenation of 1-butene to butadiene. The role of weak acid site is to adsorb basic 1-butene intermediate to proceed to the next dehydrogenation step without desorbing from

the catalyst surface to the gas phase. Therefore, the role of the support for controlling the balance of acidity and basicity is important for selective butadiene production.
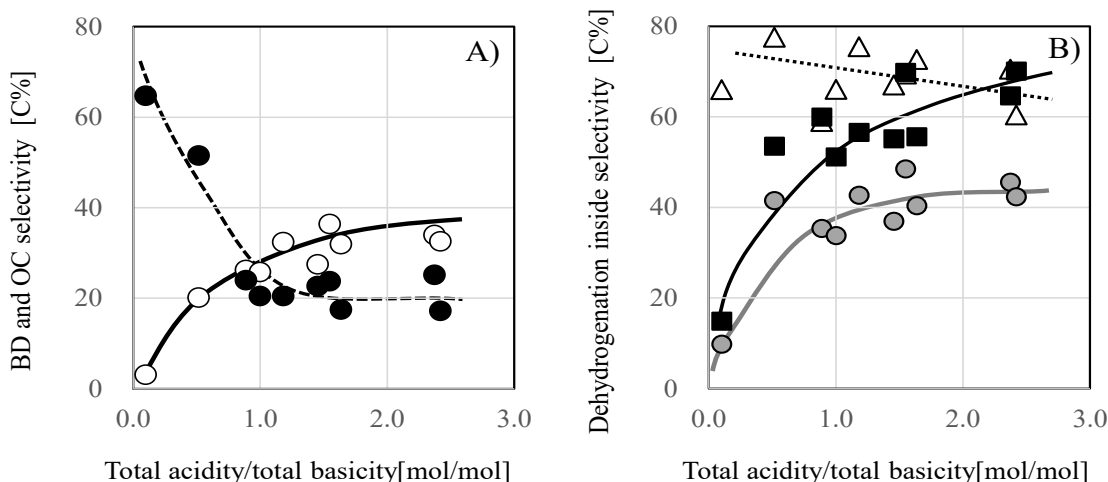
Figure 3.7 Correlation between total acidity/total basicity and selectivity: A) ○: BD and ●: OC, B) Δ: 1st step, ■: 2nd step and gray○: total dehydrogenation inside.

3.3.3   Schematic Reaction Mechanism

The mechanistic route in the ODH reaction is derived either by redox ability or by the acid-base nature of the catalyst and the reactants (n-butane, and oxidant). In the preceding discussions, the butadiene selectivity was shown to depend on the selective dehydrogenation to 1-butene. It is known that the basic character of catalyst withdraws hydrogen atoms as a proton. In our case, this occurs at the alpha-methyl carbon of n-butane. Reversely, hydrogen as hydride is selectively withdrawn by the acid catalyst from beta-methylene carbon of n-butane. The butenes (intermediate products) are basic in nature because of the double bonds, while butadiene is less basic compared to butenes due to conjugation. The catalyst for selective butadiene production from dehydrogenated basic

74

compounds should possess an adequate acidic character for olefin adsorption with basic sites for selective proton withdrawing.

Therefore, Figure 3.8 is a proposed schematic reaction mechanism with catalyst active sites for DH of n-butane selective to butadiene over Ni-Bi oxide/support catalyst.

a) Base catalyst with moderate acid (Ni-Bi-O/Al$_2$O$_3$ catalyst)

$CH_3-CH_2-CH_2-CH_3$ → $C^{-*}H_2-CH_2-CH_2-CH_3$ → $C^{-*}H_2-C^{+*}H-CH_2-CH_3$ → $CH_2=CH-CH_2-CH_3$

$B^{\delta-*}- A^{\delta+*}$ H^+-B^{-*} A^{+*} H^+-B^{-*} $A^{+*}-H^-$ $B^{\delta-*}$ $A^{\delta+*}$

$CH_2=CH-CH=CH_2$

→ $CH_2=CH-CH_2-CH_3$ → $CH_2=CH-CH_2-C^{+*}H_2$ → $CH_2=CH-C^{-*}H-C^{+*}H_2$ ↗

$A^{\delta+*}$ $B^{\delta-*}$ $A^{\delta+*}$ $B^{-*}-H^+$ H^--A^{+*} $B^{-*}-H^+$ $A^{\delta+*}$ $B^{\delta-*}$

b) Acid catalyst

$CH_3-CH=CH-CH_3$

$CH_3-CH_2-CH_2-CH_3$ → $CH_3-C^{+*}H-CH_2-CH_3$ → $CH_3-C^{+*}H-C^{-*}H-CH_3$ ↗

A^{+*} B^{-*} H^--A^{+*} B^{-*} H^--A^{+*} $B^{-*}-H^+$ A^{+*} B^{-*}

$CH_3-CH=CH-CH_3$

$CH_2=CH-CH_2-CH_3$ → $CH_2=CH=CH-CH_3$ ↗

A^{+*} B^{-*} H^--A^{+*} B^{-*} A^{+*} B^{-*}
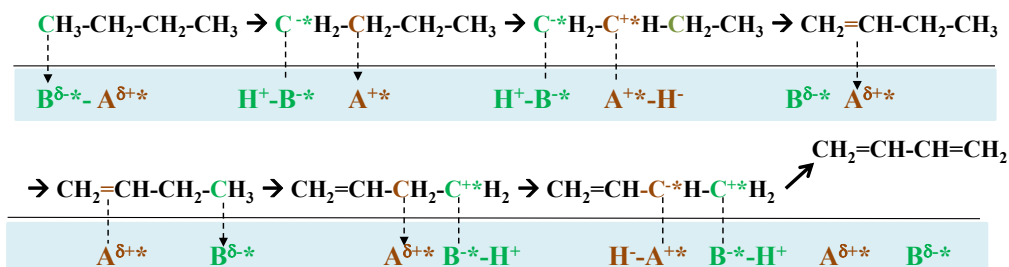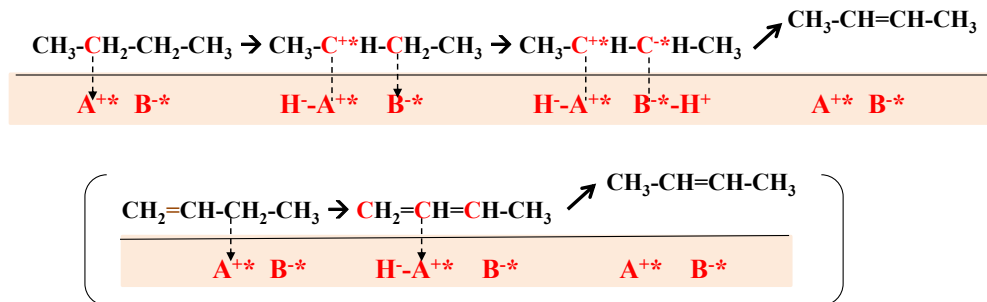
Figure 3.8 Schematic reaction mechanism and catalyst active sites for DH of n-butane selective to butadiene over Ni-Bi-O/support catalysts.

Figure 3.9 is a summarized schematic presentation of reaction over Ni-Bi-O/supports; Al$_2$O$_3$, SiO$_2$ and ZrO$_2$ catalysts with the viewpoint of a support role in butadiene ($C_4^{2=}$) selectivity from n-butane (C_4^0) over hierarchical nano-particle cohabitation catalysts. For the gel and sol-type SiO$_2$ support comparison, Figure 3.10

showed how the different support types interact with the active metal oxide species before and after calcination and the resulting performance (BD selectivity) obtained. The SiO_2 gel type (pellet shape) has a layer of less dispersed NiO over beta-Bi_2O_3 with Bi_6O_7. Because the gel type support is rigidly connected to each other (fixed pore structure), the bismuth oxides/SiO_2 connection is hard to be rearranged. In the sol type, even though there is strong dispersion of Bi_6O_7, the sol particles can be reversely and actively dispersed into the metal species as a non-hierarchical nanoparticle cohabitation hence high metal oxide-support interaction.
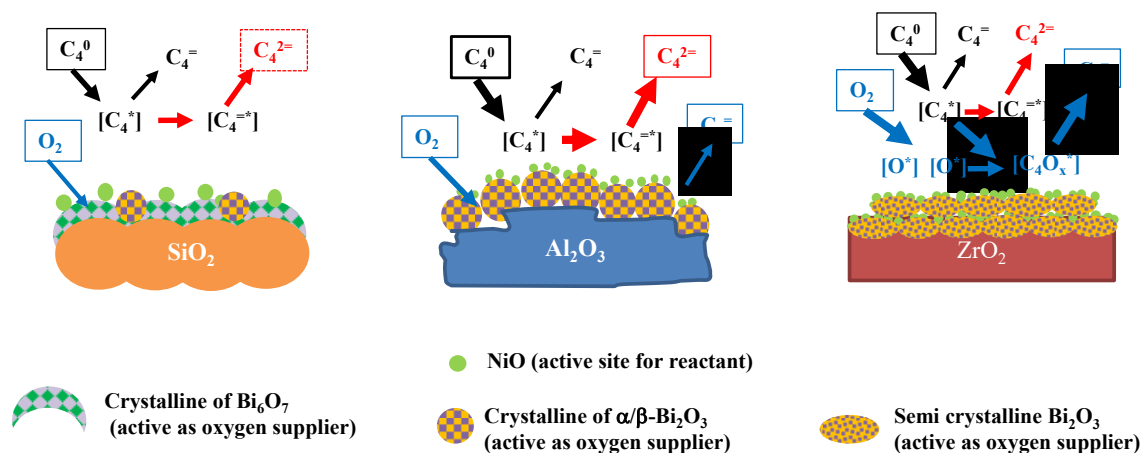
Figure 3.9 Schematic representation of DH over different supports.
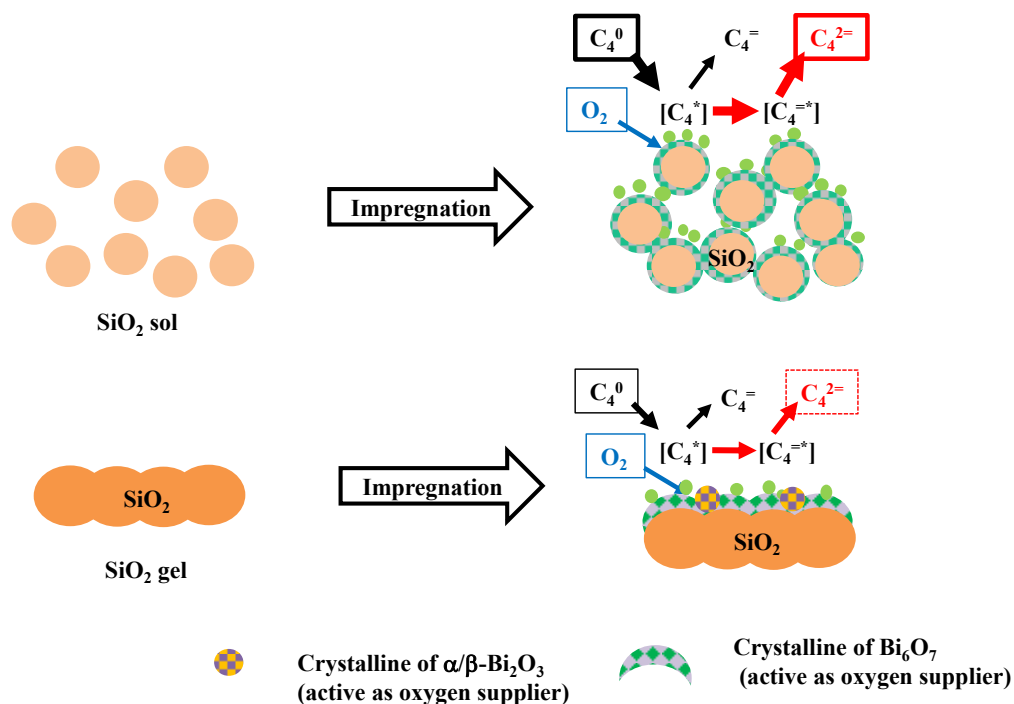
Figure 3.10 Models of gel and sol type SiO_2 support catalysts.

Conclusion

Ni-Bi-O/different support: Al_2O_3, SiO_2 (gel and sol type), ZrO_2 and none (: without support) catalysts, loaded with 20 wt% Ni and 30 wt% Bi as metal weight to support weight have been studied for DH of n-butane to butadiene. The results show that, the activity and selectivity strongly depend on the support. The order of the butadiene selectivity as support is SiO_2 sol > Al_2O_3 > SiO_2 gel > ZrO_2 >> none, where ZrO_2 and none show less dehydrogenation and high oxygenate selectivity. The trend of the butadiene selectivity reflects oxygenate formation suppressed by hierarchical or non-hierarchical nano-particle cohabitation consisting of NiO, bismuth oxide and support. The fact was verified by using the equilibrium adsorption method for the Ni-Bi-O impregnation, characterized by the

redox and acid/base property with temperature programmed reduction and desorption. Finally, acid and base balanced cooperation model was proposed schematically as reaction mechanism and catalyst active sites for ODH of n-butane selective to butadiene over Ni-Bi-O/Al$_2$O$_3$ catalyst. The result also showed SiO$_2$ support to be a potential candidate for improved catalytic performance, hence the need to investigate more of the different types of siliceous materials.

Acknowledgment

References

[1]   J. D. Burrington, R. K. Grasselli, J. Catal. 59 (1979) 79–99.

[2]   M. Bender, ChemBioEng Rev. 1 (2014) 136–147.

[3]   B. P. Ajayi, B. R. Jermy, K. E. Ogunronbi, B.A. Abussaud, S. Al-Khattaf, Catal. Today 204 (2013) 89–196.

[4]   J.C Jung, H. Lee, S. Park, Y-M Chung, T.J. Kim, S.J. Lee, S-H. Oh, Y.S. Kim, I.K Song, Korean J. Chem. Eng. 25 6 (2008) 1316-1321.

[5]   J.C Jung, H. Kim, Y.S Kim, Y-M Chung, T.J. Kim, S.J. Lee, S-H. Oh, I.K Song, Appl. Catal. A: Gen. 317 (2007) 244-249.

[6]   M. Cherian, M.S. Rao, A.M. Hirt, I.E. Wachs, G. Deo, J. Catal. 211 (2002) 482–495.

[7]   I. Marcu, I. Sandulescu, J.M. Millet, J. Mol. Catal. 203 (2003) 241–250.

[8]   J.C. Gottifredi, E.L. Sham, V. Murgia, E.M. Farfa, Appl. Catal. A: Gen. 312

(2006) 134–143.

[9]   M. Volpe, M.L. Ferrari, J. Mol. Catal. A: Chem. 164 (2000) 281-290.

[10]   I. Rossetti, G. F. Mancini, P. Ghigna, M. Scavini, M. Piumetti, B. Bonell, F. Cavani, A. Comite, J. Phy. Chem. C. 116 42 (2012) 22386-22398.

[11]   A. Hakuli, M.E. Harlin, L.B. Backman, A.O.I. Krause, J. Catal 184 (1999) 349-356.

[12] H. Armendariz, J.A Toledo, G. Aguilar-Rios, M.A. Valenzuela, P.Salas, A. Cabral, H. Jimenez, I. Schifter, J. Mol. Catal A: Chem. 92 (2012) 325-332.

[13]   H. Arriola, N. Nava, Appl Catal A: Gen. 92 (1992) 29-38.

[14]   J K. Lee, H. Lee, U. G. Hong, Y. Yoo, Y-J Cho, J. Lee, H. Jang, J. C. Jung, I. K Song, J. Ind. Eng. Chem.18 (2012) 1096-1101.

[15] H. Lee, J. K. Lee, U. G. Hong, Y. Yoo, Y.J. Cho, J. Lee, H.S. Jang, J. C Jung, I. K. Song, J. Ind. Eng. Chem. 18 (2012) 808-813.

[16]   B. Xu, X. Zhu, Z. Cao, L. Yong, W. Yang, Chinese J. Catal. 36. (2015) 1060-.

[17]   Y. Xu, J. Lu, M. Zhang, J. Wang, J. Nat. Gas Chem. 18 (2009) 88-93.

[18]   M.A. Volpe, G.M. Tonetto, H. De Lasa, Appl. Catal. A: Gen. 272 1-2 (2004) 69-78.

[19]   M. Setnicka, P. Cicmanec, R. Bulanek, A. Zukal, J. Pastva, Catal. Today. 204 (2013) 132-139.

[20]   W. Liu, S.K. Lai, H. Dai, S. Wang, H. Sun, C.T Au, Catal. Lett. 113 (2007) 1-8.

[21]   M.L. Pacheco, J. Soler, A. Dejoz, J.M.L. Nieto, J. Herguido, M. Menendez, J. Santamer, Catal. Today 61 (2000) 101-107.

[22]   R. Bulanek, A. Kaluzova, M. Setnicka, A. Zukal, P. Cicmanec, J. Mayerova, Catal. Today 179 (2012) 149-158.

[23] E. Santacesaria, M. Cozzolino, M. Di Serio, A.M. Venezia, R. Tesser, Appl. Catal. A: Gen. 270 1-2 (2004) 177-192.

[24]   B.R. Jermy, B.P. Ajayi, B.A. Abussaud, S. Asaoka, S. Al-Khattaf, J. Mol. Catal. A Chem. 400 (2015) 121–131.

[25]   B. R. Jermy, S. Asaoka, S. Al-Khattaf, Catal. Sci. Technol. 5 9 (2015) 4622–4635.

[26]   G. Tanimu, B. R. Jermy, S. Asaoka, S. Al-Khattaf, J. Ind. Eng. Chem. 45 (2017) 111-120.

[27]   T. Kimura, K. Sakashita, S. Asaoka, Mater. Res. Innovations 15 (2011) s101-s105.

[28]   T. Kimura, H. Imai, X. Li, K. Sakashita, S. Asaoka, S. Al-Khattaf, Catal. Lett. 143 (2013) 1175-1181.

[29]   T. Kimura, H. Imai, X. Li, K. Sakashita, S. Asaoka, M.N Akhtar, S. Al-Khattaf, Arabian. J. Sci. Eng. 39 (2014) 6617-6625.

[30]   A.K. Singh, U.T. Nakate, Scientific World J. (2014) 1-7.

[31]   A. Hameed, V. Gombac, T. Montini, P. Fornasiero, Chem. Phy. Lett. 472 (2009) 212-216.

CHAPTER 4

Pore Structure Effect of Support in Ni-Bi-O/mesoporous silica Catalyst on Butane ODH
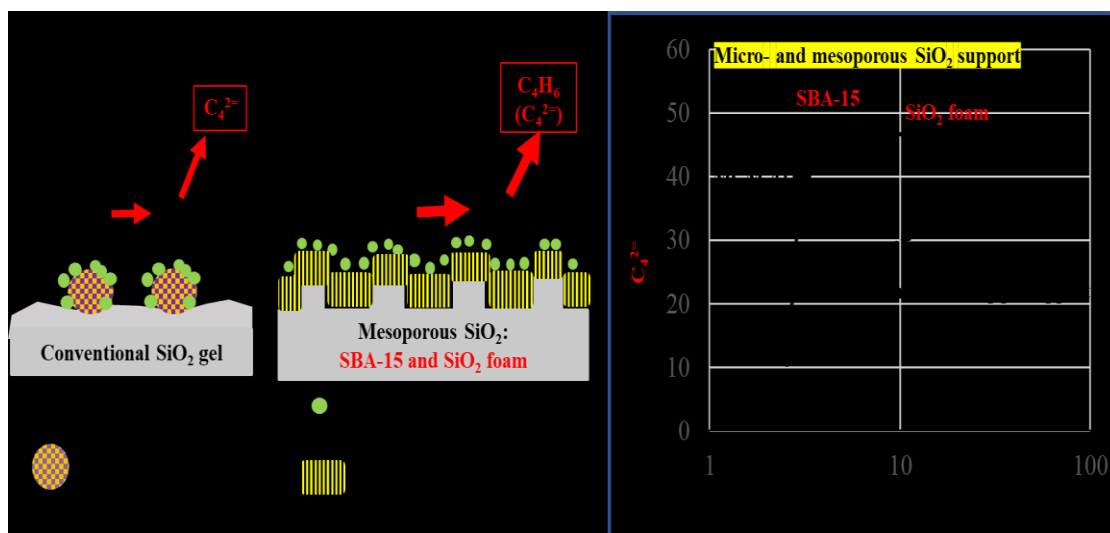
Published as:

Abstract

Ni-Bi-O/structured mesoporous (MCM-41, SBA-15, and silica foam) silica catalyst with 20wt% Ni and 30wt% Bi has been studied in oxidative dehydrogenation of n-butane to butadiene. Mesoporous SBA-15 showed a clear superiority in activity and selectivity as compared to MCM-41, silica foam and conventional silica. The order of the butadiene yield was SBA-15 > Silica foam > MCM-41 > conventional silica. SBA-15 catalyst exhibits the best performance (butadiene selectivity: 47.5% at n-butane conversion: 28.9%) due to the presence of Bi_2O_{3-a} phase (a = 0.2-0.4) as well as the strong base with weak/moderate acid sites, as evident from XRD and TPD analysis, respectively. The formation of Bi_2O_{3-a} (a = 0.2-0.4) phase is related to the template effect of structurally ordered silica.

***Keywords*:** oxidative dehydrogenation; *n*-butane; butadiene; MCM-41; SBA-15; silica foam.

4.1   Introduction

Butadiene is one of the demand-growing raw materials of a high importance for the petrochemical industry. It is mainly produced as a byproduct from naphtha cracker during ethylene and propylene production. On-purpose butadiene production technology is also expected to meet the growing demand. One of the methods is oxidative dehydrogenation of 1-butene. On the other hand, several works on oxidative dehydrogenation of n-butane to butadiene have been directed towards developing an efficient catalyst system. These efforts have resulted in preparation of vanadium based catalysts composed of V_2O_5/SiO_2 [1], V_2O_5/silica gel [2], V/supports (TiO_2, ZrO_2 and Al_2O_3) [3,4], V/TiO_2-SiO_2 [5], $Mg_3(VO_4)_2$ species over Al_2O_3, ZrO_2, MgO and CeO_2 [6,7], VOx/supports (USY, NaY, γ-Al_2O_3, α-Al_2O_3) [8], VOx/SBA-15 [9], V/supports (HMS, SBA-16, SBA-15, MCM-48) [10], VOx/Ti-HMS [11], V-MCM-41 [12], V/Ti-SBA-15 [13], Mo-V-MgO [14] and a phosphate modified CNT [15]. However, the role of catalyst in 1st (n-butane to butenes) and 2nd (1-butene to butadiene) step dehydrogenations and combination of two is not well defined in the literature.

In our previous study [16], nanostructured Ni-Bi-O species impregnated on Al_2O_3 were reported as active and selective (butadiene formation) catalyst for oxidative dehydrogenation of n-butane. Alumina-supported 20wt% Ni (as metal weight to Al_2O_3 weight) oxide was highly active but not selective. The selectivity was improved by impregnation of 30wt% Bi (as metal weight to Al_2O_3 weight) oxide with 20wt% Ni. The impregnation of Bi oxide efficiently reduces the side-reaction resulting in high butadiene selectivity (40%). In addition, the catalyst calcination plays a vital role to enhance butadiene selective by controlling the formation alpha and beta mixed Bi_2O_3 phase [17].

Furthermore, during the reaction the activity and selectivity were proved to depend on the acid-base property and NiO redox character by Ni species modification through partial substitution with Co and Fe [18]. In further investigation of the support effect, SiO_2 supported catalyst showed the best performance than Al_2O_3 and ZrO_2 [19] supported catalyst.

Mesoporous silicas (MCM-41, SBA-15, and foam) have been used as support to prepare well-dispersed tungsten oxide catalyst [20-22]. Oxidative dehydrogenation of n-butane was reported using vanadium nanoparticles impregnated over mesoporous silica support [10]. Mesoporous silica support showed an enhanced performance by stabilization of nanoparticles due to their ordered structure and well-defined pore sizes. In our present study, mesoporous silica supports such as MCM-41, SBA-15 and silica foam were synthesized and impregnated with 20wt% Ni and 30wt% Bi. The impregnated catalyst was investigated on oxidative dehydrogenation of n-butane to butadiene and the observed results are discussed.

4.2 Experimental Section

4.2.1 Catalyst Preparation

Conventional silica supports having different pore diameter (Cariact Q6, Cariact Q15 and Cariact Q30) were purchased from Fuji Silysia chemicals Ltd, Japan. Si-MCM-41 was synthesized using procedure reported in the literature [23]. Si-SBA-15 support material [24] was synthesized using tri-block copolymer, poly(ethylene glycol)-*block*-poly(propylene glycol)-*block*-poly(ethylene glycol) as a structure directing agent. 4 g of Pluronic P123 was added to 30 ml of water. After stirring for a few hours, a clear solution

was obtained. About 70 g of 0.28 M hydrochloric acid was added to it and the solution was stirred for another 2 h. Then, 9 g of tetraethyl orthosilicate (TEOS) was added and the resulting mixture was stirred for 24 h at 40 °C and finally heated to 100 °C for 48 h. The solid product was recovered by filtration, washed with water for several times and dried overnight at 100 °C. Finally, the product was calcined at 550 °C for 6 h to remove the template. Mesoporous silica foam was synthesized using procedure reported by Qi et al. [25]. In a typical synthesis, 3.0 g of neutral triblock co-polymer surfactant, Pluronic 123, was dissolved in a mixture: 3.0 g of acetic acid, 52 g of deionized water and 0.3g of ammonium fluoride at 40 °C. After stirring for 2 h, 2.35 g of sodium silicate solution in 40 g of water was added and the resultant mixture was reacted under vigorous stirring for 5 min. Then, the mixture was kept under static condition for 24 h at 40 °C followed by aging at 70 °C overnight. The solid products were washed with deionized water and collected by filtration and air dried. The obtained solid was then calcined at 560 °C for 6 h to remove the template.

The Bi-Ni-O/support catalysts were prepared by the co-impregnation method of equilibrium adsorption with enforced deposition. Nickel nitrate hexahydrate $Ni(NO_3)_2 \cdot 6H_2O$ (99 %, Fisher Scientific) was used as nickel source, while bismuth nitrate pentahydrate $Bi(NO_3)_3 \cdot 5H_2O$ (98 %, Fluka) was used as bismuth source. For the preparation of 20 wt% Ni-30 wt% Bi-O/Al_2O_3 catalyst, 0.99 g of $Ni(NO_3)_2 \cdot 6H_2O$ was added to 80 ml of distilled water. After complete dissolution, 0.70 g of $Bi(NO_3)_3 \cdot 5H_2O$ was added and stirred. Then 1.0 g of dried support was added for impregnation and left overnight for equilibrium Bi species adsorption. Then the sample mixture was dried up by evaporation at 80 °C for enforced Ni species deposition. The solid was further dried at 120

°C for 3 h and it was calcined at 350 °C (10 °C/min) for 1 h and the temperature was raised to 590 °C (15 °C/min) and kept for 2 h. The obtained catalysts were denoted as shown in Table 4.1.

Table 4.1. List of catalysts codes used for oxidative dehydrogenation of n-butane to butadiene.

Catalyst Code	Description
A	20 wt% Ni and 30 wt% Bi on Cariact Q-6
B	20 wt% Ni and 30 wt% Bi on Cariact Q-10
C	20 wt% Ni and 30 wt% Bi on Cariact Q-30
D	20 wt% Ni and 30 wt% Bi on Si-MCM-41
E	20 wt% Ni and 30 wt% Bi on Si-SBA-15
F	20 wt% Ni and 30 wt% Bi on silica foam

4.2.2 Catalyst Reaction Testing

The oxidative dehydrogenation was carried out in an automated fixed bed reactor purchased from BELCAT, Japan. 0.3g of catalyst was loaded into the reactor and calcined under air atmosphere. After calcination, the reaction started under a nitrogen atmosphere. The feed n-butane contact time was maintained at 0.42 h·g/mol. The total flow rate of reactants including n-butane, air, and nitrogen was maintained at 31.2 ml/min. The catalysts were tested at 400 °C with oxygen to n-butane ratio (O_2/n-C_4H_{10} = 1.0, 2.0 and 4.0 mol/mol) for 1 hour under each condition and followed by 450 °C (O_2/n-C_4H_{10} = 2.0 mol/mol) and 500 °C (O_2/n-C_4H_{10} = 2.0 mol/mol) for 1 hour each. The total time on stream is about 5 hours. The products were analyzed through online GC system (Agilent, 7890N). The hydrocarbons and oxygenates were analyzed using FID and GC-Gas Pro capillary column (L: 60 m and ID: 0.32 mm), while gases, N_2, O_2, CO and CO_2, and H_2, respectively were detected using TCD and Shin Carbon 80/100 mesh SS column (He carrier) and MS5A

60/80 mesh SS column (Ar carrier). The products were confirmed by comparing with standard samples. The n-butane conversion and product selectivity were calculated using carbon mass balance. The obtained results were summarized based on Scheme 4.1, which were arranged using observed products. The selectivity of the catalyst to dehydrogenation products DH (consisting mainly 1-butene, 2-butenes and 1,3-butadiene: BD), oxygenate and cracked products OC (carboxylic acids, ethylene, propylene, methane, and CO_2) and partial oxidation products PO (CO and H_2) are presented in Figure 4.1.
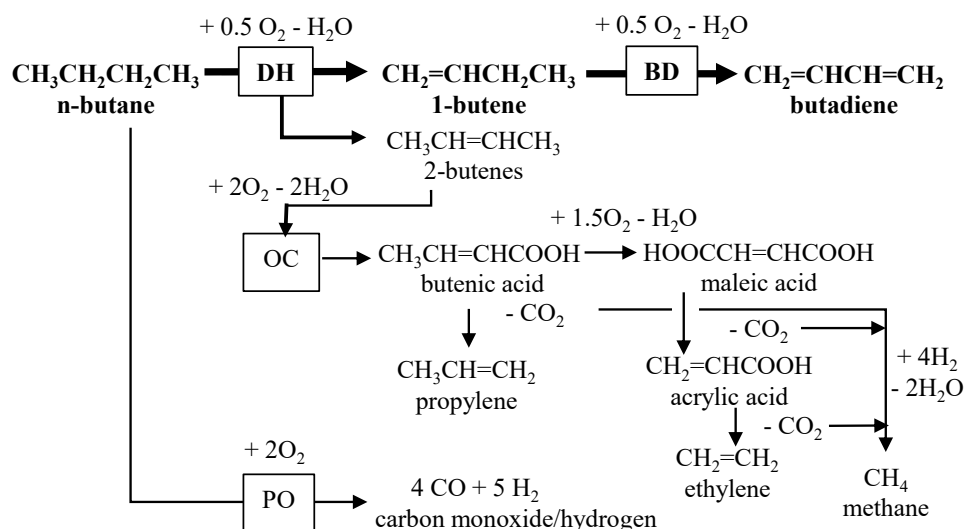
Figure 4.1 Possible reaction pathway for oxidative dehydrogenation of n-butane to butadiene

4.2.3 Catalyst Characterization

The physicochemical characteristics such as surface area and pore structure were analyzed by using nitrogen adsorption-desorption isotherm (Micromeritics ASAP 2020 instrument, Norcross, GA). The pore surface area, pore volume, and pore diameter were measured using BJH adsorption method. X-ray diffraction patterns of calcined samples were recorded from (2 theta) range of 5 ° to 90 ° using Rigaku Miniflex II desktop X-ray

diffractometer and using Cu Kα radiation (wavelength λ=1.5406 Å) and 30 mA and 40 kV as operating parameters, a step size of 0.02 º and a speed of 0.5 º/min. The catalyst morphologies were analyzed using high-resolution transmission electron microscope (HRTEM-model JEM-2100F) with an acceleration voltage of 200 kV. The redox character and acid-base property were analyzed using temperature programmed reduction (TPR) and temperature programmed desorption (TPD) using BEL-CAT-A-200 chemisorption instrument as reported earlier [16]. The redox property measurement was done using a gas mixture of Ar/H_2 (95/5 vol%) having a total flow rate of 50 cm^3/min. 0.1 g of the calcined catalyst was preheated for 3 h at 300 ºC in inert He after which it is cooled to room temperature. It was then heated at the rate of 20 ºC/min up to 900 ºC. H_2 intake was recorded with a TCD and CuO was used as a reference for calibrating the consumption of H_2. Ammonia and carbon dioxide temperature programmed desorption (NH_3 and CO_2 TPD) were carried out using the same equipment (BELCAT system) for acidity and basicity measurements respectively, the procedure is similar to that previously reported [18].

4.3   Results and Discussion

4.3.1 Catalyst Characterization

4.3.1.1 X-ray diffraction

The X-ray diffraction (XRD) patterns related to Bi oxide species for catalyst A to F are shown in Figure 4.2. The XRD patterns were measured from diffraction angle of 2θ = 5 to 90 º. Then, 2θ = 25 to 35 º was chosen to precisely examine the phases of BiO_x in the different catalysts. For the conventional SiO_2 supported catalysts, the main peaks are

attributed to beta-Bi_2O_3 and Bi_2O_{3-a} at $2\theta = 27.38\ °$ and $29.0\ °$ respectively. The intensity of these peaks increases with increase in the pore size of the support. However, the mesoporous supported catalysts showed higher intensity as compared to conventional silica catalysts. Catalyst D (MCM-41 supported) showed the two phases of BiO_x almost 40-60% ratio for beta-Bi_2O_3 and Bi_2O_{3-a} respectively. Catalyst F (Silica foam supported) on the other hand also showed the two BiO_x phases but the dominant phase is the Bi_2O_{3-a} at $2\theta = 29.0\ °$. Mesoporous SBA-15 supported Catalyst E showed a pure and highly crystalline phase of Bi_2O_{3-a}. Using the XRD pattern of the pure and highly crystalline phase of BiO_x, the phase assignment of Bi_6O_7 assigned in our previous paper [19] was re-examined to conclude Bi_2O_{3-a} (a = 0.2-0.4). Though the XRD pattern agrees with previously assigned phase Bi_6O_7 ($Bi_2O_{2.33}$) in major three peaks referring to the JCPDS Powder Diffraction File No.27-0051 [26]. The minor but fingerprint-like peaks at 2 theta = 5, 10 and 30.6 ° of (002), (004) and (0012) respectively could not be observed. Furthermore, the pattern also did not agree with $Bi_2O_{2.5}$ and $Bi_2O_{2.75}$ in the data file but the main peak position is between 27.93 and 31.92° of $Bi_2O_{2.5}$ and $Bi_2O_{2.75}$ respectively. These studies lead to the assignment of Bi_2O_{3-a} (a = 0.2-0.4) phase.
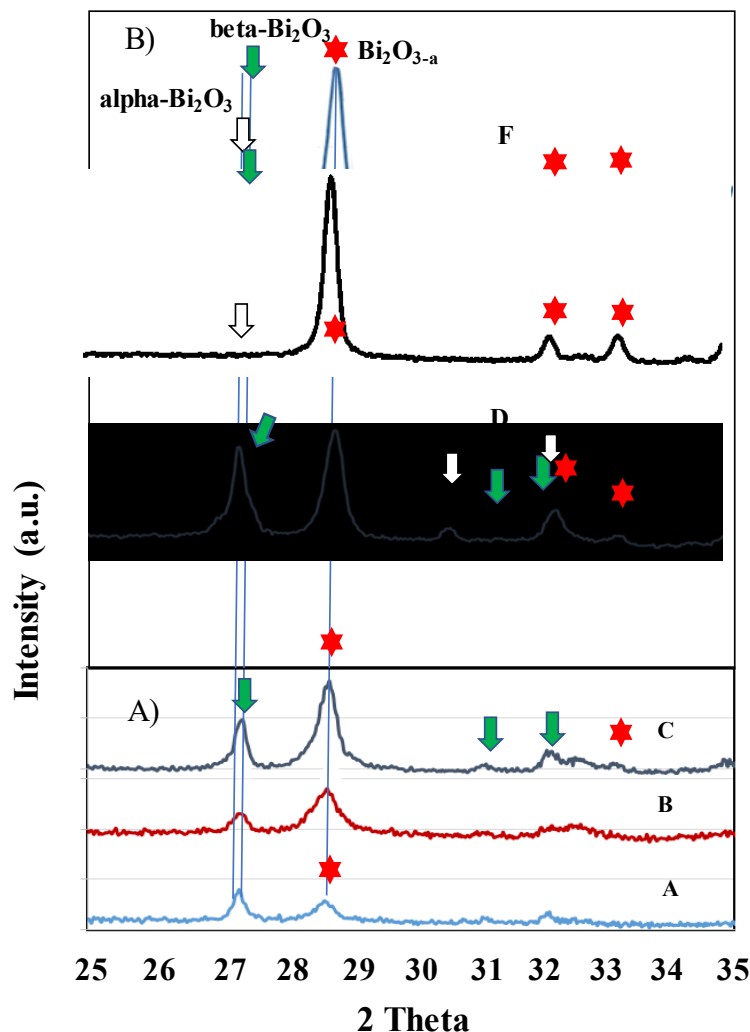
Figure 4.2 Comparison of X-ray diffraction pattern for support species in Ni-Bi-O catalyst: A) Conventional SiO$_2$ and B) mesoporous SiO$_2$.

The highly ordered mesoporous SBA-15 support was further loaded NiO and BiO$_x$, separately and the XRD patterns were compared with that of the Ni-Bi-O/SBA-15 catalyst as shown in Figure 4.3. For the NiO/SBA-15, peaks at $2\theta = 37$ and $43°$ were observed corresponding to the NiO phase. The crystal size of the NiO was found to be 10.1 nm as determined from the Scherrer's equation. And for the case of BiO$_x$/SBA-15, peaks of highly crystalline beta-Bi$_2$O$_3$ and Bi$_2$O$_{3-a}$ were observed. It clearly indicates the formation

90

of the pure and highly crystalline Bi_2O_{3-a} phase in SBA-15 supported catalyst is not only due to mesoporous SBA-15 but also accelerated by Ni species co-impregnation. Comparing Ni oxides catalyst alone with the binary catalyst, the dispersion of the NiO oxides was increased and the intensity of the peaks corresponding to the oxide was reduced as shown in Figure 4.3. Only 30% of NiO with crystal size of 20.9 nm (calculated using Scherrer's equation) was detected for catalyst E, indicating that 70% of NiO is highly dispersed on the Bi_2O_{3-a} surface. Reversely, in the case of Bi amount reduction, 80% of NiO with large crystal size of 20.9 nm was detected indicating that only 20% is highly dispersed on the Bi_2O_{3-a} ($a = 0.2$-0.4) surface.
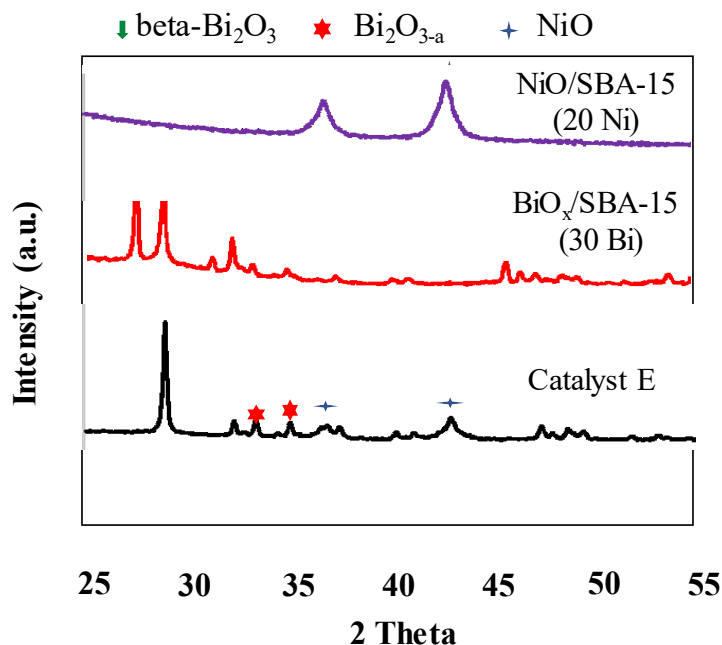
Figure 4.3 Comparison of X-ray diffraction pattern of NiO/SBA-15 (20 Ni), BiOx/SBA-15 (30 Bi) and Ni-Bi-O/SBA-15 (20 Ni-30 Bi and 20 Ni-10 Bi) catalysts.

The concentration of Bi_2O_{3-a} phase on the support pore diameter as shown in Figure 4.4. For the conventional silica supported catalyst, the concentration of the phase increases with increasing support pore diameter. This is a clear indication that the crystallinity (silica arrangement like mesoporous silica) even though within the amorphous phase increases with increase in the average pore diameter of the support. For the mesoporous structured silica supported catalysts, the Bi_2O_{3-a} phase concentration increases with increase in pore diameter up to 4.5 nm. For catalyst E, Bi_2O_{3-a} phase concentration was about 99.5%, whereas the catalyst F (with the highest average pore diameter) showed a decrease in Bi_2O_{3-a} phase concentration due to the presence of beta-Bi_2O_3 phase as observed in XRD.
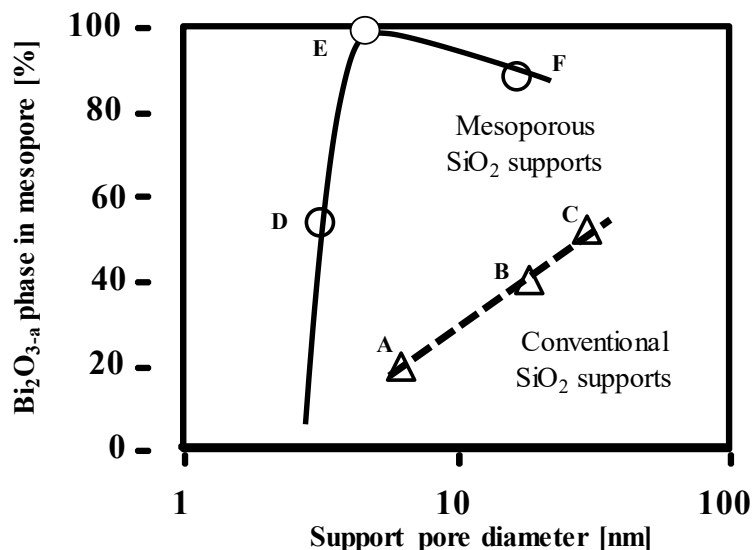
Figure 4.4 Bi_2O_{3-a} phase concentration in mesopore vs support pore diameter.

4.3.1.2 Surface area and pore structure

The BET areas, pore volumes and the average pore diameters of the various catalysts are presented with the values of the corresponding supports in Table 4.2. All the catalysts apparently showed a reduced surface area as compared to the support. The pore structure

of the catalysts also followed the same trend. But their values adjusted to support weight base showed increased or not much-reduced values for all the catalysts. It is expected due to the high loading of active metal species without leading to pore blockages. Among the conventional silica supported catalysts, Catalyst A showed a surface area of 519 m^2/g, twice that of the catalyst B (251 m^2/g). Though the mesoporous silica supports mostly have higher surface area and porosity than the conventional amorphous silica supports. The surface area of the catalysts adjusted to the support content in the catalysts is in more than half of the catalysts slightly higher than surface area of the pure support. Such observation is reported in our previous studies [16-19]. This finding was considered due to dispersion of Ni-Bi-O nano-sized particle.

Table 4.2 Physical properties of catalysts and supports.

Catalyst: (Support)	BET area		Pore volume		Average pore diameter [nm]^e
	[m^2/g-catalyst]^a	[m^2/g-support]^b	[cm^3/g-catalyst]^c	[cm^3/g-support]^d	
A	327	519	0.62	0.98	6.2
(Cariact Q6)	(426)	(426)	(0.83)	(0.83)	(6.3)
B	158	251	0.71	1.13	16.8
(Cariact Q10)	(242)	(242)	(1.22)	(1.22)	(18.6)
C	62	98	0.52	0.82	35.3
(Cariact Q30)	(166)	(166)	(1.28)	(1.28)	(29.9)
D	768	1220	0.53	0.84	2.8
(Si-MCM-41)	(914)	(914)	(0.86)	(0.86)	(3.1)
E	269	427	0.33	0.52	4.2
(Si-SBA-15)	(657)	(657)	(1.08)	(1.08)	(4.1)
F	388	616	1.55	2.46	15.6
(Silica foam)	(540)	(540)	(2.27)	(2.27)	(16.4)

^{a}BET area, ^{c,e}pore volume and average pore diameter measured using BJH isotherm, ^{b,d}Surface area and pore volume calculated to support weight base by using the equation: SA or PV×[Σ(MO$_x$/M)+100]/100, where M = metal wt%; MO$_x$= metal oxide wt%; SA = surface area; PV = pore volume.

The pore size distribution of the mesoporous silica is narrow as compared to the conventional silica as shown in Figure 4.5. It also shows the sharp (narrow) pore size distribution of the mesoporous silica catalyst is originated from that of the corresponding support without large shift in peak position.
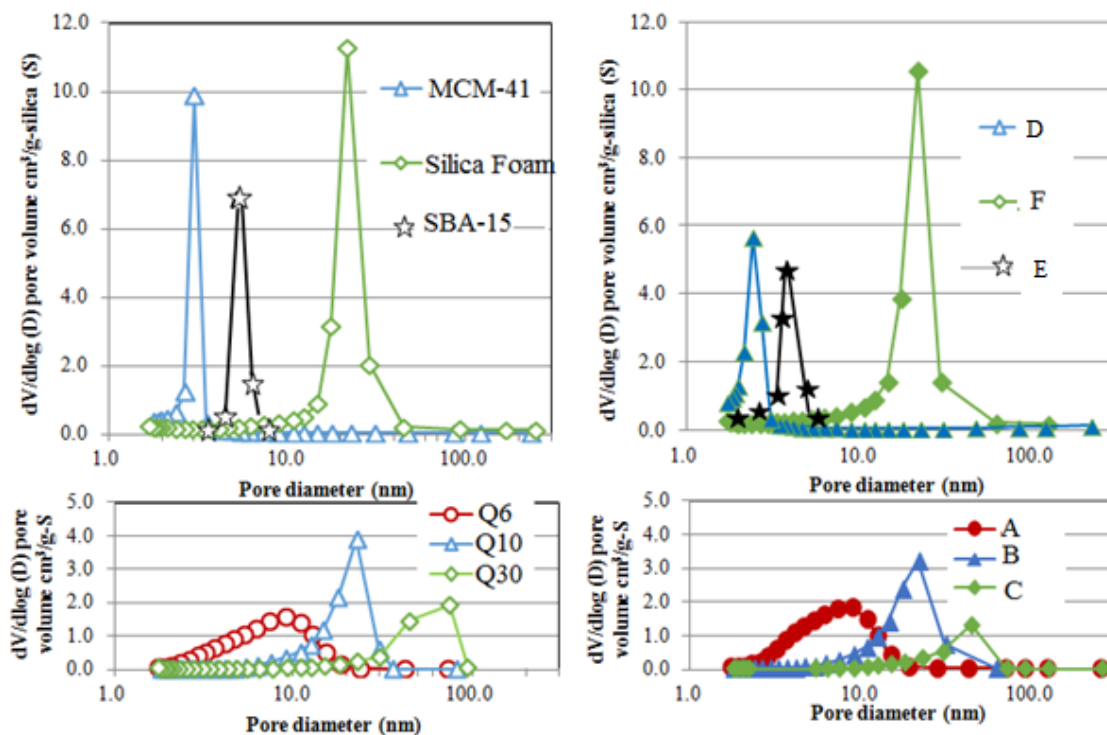
Figure 4.5 Pore size distribution of support and its catalyst A to F.

4.3.1.3 Temperature programmed reduction

The extent of active species reducibility plays an important role in the activity and selectivity of catalysts, especially in oxidative dehydrogenation reactions. This property is measured using temperature programmed reduction (TPR) and the performance of a catalyst is enhanced by an accelerated redox cycle resulting from increased active species reducibility. H_2-TPR profile of the mesoporous silica supported catalysts is shown in Figure 4.6 in comparison with the conventional silica catalyst B. The TPR maximum temperature depends on the sample mass and the speed of the reduction reaction, hence same condition in terms of sample mass, the flow rate of H_2 and temperature programming was adopted.
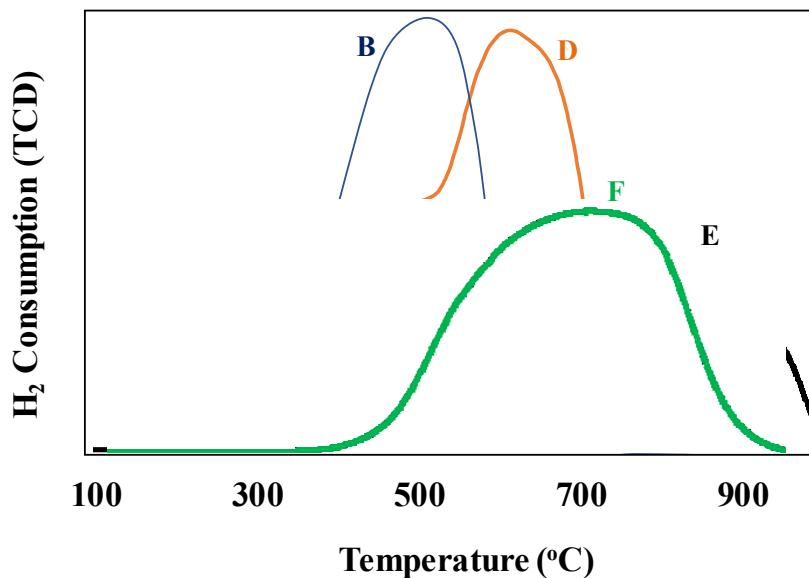
Figure 4.6 TPR profile for support species in Ni-Bi-O catalyst: B (Q10), D (Si-MCM-41), E (Si-SBA-15), and F (SiO$_2$ foam).

The TPR profile of catalyst B showed a high-intensity reduction peak at 500 ºC and a small reduction peak extending up to 700 ºC from 625 ºC. The easy reduction of Ni-Bi-O metal oxide species at 500 ºC shows the presence of larger particle not firmly interacting with the support. This change of reducibility over SiO$_2$ is related to the different state of NiO and Bi$_2$O$_3$ coordination between each other [19]. TPR profiles were divided into three parts: I) easily reducible (350-550ºC), II) moderately reducible (550-650ºC) and III) difficult to reduce (650-850ºC) with the total as shown in Table 4.3. For the case of catalyst (MCM-41), a medium reduction peak at the easily reducible region and high intensity peak at around 700 ºC were observed. It is also near the case of F (silica foam) even though the peak at the easily reducible region decreases and that of the region with difficulty increases in reducibility. The difficulty is related to the state of the smaller particles of highly dispersed active species strongly interacting with the mesoporous support species.

Table 4.3 H_2 consumption in TPR of 20wt%Ni-30wt%Bi-O supported catalysts.

Catalyst (Support)	TPR: H_2 consumption [m mol/g] (T_M[°C])			
	I (350-550 °C)	II (550-650 °C)	III (650-850 °C)	total
B (Cariact Q-10)	3.74	1.12	0.13	4.99
D (MCM-41)	1.29	2.97	0.68	4.95
E (SBA-15)	0.88	1.04	2.43	4.35
F (SiO$_2$ foam)	0.70	1.01	2.51	4.22

In the case of E (SBA-15), TPR profile showed a broad peak extending from 500-1000 °C. The broadness of the reduction peak is related to the strong dispersion/interaction of the active species of NiO and BiO_x with the supports.

4.3.1.4 Temperature programmed desorption

The basicity and acidity of the catalysts were measured using CO_2- and NH_3-temperature programmed desorption technique (CO_2- and NH_3-TPD), respectively. The amount of NH_3/CO_2 desorbed in mmol/g for catalysts of 20 wt% Ni-30 wt% Bi-O metal oxides over different conventional and mesoporous silica catalysts are presented in Table 4.4. CO_2-TPD profiles of the catalysts are decomposed into three peaks centered at ca. 170 °C, ca. 300 °C and ca. 400 °C, named as I, II and III with an assignment to weak base, moderate base, and strong base, respectively. Similarly, NH_3-TPD profiles are also deconvolved into three peaks with range at 100-250 °C, 250-400 °C and 400 °C < named as I, II and III representing weak acid, moderate acid, and strong acid, respectively.

Table 4.4 Temperature programmed desorption (CO_2- and NH_3-TPD) of 20wt% Ni-30wt% Bi-O/support.

Catalyst (Support)	CO_2-TPD Base amount [m mol/g]*[1]				NH_3-TPD Acid amount [m mol/g]*[2]				Acid /Base
	I	II	III	Total	I	II	III	Total	
A (Cariact Q-6)	0.014	0.008	-	0.022	0.019	0.010	0.003	0.032	1.5
B (Cariact Q-10)	0.031	0.002	-	0.033	0.039	0.014	0.001	0.054	1.6
C (Cariact Q-30)	0.009	0.002	-	0.011	0.011	0.002	-	0.013	1.2
D (MCM-41)	0.08	0.002	0.011	0.021	0.026	0.039	-	0.065	3.1
E (SBA-15)	0.056	0.014	0.004	0.074	0.044	0.021	-	0.065	0.9
F (Silica foam)	0.026	0.006	0.011	0.043	0.053	0.041	-	0.094	2.2

[1]: I (170°C peak): weak base, II (300°C peak): moderate base, III (400°C peak): strong base[2]: I (100-250°C): weak acid, II (250-400°C): moderate acid, III (>400°C): strong acid

Our previous reports showed that moderate and strong bases are required for efficient abstraction of H from terminal methyl of n-butane and 1-butene, and a weak acid site is required for 1-butene intermediate adsorption [18, 19]. All the conventional silica supported catalysts do not possess moderate and strong basic sites, whereas mesoporous silica supported catalysts have both moderate and strong basic sites. Catalyst B has the highest total basic sites and weak acid sites among the conventional silica supported catalysts. All the mesoporous silica supported catalysts have both weak and moderate acid sites without strong acid sites. Catalyst E has the highest moderate basic sites, which plays an important role in butadiene selectivity.

4.3.1.5 TEM analysis

Transmission electron microscopy images (TEM) of the mesoporous supported catalysts having 20 wt% Ni and 30 wt% Bi are shown in Figure 4.7. TEM of conventional silica have been reported in our previous report [19]. The crystals of BiO_x in the conventional silica were too small to be observed by TEM probably due to a low crystallinity as evident from XRD study. The TEM images showed the dispersion of the NiO with the BiO_x on the various supports. The mesoporous support showed a similar pattern of active species dispersion. To precisely study the active species dispersion, high-resolution transmission electron microscopy (HRTEM) was carried out on the D catalyst to enable the determination of the Bi_2O_{3-a} crystal and NiO crystal. Figure 4.8 shows the HRTEM image of the Catalyst E. The observed HRTEM image showed a lattice spacing of 0.21 nm and 1.4 nm corresponding to that of NiO and SBA-15, respectively. As the 1.4 nm lattice of SBA-15 reflects the orientation of silica chains, the lattices of NiO are also oriented in the same direction. A major part of NiO is dispersed not directly on SBA-15, but through Bi_2O_{3-a} phase in SBA-15. This means the three oxide chains, (i) silica chain in SBA-15 mesopore, (ii) Bi-O chain of Bi_2O_{3-a} phase and (iii) Ni-O dispersed on Bi_2O_{3-a} phase have the same orientation. The TEM image of the SBA-15 supported catalyst agreed with that reported in literature [27].
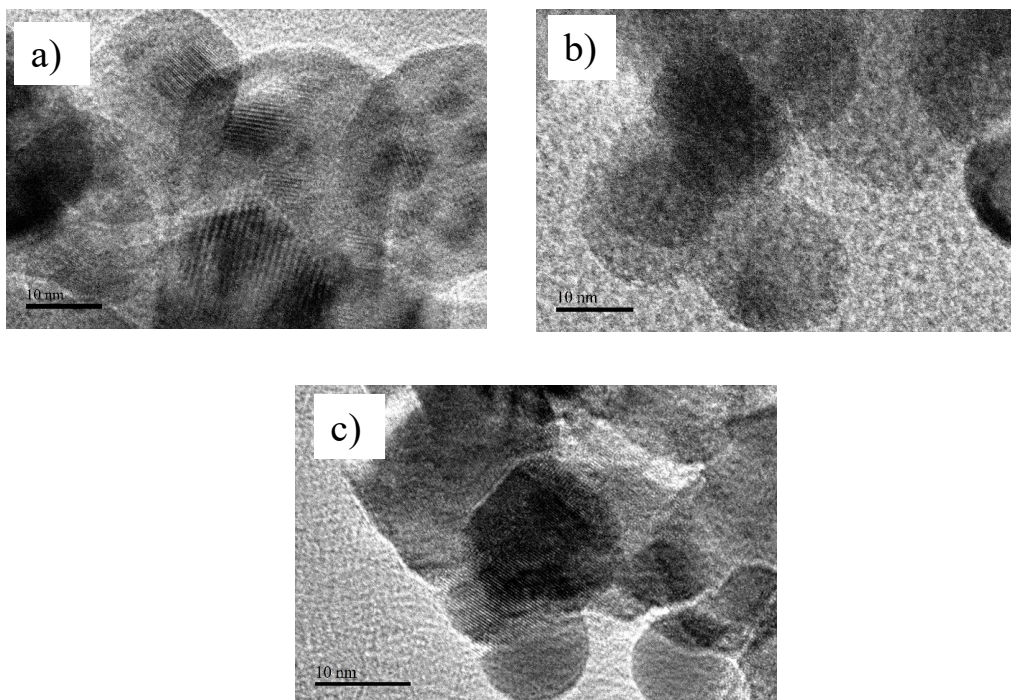
Figure 4.7 TEM image of catalyst a) Catalyst D, b) Catalyst E and c) Catalyst F.
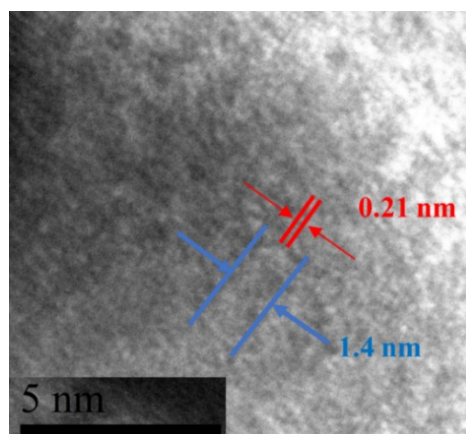
Figure 4.8 HRTEM image of Catalyst E (20 wt% Ni and 30 wt% Bi on Si-SBA-15).

4.3.2 Catalyst Evaluation

4.3.2.1 Effect of reaction condition

The reaction temperature and O_2/n-C_4H_{10} feed ratio were varied to test the performance of

Catalyst E. The dependence of activity/selectivity on time-on-stream was observed only

until one hour (second sampling) due to initial oxygen species on catalyst surface. The result obtained at 5 h time-on-stream is presented in Table 4.5. The result confirms the reaction pathway shown in Scheme 4.1 that oxygenate and cracking products are obtained mainly from 2-butene after the 1st dehydrogenation step. With increase in the reaction temperature, the conversion increased, while dehydrogenation selectivity decreased. BD selectivity did not change but OC production increased two folds with increase in the temperature. This is due to excess NiO species, which are more active at higher temperatures and they favor cracking reaction pathway. Upon increasing $O_2/n-C_4H_{10}$ feed ratio, the conversion increased up to 2.0 ratio, thereafter slight decrease in conversion was observed. With increase in $O_2/n-C_4H_{10}$ feed ratio, the dehydrogenation selectivity (and butadiene selectivity) decreased. OC and PO selectivity were increased due to excess oxygen supply that facilitates cracking and oxidation reactions. The decrease in conversion with increasing $O_2/n-C_4H_{10}$ feed ratio from 2.0 to 4.0 suggest oxygen species saturation of major and selective dehydrogenation site. Oxygenates byproduct suppress main reaction, resulting to a decrease in conversion.

Table 4.5 Comparison of catalytic performance over 20 wt% Ni-30 wt% Bi-O/SBA-15 catalyst
for different reaction conditions

Reaction temperature [$^{\circ}$C]	400	400	400	450	500
$O_2/n\text{-}C_4H_{10}$ molar ratio	1.0	2.0	4.0	2.0	2.0
$n\text{-}C_4H_{10}$ conversion [%]	**21.5**	**26.5**	**25.4**	**28.9**	**37.7**
Selectivity*[1] [C%]					
DH	91.6	87.6	80.1	75.2	49.6
$2\text{-}C_4H_8$	23.3	20.5	19.7	15.4	15.5
$1\text{-}C_4H_8$	18.8	19.1	18.9	12.3	4.3
BD	**49.5**	**48.0**	**41.5**	**47.5**	**38.2**
OC	6.7	9.3	11.3	19.7	43.3
PO	1.7	3.2	8.5	5.1	7.1
($1\text{-}C_4H_8$ + BD)*[2]	68.3	67.1	60.4	59.8	42.5
BD/($1\text{-}C_4H_8$+ BD) %*[3]	72.5	71.5	68.7	79.4	89.8
BD yield	**10.7**	**12.7**	**10.5**	**13.7**	**14.4**

*[1] DH: dehydrogenation, BD: butadiene, OC: oxygenate and the cracked, PO: partial oxidation.
*[2] selectivity at 1st step dehydrogenation, *[3] selectivity at 2nd step dehydrogenation

4.3.2.2 Effect of conventional silica support

Commercially available silica materials having different pore sizes were used as supports and their activity was studied at 450 $^{\circ}$C and $O_2/n\text{-}C_4H_{10}$ = 2.0. From Table 4.6, all the catalysts showed almost similar n-butane conversion, but catalyst B gave the highest dehydrogenation selectivity with the least oxygenate and cracked products selectivity. Catalyst A produced the highest 2-butenes with higher cracked products selectivity.

Butadiene selectivity is similar for catalyst B and C and slightly lower in the case of the catalyst A. It indicates that for conventional silica support to effectively and efficiently disperse BiO_x and then NiO species, a relatively large pore size is required.

Table 4.6 Comparison of catalytic performance for conventional SiO_2 supports with different pore size in Ni-Bi-O catalyst.

Catalyst	A	B	C
Support APD [nm]	6.3	18.6	29.9
n- C_4H_{10} conversion [%]	**19.8**	**17.6**	**18.2**
(O_2 conversion)	(32)	(25)	(31)
Selectivity*[1] [C%]			
DH	74.3	79.1	75.9
2- C_4H_8	24.5	21.7	18.4
1- C_4H_8	22.3	25.5	25.1
BD	**27.5**	**31.9**	**32.4**
OC	22.7	17.5	21.5
PO	3.0	3.4	2.5
(1- C_4H_8 + BD)*[2]	49.8	57.4	57.5
BD/(1- C_4H_8 + BD) %*[3]	55.2	55.6	56.4
BD yield	**5.4**	**5.6**	**5.9**

*[1] DH: dehydrogenation, BD: butadiene, OC: oxygenate and the cracked, PO: partial oxidation. *[2] selectivity at 1st step dehydrogenation, *[3] selectivity at 2nd step dehydrogenation

4.3.2.3 Effect of mesoporous silica support

Mesoporous silica supports have highly ordered pore structures and high surface areas, which can enhance dispersion of active species thereby generating more active sites as compared to conventional silica supports. Also, their pore sizes are well defined, can be controlled and have thick pore walls [28-30]. Three different mesoporous silica supports (MCM-41, SBA-15 and SiO_2 foam) were synthesized and impregnated with the active metal species and tested for n-butane oxidative dehydrogenation. The results obtained are presented in Table 4.7.

Table 4.7 Comparison of catalytic performance for mesoporous SiO_2 support species in Ni-Bi-O catalyst

Catalyst	D	E	F
Support	MCM-41	SBA-15	SiO_2 foam
APD[nm]	3.1	4.5	16.4
n- C_4H_{10} conversion [%]	**18.0**	**28.9**	**29.2**
(O_2 conversion)	(27)	(57)	(55)
Selectivity[1] [C%]			
DH	74.6	75.2	77.6
2- C_4H_8	20.5	15.4	17.2
1- C_4H_8	14.0	12.3	14.8
BD	**40.1**	**47.5**	**45.6**
OC	18.8	19.7	21.0
PO	6.6	5.1	1.4
(1- C_4H_8 + BD)[2]	54.1	59.8	60.4
BD/(1- C_4H_8 + BD) %[3]	74.1	79.4	75.4
BD yield	**7.2**	**13.7**	**13.3**

The conversion of the catalysts is in the order catalyst D < E = F. The conversion was improved as compared to the conventional silica supported catalysts. Dehydrogenation products selectivity of the catalysts is almost similar even though it increased slightly going from catalyst E through D and F, while oxygenate and cracked products selectivity showed an opposite trend. Partial oxidation selectivity increased in the order catalyst F < E < D. Butadiene selectivity is slightly higher in Catalyst E, which directly relates to the selective 2nd step dehydrogenation ability as observed low amount of 1-butene in product distribution.
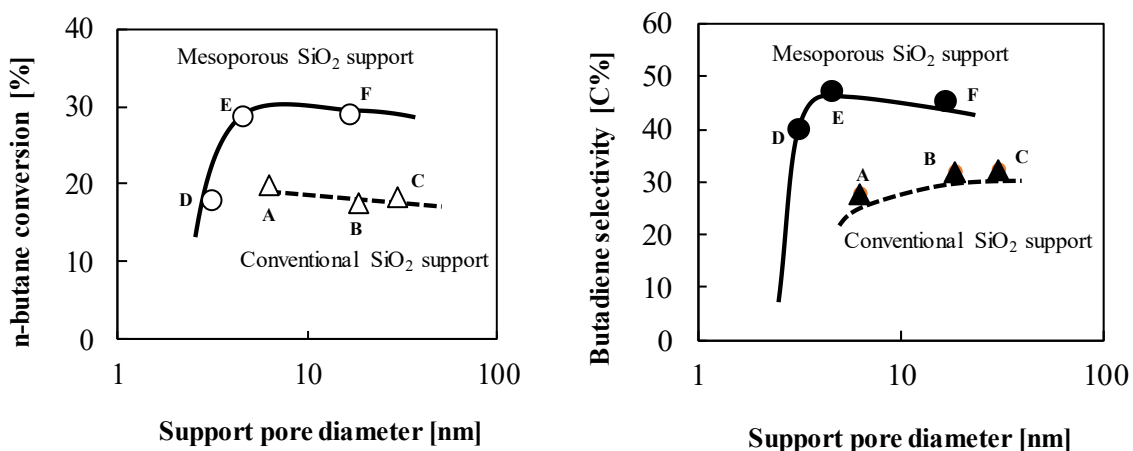
Figure 4.9 n-Butane conversion and butadiene selectivity *vs* support pore diameter

It was reported that the dispersion of active species, their reducibility, and catalytic performance are effectively controlled by the pore sizes of both the conventional and mesoporous supports [31]. In our case, the effect of support pore diameter on the main catalytic performances (n-butane conversion and butadiene selectivity) showed a completely different trend between mesoporous silica and conventional silica, as shown in Figure 4.9. Catalytic activity and butadiene selectivity of the mesoporous silica shows clear superiority over the conventional silica even at similar pore diameter region. Therefore, the

superiority is considered not only due to the pore size or the porosity but also owing to the ordered silica structure.
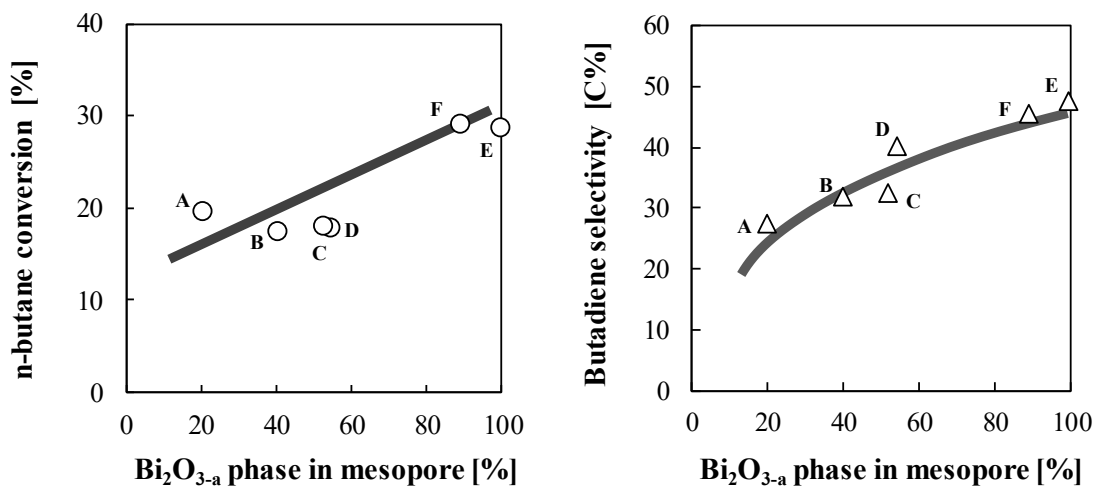
Figure 4.10 Conversion and butadiene selectivity vs Bi_2O_{3-a} (a = 0.2-0.4) phase concentration in mesopore.

The peak intensity of the Bi_2O_{3-a} (a = 0.2-0.4) phase has been correlated to the n-butane conversion and butadiene selectivity as presented in Figure 4.10. For both the conventional and mesoporous silica supported catalysts, an increase in the concentration of the Bi_2O_{3-a} phase increases both the conversion and selectivity. This is an indication that the phase serves as an active phase for dispersing NiO which is active and selective for dehydrogenation to butadiene. The trends of conversion and butadiene selectivity are merely indicated by one trend of butadiene yield as shown in Figure 4.11. It is clear that the Bi_2O_{3-a} phase in mesopore strongly affects butadiene yield.
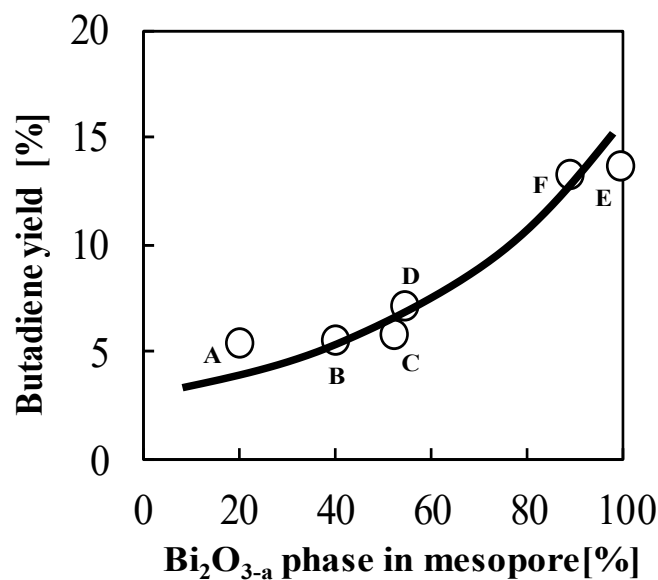
Figure 4.11 Butadiene yield vs Bi_2O_{3-a} phase concentration in mesopore.

4.3.3 Modelling of Reaction and Catalyst

4.3.3.1 Role of support in catalyst preparation

The active species of NiO and BiO_x interact and disperse differently in the different mesoporous silica supports. This interaction generates different active sites and active oxygen supplier for a continuous redox cycle of the active species. The effect of mesoporous silica support is important to NiO on hierarchical NiO-Bi_2O_{3-a} nano-particle cohabitation. The SBA-15 support works with the NiO species to produce Bi_2O_{3-a} and high dispersion of NiO on it.

4.3.3.2 Model of support effect on butadiene ($C_4^{2=}$) selectivity

The schematic representation of the silica support effect on the selectivity to butadiene is shown in Figure 4.12. Conventional SiO_2 supported catalysts mainly have a mixture of beta-Bi_2O_3 and Bi_2O_{3-a} as active oxygen supplier, hence the catalyst showed an

overall high dehydrogenation selectivity but low 1st and 2nd step dehydrogenation selectivity to butadiene. This resulted in relatively high 1-butene desorbed into the gaseous phase because 2nd step dehydrogenation selectivity requires moderate and strong base more than 1st step dehydrogenation selectivity. Mesoporous silica supported catalysts have a highly crystalline Bi_2O_{3-a} phase which acts as active and selective oxygen supplier as well as selective active site (moderate and strong base) for butadiene production. Finally, the catalysts showed very high 2nd step dehydrogenation selectivity and improved overall butadiene selectivity.
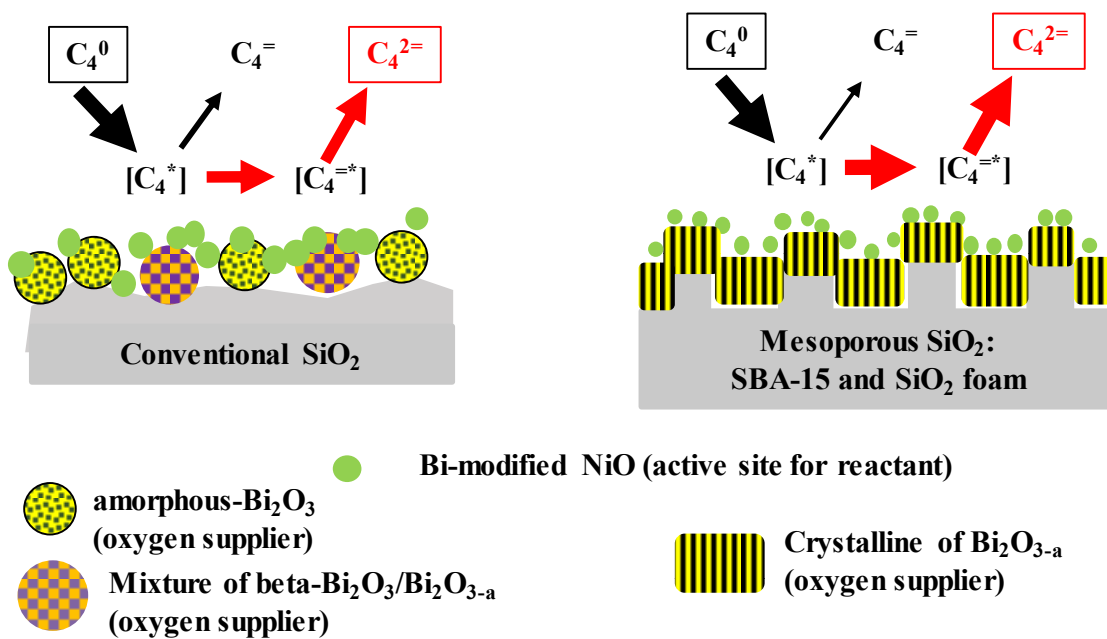
Figure 4.12 Model of reaction and catalyst for oxidative dehydrogenation of n-butane to butadiene over Bi-Ni oxide/SiO$_2$ catalyst

Conclusion

Ni-Bi-O/structured mesoporous (MCM-41, SBA-15, and foam) SiO$_2$ catalysts showed high performance for oxidative dehydrogenation of n-butane to butadiene. The mesoporous SiO$_2$ supports showed enhanced activity and selectivity as compared to

conventional SiO_2 support. The order of butadiene yield is SBA-15 > SiO_2 foam> MCM-41 > conventional SiO_2. The performance is strongly due to the combination of both Bi_2O_{3-a} (a=0.2-0.4) phase as well as strong basic sites with weak/moderate acid sites. SBA-15 catalyst showed the best performance among other mesoporous silica materials due to highly crystalline Bi_2O_{3-a} peak (contained 99.5 % of the Bi_2O_{3-a} phase) as evident from XRD study. The Bi_2O_{3-a} (a=0.2-0.4) phase is oriented along SBA-15 silica lattice as observed from TEM study. The support effect on the catalytic performance directly relates to the BiO_x phase and the hierarchical cohabitation of the Bi-Ni-O active sites.

Acknowledgment

References

[1]   J.C. Gottifredi, E.L. Sham, V. Murgia, E.M. Farfa, Appl. Catal. A: Gen. 312 (2006) 134.

[2]   Y. Xu, J. Lu, M. Zhang, J. Wang, J. Nat. Gas Chem. 18 (2009) 88.

[3]   B.M. Weckhuysen, D.E. Keller, Catal. Today 78 (2003) 25.

[4]   I. Rossetti, G. F. Mancini, P. Ghigna, M. Scavini, M. Piumetti, B. Bonell, F. Cavani, A. Comite, J. Phy. Chem. C. 116 (2012) 22386.

[5]   E. Santacesaria, M. Cozzolino, M. Di Serio, A.M. Venezia, R. Tesser, Appl. Catal. A: Gen. 270 (2004) 177.

[6]   A. Dejoz, J.M. Lopez Nieto, F. Marquez, M.I. Vazquez, Appl. Catal. A: Gen 180 (1999) 83.

[7]   J. K. Lee, H. Lee, U. G. Hong, Y. Yoo, Y-J. Cho, J. Lee, H-S. Jang, J. C. Jung, I. K. Song, J. Ind. Eng. Chem. 18 (2012) 1096

[8]   M.A. Volpe, G.M. Tonetto, H. De Lasa, Appl. Catal. A: Gen. 272 (2004) 69.

[9]   W. Liu, S.K. Lai, H. Dai, S. Wang, H. Sun, C.T Au, Catal. Lett. 113 (2007) 147

[10]   R. Bulanek, A. Kaluzova, M. Setnicka, A. Zukal, P. Cicmanec , J. Mayerova, Catal. Today 179 (2012) 149.

[11]   M. Setnicka, P. Cicmanec, R. Bulanek, A. Zukal, J. Pastva, Catal. Today. 204 (2013) 132.

[12]   X. Wang, G. Zhou, Z. Chen, W. Jiang, H. Zhou, Microporous Mesoporous Mater. 223 (2016) 261.

[13]   C. Wang, J-G. Chen, T. Xing, Z-T. Liu, Z-W. Liu, J. Jiang, J. Lu, Ind. Eng. Chem. Res. 54 (2015) 3602.

[14]   J. Rischard, C. Antinori, L. Maier, O. Deutschmann, Appl. Catal. A: Gen. 511 (2016) 23.

[15]   Y. Zhang, R. Huang, Z. Feng, H. Liu, C. Shi, J. Rong, B. Zong, D. Su, J. Energy Chem. 25 (2016) 349.

[16]   B.R. Jermy, B.P. Ajayi, B.A. Abussaud, S. Asaoka, S. Al-Khattaf, J. Mol. Catal. A Chem. 400 (2015) 121.

[17]   B. R. Jermy, S. Asaoka, S. Al-Khattaf, Catal. Sci. Technol. 5 (2015) 4622.

[18]   G. Tanimu, B. R. Jermy, S. Asaoka, S. Al-Khattaf, J. Ind. Eng. Chem. 45 (2017) 111.

[19]   G. Tanimu, S. Asaoka, S. Al-Khattaf, Mol. Catal. 438 (2017) 245.

[20]   T. Bhuiyan, P. Arudra, M. Akhtar, A. Aitani, R. Abudawoud, M. Al-Yami, S. Al-Khattaf, Appl. Catal. A: Gen 467 (2013) 1025.

[21]   T. Bhuiyan, P. Arudra, M. Akhtar, A. Aitani, R. Abudawoud, M. Al-Yami, S. Al-Khattaf, Can. J. Chem. Eng. 92 (2014) 1271.

[22]   M. A. Ibrahim, M. N. Akhtar, J. Cejka, E. Montanari, H. Balcar, M. Kubu, S. Al-Khattaf, J. Ind. Eng. Chem. 53 (2017) 119.

[23]   A. Palani, A. Pandurangan, J. Mol. Catal. A 226 (2005) 129.

[24]   A. Palani, H-Y. Wu, C-C. Ting, S. Vetrivel, K. Shanmugapriya, A.S.T Chiang, H-M. Kao, Microporous Mesoporous Mater. 131 (2010) 385.

[25]   G. Qi, L. Fu, B. H. Choi, E. P. Giannelis, Energy Environ. Sci. 5 (2012) 7368.

[26]   S. Liu, S. Kang, H. Wang, G. Wang, H. Zhao, W. Cai, Chem. Eng. J. 289 (2016) 219.

[27]   C. J. Gommes, H. Friedrich, M. Wolters, P.E. de Jongh, K. P. de Jong, Chem. Mater. 21 (2009) 1311.

[28]   T. Shimizu, M. Ota, Y. Sato, H. Inomata, Chem. Eng. Res. Des. 104 (2015) 174.

[29]   A. Zukal, H. Siklova, J. Cejka, Langmuir 24 (2008) 9837.

[30]   K. Cheng, M. Virginie, V.V. Ordomsky, C. Cordier, P. A. Chernauskii, M. I. Ivantsov, S. Paul, Y. Wang, A. Y. Khodakov, J. Catal. 328 (2015) 139.

[31]   D. Song, J. Li, J. Mol. Catal. A: Chem. 247 (2006) 206.

CHAPTER 5

New Mesoporous Catalyst System containing Bi₂SiO₅ for n-Butane ODH
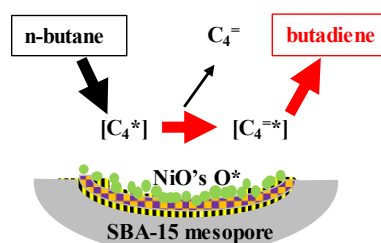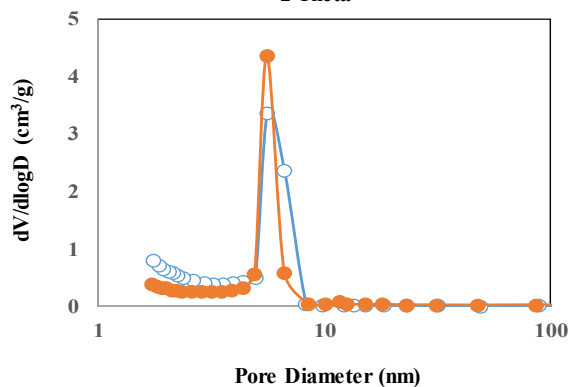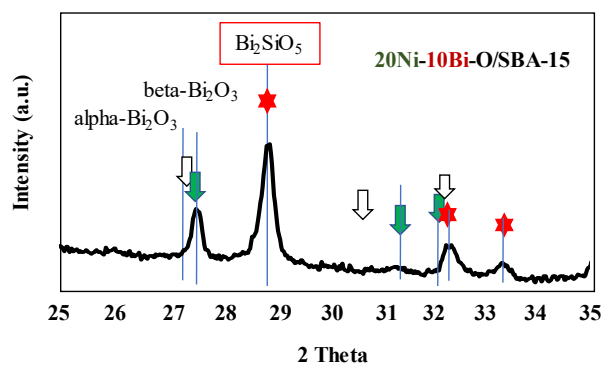
Submitted as:

G. Tanimu, Sachio Asaoka

Microporous and Mesoporous Materials

Abstract

NiO-beta-Bi_2O_3-Bi_2SiO_5/SBA-15 catalysts, containing 10-20 wt% Ni and 10-30 wt% Bi as metal loading on mesoporous SiO_2 support (SBA-15), were utilized for the oxidative dehydrogenation of n-butane to butadiene, comparing from the viewpoint of Bi oxide phase and combination balance with Ni oxide and the support. The phase change between Bi_2SiO_5 and beta-Bi_2O_3 depending on Ni/Bi ratio and loading ratio to the support is mainly due to template effects of Ni and mesoporous SiO_2 support to Bi oxide. The formation degree of oxide phase Bi_2SiO_5 and beta-Bi_2O_3 phase reflected in the butadiene selectivity through changing the reducibility and dispersion properties. The catalyst with moderate loading of both Ni and Bi exhibited a high advantage in the n-butane conversion and butadiene selectivity to the less and excess loaded catalysts. Increasing Ni loading resulted in higher activity, while increasing Bi loading led to improved butadiene selectivity. The catalytic performance of other mesoporous support catalysts depended on Ni and Bi loading. The characteristics of the catalysts agreed with their performance in the view of the catalytic scheme for selective production of butadiene via butenes.

Keywords: n-butane; dehydrogenation; butadiene; SBA-15; Bi_2SiO_5.

5.1 Introduction

The global demand for butadiene in the manufacturing of synthetic rubber was about 12.3 million tons in 2018 and it is expected to grow by 4.5 % annually during the next five years [1]. On-purpose production methods have been investigated to supplement the decrease in butadiene supply due to the shift from naphtha to ethane crackers. Oxidative dehydrogenation (ODH) reaction is one of the promising methods aimed at bridging the gap between the growing demand and supply of butadiene. Many researchers have investigated n-butane oxidative dehydrogenation to butenes/butadiene using mainly vanadia/molybdena on metal oxides supports [2-10]. The function of the catalysts in the first (butane to 1-butene/2-butenes) and second (butenes to 1,3-butadiene) step dehydrogenations is not well discussed in those literatures.

Our prior studies [11-14] utilized nanoparticles of Ni-Bi-O species deposited on commercially available Al_2O_3, SiO_2, and ZrO_2 for the ODH of n-butane with high selectivity to butadiene. The contribution of Bi oxide in stabilizing the NiO nanoparticles selective to butadiene [11], role of calcination (two steps of 350 and 590 ℃ in air) in controlling the Bi oxide phase formations [12], and the synergetic effects of NiO modification by partial substitution with Co and Fe [13], have been reported. The role of support in controlling the redox character of the active species, metal-support interaction and acid-base properties have been highlighted [14]. In an advanced studies on the effect of supports, an enhanced performance was obtained with SiO_2 sol supported catalyst compared to the unsupported, Al_2O_3 and ZrO_2 gel supported catalysts or the sol supported ones.

114

Mesoporous silica support showed enhanced performance in catalytic applications through stabilizing the performance of the impregnated metal oxides nanoparticles with a uniform dispersion. This is mainly due to their ordered structure, high surface area, high chemical and thermal stabilities, and well-defined pore sizes [15-18]. Mesoporous silica supports (MCM-41, SBA-15, and silica foam) were utilized in the synthesis of highly-dispersed tungsten oxide catalyst for butene metathesis reaction [19-21]. Nanoparticles of vanadium deposited on mesoporous silica supports have been utilized for the ODH of n-butane [22-26]. Supports of highly ordered mesoporous silica (SBA-15, silica foam, and MCM-41) loaded with 20wt% Ni and 30wt% Bi, were also utilized in our previous study [27]. The binary-oxide impregnated catalysts were probed for n-butane ODH to butadiene and compared with traditional silica gel catalysts. Mesoporous silicas as catalyst support are superior to the traditional silica gels, where the mesoporous silica SBA-15 supported catalyst gave the best performance [27]. As a follow-up to the previous investigations, the SBA-15 supported catalysts have been studied in this paper from the viewpoint of Bi oxide phase and combination balance with Ni oxide and mesoporous silica support. The silica foam, the silica sol, and the traditional silica gel catalysts have been utilized in this study as references.

5.2   Experimental Section

5.2.1 Catalyst Preparation

Si-SBA-15 carrier was prepared using tri-block copolymer as a structure directing agent. 4 g of Pluronic P123 was introduced into 30 ml of de-ionized water. Stirring continued until clear solution was achieved. 70 g of 0.28 M HCl was added to the solution with continuous stirring for 2 h. 9 g of TEOS was introduced and stirring continued for 24

h at 40 ℃ and finally heated for 48 h at 100 ℃. Filtration was utilized in recovering the solid product, de-ionized water was used several times for washing the residue and then dried at 100 ℃ overnight. Calcination was done at 550 ℃ for 6 h for template removal [28]. The other mesoporous silicas used were silica gel Q10 was procured from Fuji Silysia Chemicals Limited, Japan. Si-MCM-41 was prepared using the method obtained in the literature [29]. The procedure reported by Qi et al [30] was used in preparing silica foam, and silica sol was purchased from Sigma Aldrich.

Co-impregnation technique of equilibrium adsorption with enforced deposition was utilized in synthesizing all the supported catalysts to reduce waste streams [31]. $Ni(NO_3)_2 \cdot 6H_2O$ (99 %, Fisher Scientific) and $Bi(NO_3)_3 \cdot 5H_2O$ (98 %, Fluka Garantie) were utilized as Ni and Bi precursors, respectively. In a typical synthesis, 0.99 g of Ni precursor was dissolved in 80 ml of de-ionized water. 0.70 g of Bi precursor was introduced after dissolution with continuous stirring. 1.0 g of the support was added for impregnation. The mixture was left overnight for equilibrium adsorption of Bi species and followed by evaporative drying at 80 °C for Ni species enforced deposition. The product was further dried at 120 °C for 3 h and calcined in two steps at 350 °C for 1 h and 590 °C for 2 h at the rates of 10 °C/min and 15 °C/min, respectively.

5.2.2 Catalyst Testing

ODH reaction of n-butane was conducted in an automated fixed-bed reactor obtained from Microtrac Bel Company, Japan. 300 mg of the synthesized catalyst was introduced into the reactor to form the catalyst bed. The contact time of n-butane was maintained at 0.42 h·g/mol. The total reactants flow rate was kept at 31.2 ml/min. The performance of the catalysts were evaluated at 400 °C and $O_2/n\text{-}C_4H_{10} = 1.0$, 2.0 and 4.0 mol/mol and then

followed by 450 °C (O_2/n-C_4H_{10} = 2.0 mol/mol) and 500 °C (O_2/n-C_4H_{10} = 2.0 mol/mol). The total time on stream is about 5 h. Products analyses was achieved with an online gas chromatograph (GC) system (Agilent, 7890N). FID and GC-Gas Pro capillary column (L: 60 m and ID: 0.32 mm) was used in analyzing the hydrocarbons and oxygenates. Gases including CO_x, N_2, O_2, and H_2, were identified using TCD and Shin Carbon 80/100 mesh SS column having He as a carrier and MS5A 60/80 mesh SS column with Ar as carrier. Standard samples were used for confirming the products. The conversion of n-butane and the selectivities of the products were obtained using based on carbon mass balance.

5.2.3   Characterization of Catalysts

The BET surface area and pore characteristics were obtained using N_2 adsorption-desorption isotherm with Micromeritics ASAP 2020 instrument, Norcross, GA. BJH adsorption method was used in obtaining the pore volume, pore surface area, and average pore diameter. The XRD patterns of the calcined catalysts were measured in the 2θ range of 5 ° to 90 ° with a Rigaku Miniflex II desktop X-ray diffractometer utilizing Cu Kα radiation at a wavelength of λ=1.5406 Å and operating parameters of 30 mA and 40 kV with a step size of 0.02 ° and speed of 0.5 °/min. A high-resolution transmission electron microscope (JEM-2100F model) having an acceleration voltage of 200 kV was used in analyzing the morphologies of the catalysts. TPR was used in determining the catalysts reducibility. This was achieved using BEL-CAT-A-200 chemisorption instrument [27]. A gas mixture of Ar/H_2 (95/5 vol%) with a total flow rate of 50 cm^3/min was used in the TPR measurement. 100 mg of the catalyst was preheated at 300 °C for 3 h under inert He atmosphere and then cooled to room temperature. It was then increased up to 1000 °C at the rate of 20 °C /min. The intake of H_2 was measured with TCD and CuO was utilized as

a reference for H_2 consumption calibration. The catalysts binding energy and bonding states were analyzed using X-ray photoelectron spectroscopy (XPS) with a PHI 5000 Versa Probe II, ULVAC-PHI Inc. spectroscope. The samples were disc-pelletized and put under a high vacuum prior to the XPS measurement.

5.3   Results and Discussion

5.3.1 Catalyst Properties

5.3.1.1 Surface area and porosity

The dispersion of active sites is mainly determined using the specific surface area and pore structure of the catalysts [32]. The surface areas calculated using the BET equation in the linear region of the N_2 adsorption-desorption isotherms (P/P_o = 0.05-0.3), pore volumes and the average pore diameters of the various catalysts calculated using the BJH method, are presented together with the support values in Table 5.1. A decrease in surface area was observed for all the catalysts compared to that of the support. The same trend was also observed in the catalysts pore structure. However, their values adjusted to support weight base showed increased or not much-reduced values with the exception of SBA-15 supported catalyst.

Table 5.1 Catalysts and supports physical properties.

Catalyst: (Support)	BET surface area		Pore surface area		Pore volume		Average pore diameter
	$[m^2/g\text{-}catalyst]^a$	$[m^2/g\text{-}support]^b$	$[m^2/g\text{-}catalyst]^c$	$[m^2/g\text{-}support]^d$	$[cm^3/g\text{-}catalyst]^e$	$[cm^3/g\text{-}support]^f$	$[nm]^g$
CSGM (SiO$_2$ gel: SGM)	158	251 (242)	171	272 (263)	0.71	1.13 (1.22)	16.8 (18.6)
CSB (SBA-15: SB)	269	427 (657)	309	491 (1080)	0.33	0.52 (1.08)	4.2 (4.1)
CSF (SiO$_2$ foam: SF)	388	616 (540)	397	630 (554)	1.55	2.46 (2.27)	15.6 (16.4)
CSS (SiO$_2$ sol)	91	144	87	138	0.64	1.02	29.1

The definition of the notations: a, b, c, d, e, f, and g can be found elsewhere [14]

The N$_2$ adsorption-desorption isotherm of the Ni-Bi-O/SBA-15 catalyst (normalized to support weight) and SBA-15 support is presented in Figure 5.1(a) while the pore size distribution (normalized to support weight) using the adsorption branch isotherm is shown in Figure 5.1(b). The isotherms are typical of type IV of the IUPAC classification due to the existence of the type H1 hysteresis loop, which is common for mesoporous materials having a well-defined cylindrical-like pore channel [32]. Adsorption and desorption paths of the isotherm coincide at low relative pressure (up to $P/P_o \approx 0.5$) which is an indication that there exists monolayer-multilayer adsorption [33]. The beginning of the hysteresis

loop signifies capillary condensation within the pores, and its end corresponds to the filling of the pores. Metal loading resulted in the decrease in the height of the loop due to pore volume decrease caused by the introduction of metal species within the support mesopore [34]. The pore size distribution gave a sharp peak for both the support and the catalyst indicating a narrow mesopore size distribution, typical of mesoporous SBA-15 material [34, 35].
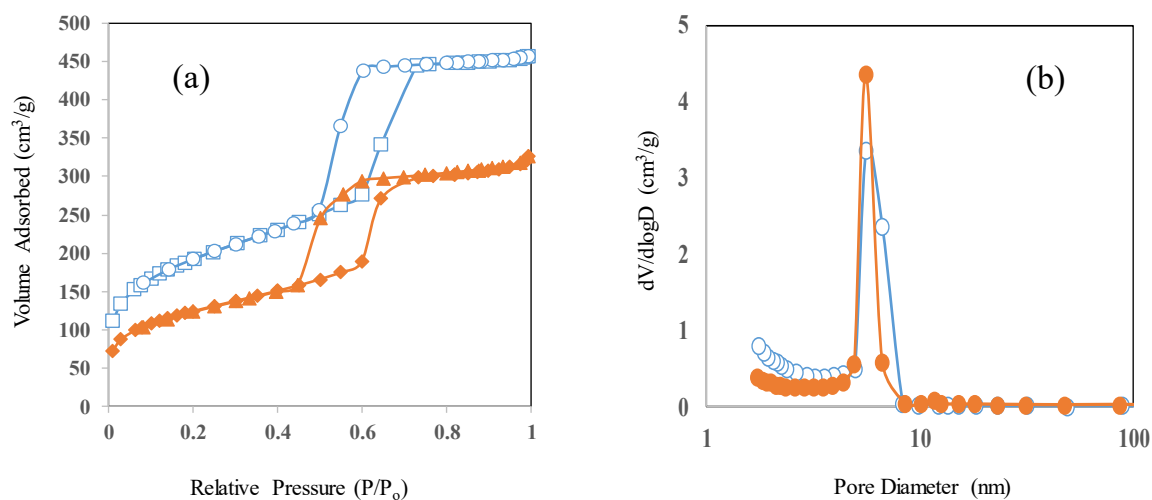
Figure 5.1 (a) N_2 adsorption-desorption isotherm; (b) pore size distribution (Blue/unfilled: SBA-15, Red/Filled: Ni-Bi-O/SBA-15).

The pore size distribution was divided into three regions to carefully examine the effect of the metal loading on the support. The pore surface area and pore volume of the support and catalyst are presented in Table 5.2. The pore surface area and the pore volume of the catalysts reduced to almost 50 % of the support. The main reduction is observed in the region of lower pore diameter (1.7-3.9 nm). An approximately 1.1 nm thickness of the pore inside surface of the support has been covered by the metal oxides impregnation.

Table 5.2 Pore size distribution of Ni-Bi-O/SBA-15 catalyst and support.

Material	Support: SBA-15		Catalyst: Ni-Bi-O/SBA-15	
Pore diameter (nm)	Pore surface area (m^2/g)	Pore volume (cm^3/g)	Pore surface area $(m^2/g\text{-support})$	Pore volume $(cm^3/g\text{-support})$
1.7-3.9	714 (66.1)	0.523 (48.4)	213 (43.2)	0.096 (18.5)
3.9-5.6	60 (5.5)	0.066 (6.1)	53 (10.9)	0.060 (11.5)
5.6-266	306 (28.4)	0.491 (45.5)	225 (45.9)	0.364 (70.0)
Total	1080 (100)	1.080 (100)	491 (100)	0.520 (100)

The surface area, pore volume and the average pore diameter of the catalysts with reduced Ni and/or Bi loading can be found in the supplementary material [S1]. All the catalysts exhibited a reduced surface area and pore volumes compared to the supports. The average pore diameter remained unchanged in all the catalysts.

5.3.1.2 X-ray diffraction

The X-ray diffraction (XRD) patterns related to Bi oxide species for the mesoporous and conventional silica supported catalysts are presented in Figure 5.2. The XRD patterns were recorded from a diffraction angle of $2\theta = 5$ to 90 °. Then, $2\theta = 25$ to 35 ° was selected to examine the phases of Bi oxide in the different catalysts precisely. For the conventional SiO_2 supported catalyst, the main peaks are attributed to beta-Bi_2O_3 and Bi_2SiO_5 at $2\theta =$

27.38 º and 29.0 º respectively. This new phase was previously assigned as Bi_2O_{3-a} in our previous report [27]. However, this has been confirmed as bismuth silicate phase (JCPDS 00-0287), resulting from the interaction of Bi oxide and silica support. All the characteristic peaks associated with this new phase have been successfully identified in the silica sol supported catalyst and the mesoporous (SBA-15 and silica foam) supported catalysts. A pure Bi_2SiO_5 phase with peaks at $2\theta = 28.95$ º, 32.33 º and 33.38 º with (3,1,1), (0,2,0) and (0,0,2) diffraction lines, respectively, were identified in Ni-Bi-O/SBA-15 catalyst. This new phase assignment as Bi_2SiO_5 agreed with the reports in the literature [36-40].
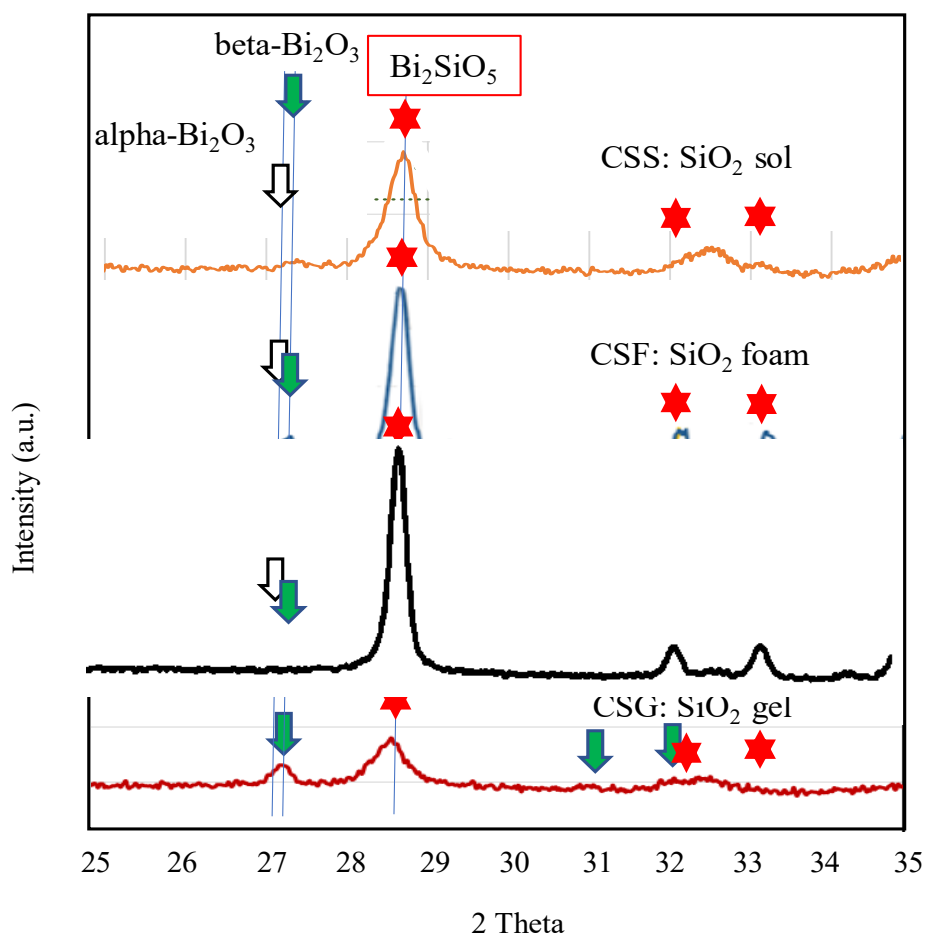
Figure 5.2 X-ray diffraction profiles for support species in 20wt%Ni-30wt%Bi-O catalyst: micro-mesoporous SiO_2: CSS, CSG, CSB, CSF

To further study the degree of formation of the new Bi_2SiO_5 phase, the metal loadings of Ni and Bi on SBA-15 were varied and the results are presented in Figure 5.3. The extent of the new phase formation depended on the presence of Ni and mainly Bi species. For NiO/SBA-15 catalyst, only NiO phase (JCPDS 00-1159) diffraction peaks at $2\theta = 36.8\,^{\circ}$ and $42.9\,^{\circ}$ were identified. BiO_x/SBA-15 showed two main diffraction peaks for beta-Bi_2O_3 and Bi_2SiO_5. The ratio of beta-Bi_2O_3 and Bi_2SiO_5 varied according to the Ni and Bi loadings on the SBA-15 support. An optimum loading for pure Bi_2SiO_5 phase is the 20 wt% Ni and 30 wt% Bi on SBA-15 as presented in Figure 5.2.
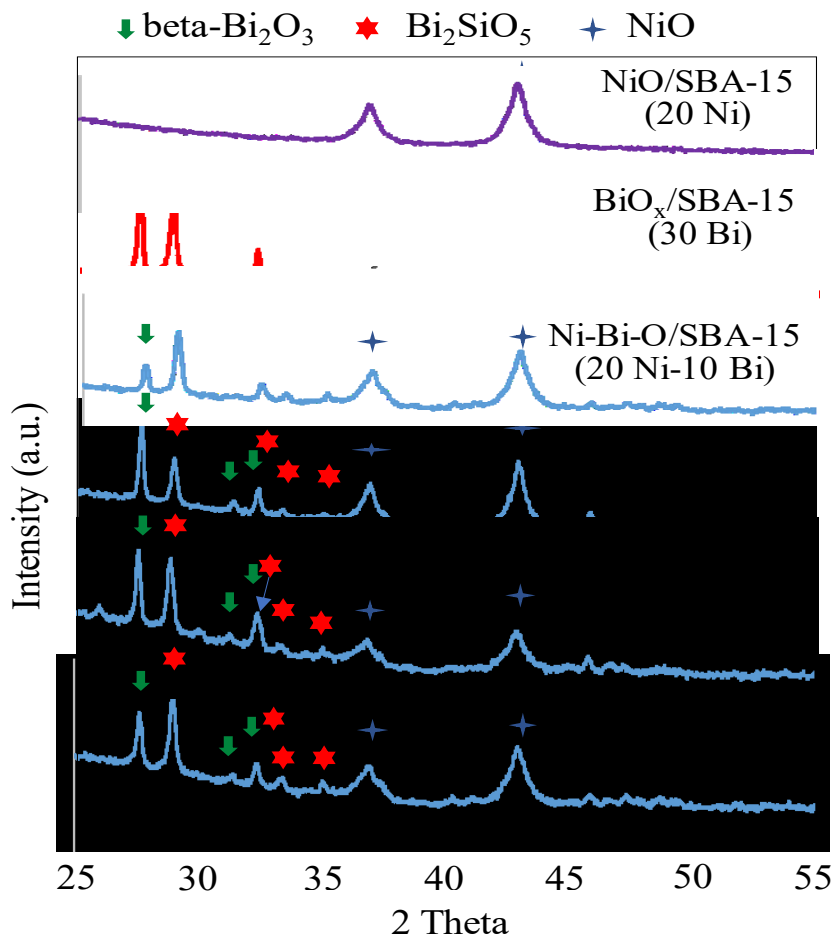
Figure 5.3 X-ray diffraction patterns for loaded species in NiO/SBA-15, BiO_x/SBA-15, and Ni-Bi-O/SBA-15 catalysts.

5.3.1.3 Temperature programmed reduction

Temperature programmed reduction (TPR) was utilized to determine the level of active species reducibility (reduction temperature and extent of reduction) which is very significant for catalysts activity and selectivity to butadiene. H_2-TPR profiles of the mesoporous silica supported catalysts are presented in Figure 5.4, and was compared with conventional silica gel and sol catalysts.
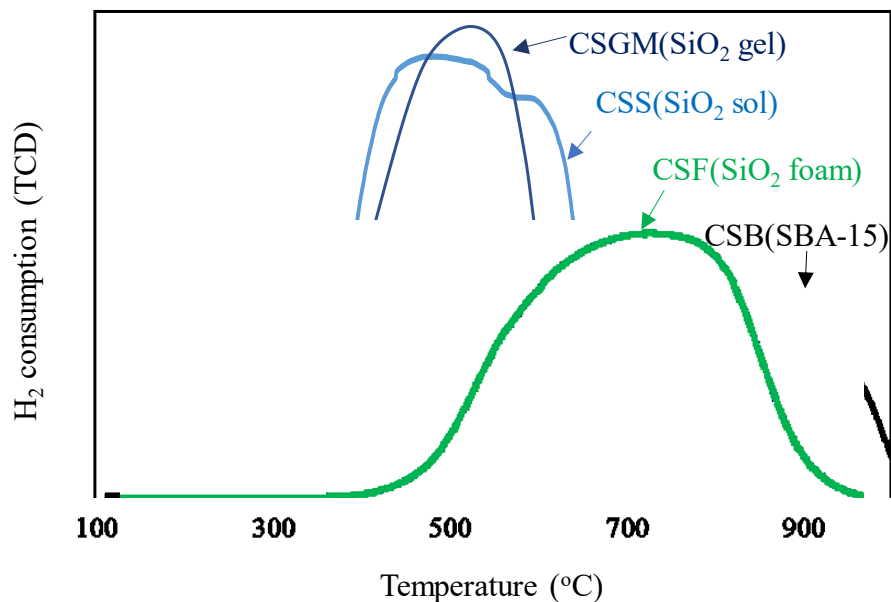
Figure 5.4 TPR profile for support species in Ni-Bi-O catalyst: CSGM (Silica gel), CSS (Silica sol), CSB (SBA-15) and CSF (SiO$_2$ foam)

SiO$_2$ gel supported catalyst (CSGM) showed a reduction peak of high intensity at 500 °C and a small reduction peak from 625 °C to 700 °C. This ease of reduction indicates the presence of NiO and BiO$_x$ species with large particles and having weak metal-support interaction. The SiO$_2$ sol supported catalyst showed a similar pattern with SiO$_2$ gel catalyst even though it produced a shoulder peak with high intensity aside from the main peak at 500 °C. Mesoporous supported catalysts (CSB and CSF) however produced a broad peak at higher reduction temperature indicating the formation of non-reducible Bi$_2$SiO$_5$ species (caused by the strong interaction of Bi oxide species with mesoporous supports). This confirmed the existence of surface heterogeneity which is having more than one species contributing to the overall reduction process [32]. The amount H$_2$ consumed by the various catalysts is presented in Table 5.3. The values were based on the three temperature reduction ranges (low temperature, medium temperature, and high temperature) depicted

by the catalysts. The overall hydrogen consumption depended on the availability of easily reducible oxide species that are weakly bonded to the support surface. The medium temperature region reflects the stability of the redox cycle for dehydrogenation

Table 5.3 Amount of H_2 consumed in TPR of supported 20wt%Ni-30wt%Bi-O catalysts.

| Catalyst (Support) | Amount of H_2 consumed [m mol/g] (T_M [ºC]) | | | |
	I (350-550 ºC)	II (550-650 ºC)	III (650-850 ºC)	Total
CSGM(SiO$_2$ gel)	3.74	1.12	0.13	4.99
CSB (SBA-15)	0.88	1.04	2.43	4.35
CSF (Foamed SiO$_2$)	0.70	1.01	2.51	4.22
CSS (SiO$_2$ sol)	3.75	1.10	0.38	5.23

The TPR profile comparison for conventional SiO$_2$ gel supported catalyst (20 wt% Ni-30 wt% Bi/SiO$_2$ gel) and a catalyst formed using equilibrium adsorption (5 wt% Ni -30 wt% Bi/SiO$_2$ gel) as previously reported [14], is shown in Figure 5.5. The EQA catalyst contained a reduced amount of NiO species, hence the main component present is Bi oxide species. Two Bi species exist on the support surface which are Bi$_2$O$_3$ and Bi$_2$SiO$_5$ and these are responsible for the two distinct reduction peaks at 500 °C and 700 °C, respectively. The reduced Ni amount resulted in a stronger anchoring of Bi species on the support. This has increased the difficulty in reducibility of the EQA catalyst compared to the conventional silica supported catalyst.
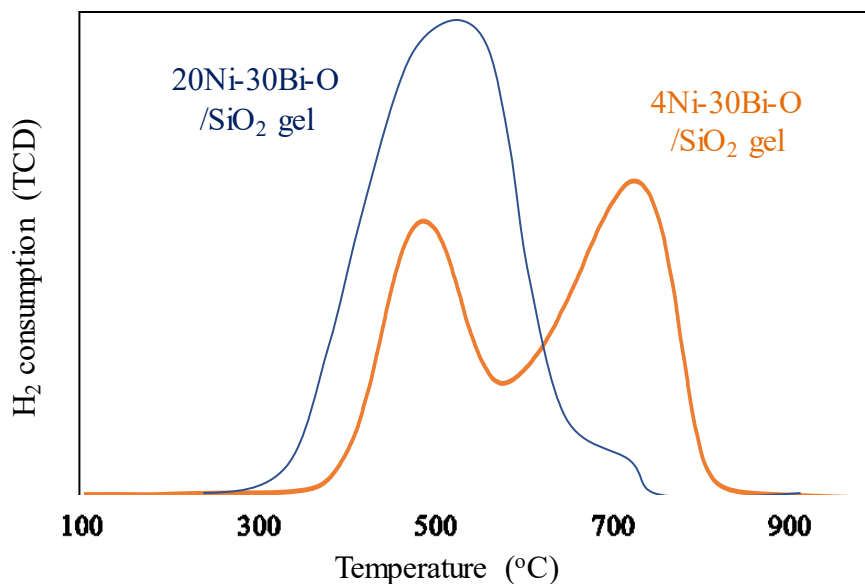
Figure 5.5 TPR profile for impregnation method in Ni-Bi-O, catalyst: CSGM (SiO_2 gel) and EQA-CSGM (SiO_2 gel).

To further study the reduction profile of mesoporous support and its interaction separately with the active metal species, TPR measurement was carried out on NiO/SBA-15 and BiO_x/SBA-15 and the result is presented in Figure 5.6. Structured SBA-15 can anchor both Ni and Bi species strongly more than the conventional silica. The TPR profile showed the difficulty in the reducibility of NiO and Bi oxide species on SBA-15 separately still remained after co-impregnation. It is evident that oxygen species of NiO are strongly bound to the support surface. Similarly, the Bi oxide deposition on the support led to the formation of two species similar to the case of EQA catalyst. This also agrees with the XRD profiles discussed earlier. The TPR profiles of the various combination of Ni and Bi oxides on SBA-15 support are shown in Figure S1 (Supplementary information). All the profiles followed the same pattern indicating a stable active species redox cycle.
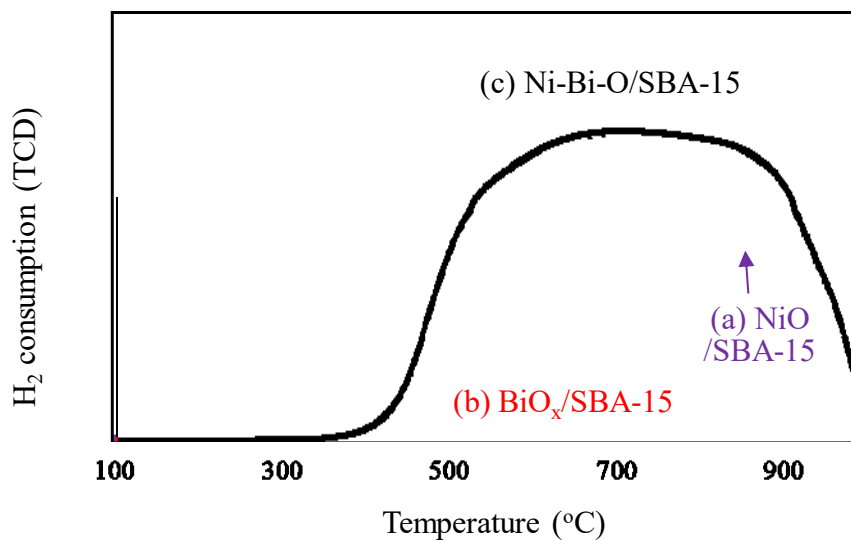
Figure 5.6 H$_2$-TPR profiles for catalysts of Ni-Bi-O over SBA-15: (a) 20wt% Ni-O, (b) 30 wt% Bi-O and (c) 20 wt% Ni-30 wt% Bi-O

5.3.1.4 X-ray photoelectron spectroscopy

The chemical states and dispersion of the active metal oxide species in the catalysts were examined using x-ray photoelectron spectroscopy (XPS) using the Ar-etching method. The XPS spectra are presented in Figure 5.7. The spectra showed before (upper layer) and after (lower layer) etching spectrum of Bi and Ni species. Surface Bi species showed XPS peaks of Bi 4f$_{7/2}$ at 158.9 eV and 4f$_{5/2}$ at 164.3 eV which gave good agreement with reference data of Bi$_2$O$_3$ [41], identified as beta phase using XRD result. Inner surface Bi species showed XPS peaks of Bi 4f$_{7/2}$ at 158.4 eV and 4f$_{5/2}$ at 163.8 eV have 0.5 eV decrease of binding energy from reference data of Bi$_2$O$_3$, which was assigned as Bi$_2$SiO$_5$ phase using XRD result. Bi in this phase is slightly reduced to lower valency like Bi$_2$O$_{3-a}$ where a is estimated around 0.6 based on decreasing percentage to Ni metal's value.

128

Surface Ni species showed XPS peaks of Ni 2p$_{3/2}$ at 854.4 eV which also gave good agreement with reference data of NiO [42], which is identified as nano-particle NiO using XRD result. Inner surface Ni species showed XPS peaks of Ni 2p$_{3/2}$ at 853.7 eV having 0.7 eV decrease of binding energy from reference data of NiO, which was assigned for partially reduced NiO phase using XRD result. Ni in this phase is slightly reduced to lower valency like NiO$_{1-b}$ where b is estimated around 0.4 based on decreasing percentage to Ni metal's value.
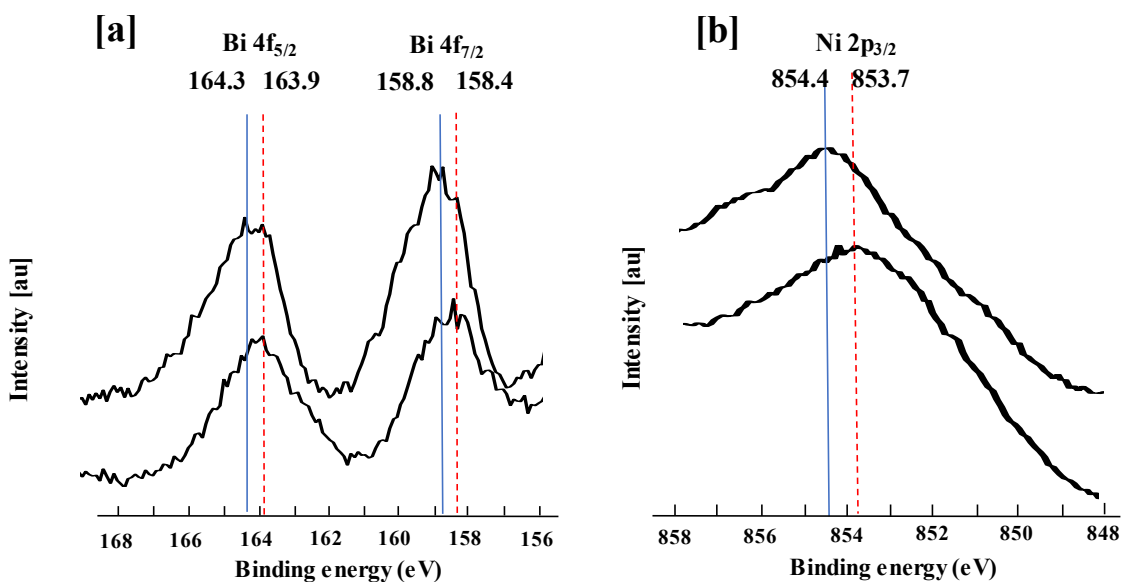
Figure 5.7 XPS study for catalysts of 20 wt% Ni- 30 wt% Bi-O over SBA-15: [a] Bi [b] Ni, upper: surface, lower: inner surface.

5.3.1.5 High-resolution transmission electron microscopy (HRTEM)

The HRTEM image of SBA-15 supported catalyst as presented in Figure 5.8 shows the size and morphology of the highly ordered pores in an array with long 1D channels. The HRTEM image agrees with the result of pore distribution measurement by N_2 adsorption. A lattice spacing of 0.21 nm which corresponded to that of NiO has already been presented previously [27]. NiO is dispersed mainly not directly on SBA-15, but through Bi species phase in SBA-15. This means that the three oxides, (i) silica ordered in SBA-15 mesopore, (ii) Bi_2SiO_5 (and beta-Bi_2O_3) ordered on the silica of SBA-15 in the mesopore and (iii) Ni oxide species dispersed on the Bi species phase form into hierarchically layered catalyst system.
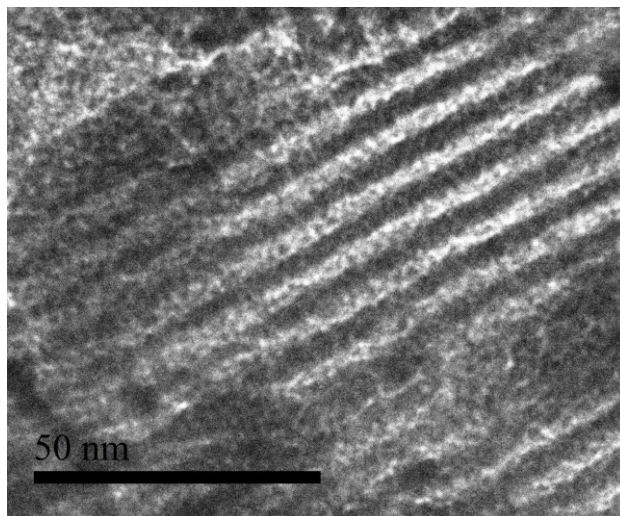
Figure 5.8 High-resolution transmission electron microscopy (HRTEM) micrographs of SBA-15 mesoporous silica catalyst.

5.3.2 Catalyst Performance Evaluation

The proposed conversion route from the n-butane to the main product together with the byproducts is presented in Figure 5.9. The major pathways are the 1st dehydrogenation from n-butane to butenes (1-butene and 2-butene), 2nd step dehydrogenation to butadiene, and cracking (to mainly ethylene, propylene, methane, CO, and CO_2). The selectivity to either dehydrogenation or cracking pathways depend on the strength of the acid and basic sites. The role of the active metal oxide species in enhancing the production of the desired product is discussed in the next section.
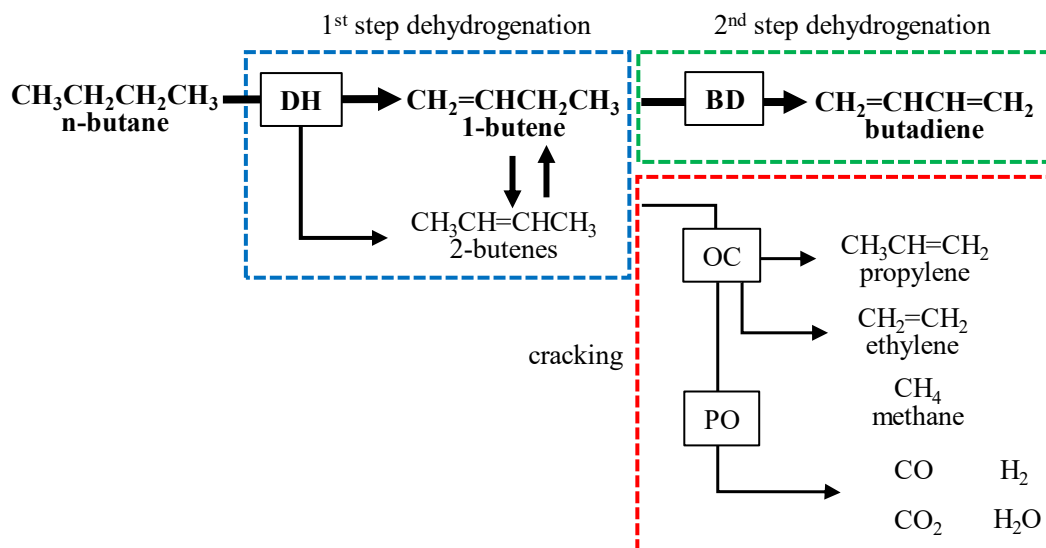
Figure 5.9 Conversion route from the n-butane to the products including co-product formation.

5.3.2.1 Effect of bismuth oxide loading

The effect of Bi species amount available on the mesoporous SBA-15 support surface on the catalyst performance is presented in Table 5.4. Reducing BiO_x species increased the ratio of the $Bi_2SiO_5/\beta\text{-}Bi_2O_3$ species as depicted by XRD measurements. The presence of

bismuth silicate species improved NiO species dispersion thereby enhancing the catalyst activity with selectivity towards both 2nd step dehydrogenation and cracking pathways.

Table 5.4 Comparison of Ni/Bi as the metal amount in the supported catalysts.

Catalyst	HN-HB	HN-LB	MN-LB	LN-LB
Support	SBA-15	SBA-15	SBA-15	SBA-15
Ni/Bi [wt%]/[wt%] (Ni/Bi atomic ratio)	20/30 (2.4)	20/10 (7.2)	14/10 (5.0)	10/10 (3.6)
n-C_4H_{10} conversion [%]	28.9	30.0	27.7	23.5
Selectivity[*1] [C%]				
DH	75.2	71.8	78.4	83.5
2-C_4H_8	15.4	14.6	15.0	17.8
1-C_4H_8	12.3	7.8	10.2	11.2
BD	47.5	49.4	53.2	54.5
PO	24.8	28.2	21.6	16.5
OC	19.7	28.2	17.1	12.1
CO	5.1	0.0	4.5	4.4
(1-C_4H_8 + BD)[*2]	59.8	57.2	63.4	65.7
BD/(1-C_4H_8 + BD) %[*3]	79.4	86.3	83.9	82.9
BD yield	13.7	14.8	14.7	12.8

5.3.2.2 Effect of nickel oxide loading

The effect of reducing the amount of NiO species deposited on the support is presented in Table 5.4. The activity of the catalysts reduced with a successive reduction in NiO amount, which reduces the selectivity of the catalyst towards the undesired cracking products. However, the dehydrogenation (and butadiene selectivity) increased mainly because of the increase in the ability of the BiO_x to effectively disperse the NiO species for stable and continuous performance.

5.3.2.3 Effect of Bi-loading on Bi-phase and Performance of Mesoporous SiO_2 Catalysts

The amount of Bi was reduced from 30 wt% to 10 wt% to investigate the NiO active species dispersion ability through dispersed BiO_x of the different mesoporous support. The results are presented in Table 5.5. Reducing Bi amount changed the surface concentration of the BiO_x species on the support that influenced the resultant dispersion of NiO. A sol-type and gel-type conventional silica supported catalysts were included for comparison with the different mesoporous supports. For the sol-type silica supported catalyst, the activity of the catalyst remained unaffected with a reduction in Bi amount while the dehydrogenation selectivity and butadiene selectivity were greatly decreased. It is an indication that the reduction in the surface of dispersed BiO_x on silica sol affects the dispersion and ease of reducibility of NiO species. For the gel-type supported catalyst, the catalyst activity improved with reduction of Bi amount indicating that for effective NiO dispersion, low Bi is enough. The increased activity reflected in increasing OC products selectivity with a reduced dehydrogenation selectivity. The selectivity for butadiene is similar for the two catalysts even though there is an improved 2nd step dehydrogenation selectivity with the

133

reduced Bi amount resulting from increased 1-butene adsorption. Hence yield of butadiene greatly improved for the reduced Bi amount among the gel-type supported catalyst.

For the mesoporous silica foam supported catalyst, conversion was increased with a reduction in Bi amount but DH selectivity (and BD selectivity) decreased. OC selectivity increased due to increase in NiO concentration on the catalyst surface. The 2nd step dehydrogenation selectivity slightly improved while the overall butadiene yield remained unchanged. In the case of SBA-15 supported catalyst, the activity remained the same for both cases, but dehydrogenation selectivity improved slightly. OC selectivity also increased due to an increase in NiO dispersion on the surface which interacts with oxygen species active for cracking reactions. Due to the fact that SBA-15 support has high dispersion ability and NiO adsorption capacity, the 2nd step dehydrogenation selectivity and butadiene yield were improved even with the reduction in Bi amount.

Table 5.5 Comparison of Bi/Ni 0.42 to 0.14 as sub metal amount in Ni-Bi-O/support catalysts.

Catalyst	CSGM-LB (CSGM)	CSB-LB (CSB)	CSF-LB (CSF)	CSS-LB (CSS)
Support	SiO_2 gel	SBA-15	SiO_2 foam	SiO_2 sol
Bi/Ni	0.14 (0.42)	0.14 (0.42)	0.14 (0.42)	0.14 (0.42)
n- C_4H_{10} conversion [%]	**29.3 (17.6)**	**30.0 (28.9)**	**34.1 (29.2)**	**35.7 (35.6)**
Selectivity*[1] [C%]				
DH	67.5 (79.1)	71.8 (75.2)	69.0 (77.6)	57.4 (78.3)
2- C_4H_8	16.6 (21.7)	14.6 (15.4)	18.8 (17.2)	11.3 (18.6)
1- C_4H_8	18.0 (25.5)	7.8 (12.3)	11.4 (14.8)	11.1 (18.1)
BD	**32.9 (31.9)**	**49.4 (47.5)**	**38.8 (45.6)**	**35.0 (41.6)**
PO	32.6 (20.9)	28.2 (24.8)	31.0 (22.4)	42.6 (21.6)
OC	26.7 (17.5)	28.2 (19.7)	30.5 (21.0)	41.2 (20.5)
CO	5.9 (3.4)	0.0 (5.1)	0.5 (1.4)	1.4 (1.1)
(1- C_4H_8 + BD)*[2]	50.9 (56.4)	57.2 (59.8)	50.2 (60.4)	46.1 (59.7)
BD/(1- C_4H_8 + BD) %*[3]	64.6 (55.6)	86.3 (79.4)	77.3 (75.4)	76.0 (69.7)
BD yield	**9.6 (5.6)**	**14.8 (13.7)**	**13.2 (13.3)**	**12.5 (14.8)**

*[1], *[2] and *[3] are same as reported previously [27]

5.3.3 Modeling of Catalyst Character and Performance

The schematic representation of the effect of SBA-15 support, its interaction with the metal oxide species, and the effect of varying the amount of the active species on the selectivity to butadiene is shown in Figure 5.10. The production of butadiene depended on the formation of active Bi_2SiO_5 and β-Bi_2O_3 species due to their role in active oxygen supply and stabilizing the NiO species for the successive dehydrogenations at low cracking. The

proposed model for the selective production of butadiene from n-butane is shown in Figure 5.11.

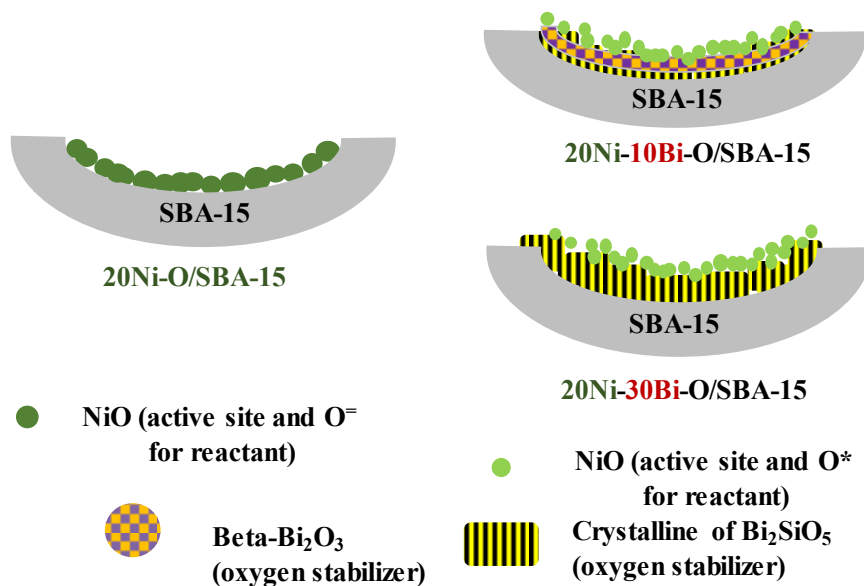Figure 5.10 Preparation scheme for Bi-Ni oxide/SBA-15 catalyst: Effect of support and NiO on hierarchical NiO-Bi$_2$SiO$_5$ nano-particle cohabitation.
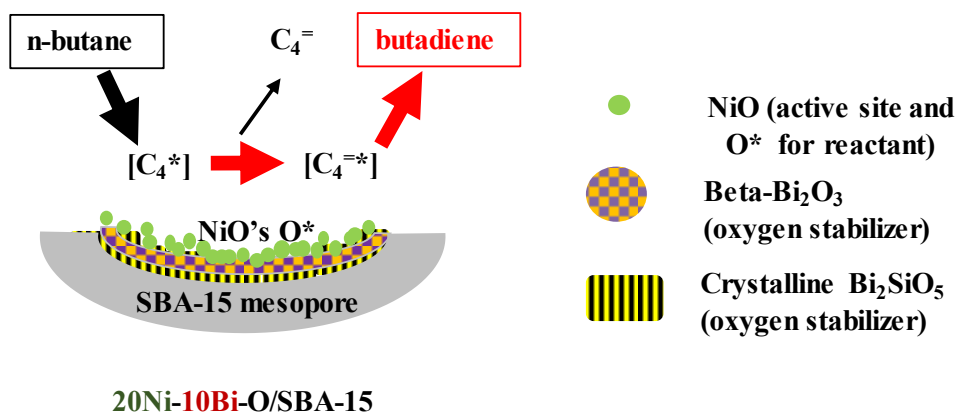

Figure 5.11 Model for a selective butadiene production from n-butane on SBA-15 supported catalyst.

Conclusion

NiO-beta-Bi_2O_3-Bi_2SiO_5/SBA-15 catalyst system showed good performance in the oxidative dehydrogenation of n-butane to butadiene, resulting from the formation of Bi_2O_3 and Bi_2SiO_5 phases on the catalyst. The change in phase between Bi_2SiO_5 and beta-Bi_2O_3 was determined by the Ni/Bi ratio and loading ratio to the support due to the template effects of Ni and mesoporous SiO_2 support to Bi oxide. The formation degree of oxide phase Bi_2SiO_5 and beta-Bi_2O_3 phase reflected in the butadiene selectivity through reducibility and dispersion properties as evident from TPR and XRD studies. The catalyst with moderate loadings of both Ni and Bi exhibited a clear superiority in the catalytic performance compared to the other catalysts. The increase of Ni loading resulted in increased activity, while the increase of Bi loading led to the butadiene selectivity improvement. The catalytic performance of other mesoporous support catalyst also depends on Ni and Bi loaded amount. The catalyst characteristics agree with the catalytic performance in the view of the proposed scheme for selective production of butadiene via intermediate butenes.

Acknowledgment

References

[1] IHS, Butadiene: Chemical Economics Handbook, HIS Markit, (2018) London.

[2] J.C. Gottifredi, E.L. Sham, V. Murgia, E.M. Farfa, Appl. Catal. A: Gen. 312 (2006) 134-143.

[3]   Y. Xu, J. Lu, M. Zhang, J. Wang, J. Nat. Gas Chem. 18 (2009) 88-93.

[4]   B.M. Weckhuysen, D.E. Keller, Catal. Today 78 (2003) 25-46.

[5]   I. Rossetti, G. F. Mancini, P. Ghigna, M. Scavini, M. Piumetti, B. Bonell, F. Cavani, A. Comite, J. Phy. Chem. C. 116 (2012) 22386-22398.

[6]   E. Santacesaria, M. Cozzolino, M. Di Serio, A.M. Venezia, R. Tesser, Appl. Catal. A: Gen. 270 (2004) 177-192.

[7]   A. Dejoz, J.M. Lopez Nieto, F. Marquez, M.I. Vazquez, Appl. Catal. A: Gen 180 (1999) 83-94.

[8]   J. K. Lee, H. Lee, U. G. Hong, Y. Yoo, Y-J. Cho, J. Lee, H-S. Jang, J. C. Jung, I. K. Song, J. Ind. Eng. Chem. 18 (2012) 1096-1101.

[9]   M.A. Volpe, G.M. Tonetto, H. De Lasa, Appl. Catal. A: Gen. 272 (2004) 69-78.

[10] J. Rischard, C. Antinori, L. Maier, O. Deutschmann, Appl. Catal. A: Gen. 511 (2016) 23-30.

[11] B.R. Jermy, B.P. Ajayi, B.A. Abussaud, S. Asaoka, S. Al-Khattaf, J. Mol. Catal. A Chem. 400 (2015) 121-131.

[12] B. R. Jermy, S. Asaoka, S. Al-Khattaf, Catal. Sci. Technol. 5 (2015) 4622-4635.

[13] G. Tanimu, B. R. Jermy, S. Asaoka, S. Al-Khattaf, J. Ind. Eng. Chem. 45 (2017) 111-120.

[14] G. Tanimu, S. Asaoka, S. Al-Khattaf, Mol. Catal. 438 (2017) 245-255.

[15] J. Liang, Z. Liang, R. Zou, Y. Zhao, Adv. Mater. 29 (2017) 1-21.

[16] C-Y. Lai, J. Thermodyn. Catal. 5 (2013) 1-3.

[17] R. H-Acuna, R. Nava, C. L. P-Ledesma, J. L-Romero, G. A-Nunez, B. Pawelec, E. M. R-Munoz, Mater. 6 (2013) 4139-4167.

[18] A. Ramanathan, B. Subramanian, Molecules 23 (2018) 263-276.

[19] T. I. Bhuiyan, P. Arudra, M. Akhtar, A. Aitani, R. Abudawoud, M. Al-Yami, S. Al-Khattaf, Appl. Catal. A: Gen 467 (2013) 224-234.

[20] T. I. Bhuiyan, P. Arudra, M. Akhtar, A. Aitani, R. Abudawoud, M. Al-Yami, S. Al-Khattaf, Can. J. Chem. Eng. 92 (2014) 1271-1282.

138

[21]   M. A. Ibrahim, M. N. Akhtar, J. Cejka, E. Montanari, H. Balcar, M. Kubu, S. Al-Khattaf, J. Ind. Eng. Chem. 53 (2017) 119-126.

[22]   W. Liu, S.K. Lai, H. Dai, S. Wang, H. Sun, C.T Au, Catal. Lett. 113 (2007) 147-154.

[23]   R. Bulanek, A. Kaluzova, M. Setnicka, A. Zukal, P. Cicmanec , J. Mayerova, Catal. Today 179 (2012) 149-158.

[24]   M. Setnicka, P. Cicmanec, R. Bulanek, A. Zukal, J. Pastva, Catal. Today. 204 (2013) 132-139.

[25]   X. Wang, G. Zhou, Z. Chen, W. Jiang, H. Zhou, Microporous Mesoporous Mater. 223 (2016) 261-267.

[26]   C. Wang, J-G. Chen, T. Xing, Z-T. Liu, Z-W. Liu, J. Jiang, J. Lu, Ind. Eng. Chem. Res. 54 (2015) 3602-3610.

[27]   G. Tanimu, A. Palani, S. Asaoka, S. Al-Khattaf, Catal. Today 324 (2019) 97-105.

[28]   A. Palani, H-Y. Wu, C-C. Ting, S. Vetrivel, K. Shanmugapriya, A.S.T Chiang, H-M. Kao, Microporous Mesoporous Mater. 131 (2010) 385-392

[29]   A. Palani, A. Pandurangan, J. Mol. Catal. A 226 (2005) 129-134

[30]   G. Qi, L. Fu, B. H. Choi, E. P. Giannelis, Energy Environ. Sci. 5 (2012) 7368-7375

[31]   P. Munnik, P. E. de Jongh, K. P. de Jong, Chem. Rev. 115 (2015) 6687-6718.

[32]   M. R. Quddus, M. M. Hossain, H. I. de Lasa, Catal. Today 210 (2013) 124-134.

[33]   S. Adamu, M. Y. Khan, S. A. Razzak, M. M. Hossain, J. Porous Mater. 24 (2017) 1343-1352.

[34]   P. E. Boahene, K. P. Soni, A. K. Dalai, J. Adjaye, Appl. Catal. A: Gen. 402 (2011) 31-40.

[35]   Y. Wang, M. Noguchi, Y. Takahashi, Y. Ohtsuka, Catal. Today 68 (2001) 3-9.

[36]   H. Lu, Q. Hao, T. Chen, L. Zhang, D. Chen, C. Ma, W. Yao, Y. Zhu, Appl. Catal. B: Environ. 237 (2018) 59-67.

[37]   K. Hayashi, K. Yameda, M. Shima, Mater. Lett. 200 (2017) 24-26.

[38]   H. W. Gao, X. F. Wang, D. N. Gao, Mater. Lett. 67 (2012) 280-282.

[39]   L. Zhang, W. Wang, S. Sun, J. Xu, M. Shang, J. Ren, Appl. Catal. B: Environ. 100 (2010) 97-101.

[40]   J. Lu, X. Wang, Y. Wu, Y. Xu, Mater. Lett. 74 (2012) 200-202.

[41]   https://xpssimplified.com/elements/bismuth.php Retrieved: 12th February, 2019.

[42]   T. Kimura, H. Imai, X. Li, K. Sakashita, S. Asaoka, M. N. Akhtar, S. S. Al-Khattaf,
       Arab. J. Sci. Eng. 39 (2014) 6617-6625.

CHAPTER 6

Elucidation of the Reaction Network for n-Butane ODH and Kinetic Modelling

[1]   Center of Research Excellence in Petroleum Refining and Petrochemicals, King Fahd University of Petroleum & Minerals, Dhahran 31261, Saudi Arabia

[2]   Department of Chemical Engineering, King Fahd University of Petroleum & Minerals, Dhahran 31261, Saudi Arabia

[3]   Department of Chemical and Biomolecular Engineering, University of Delaware, Newark, Delaware 19716, United States.

Abstract

The reaction network for the oxidative dehydrogenation of n-butane to butadiene was examined. Delplots for experiments with n-butane, 1-butene, and 2-butene feeds were constructed. These analyses revealed that butadiene formed from both 1-butene and 2-butene. The experimental ratio of 2-butene and 1-butene was far from the equilibrium value, suggesting that the 2-butene to 1-butene equilibrium was not established, supporting the existence of the direct reaction of 2-butene to butadiene.

Keywords: Reaction network, Oxidative dehydrogenation, n-Butane, 1,3-Butadiene, Delplots

6.1   Introduction

Butadiene is an important petrochemical raw material used mainly in the production of synthetic rubbers and automobile tires. Increased demand for this raw material has resulted in an intensive search toward an on-purpose production method to complement the conventional production methods. The oxidative dehydrogenation (ODH) reaction of n-butane involves the use of gas-phase oxygen as a co-feed, thereby prolonging the catalyst life. This reaction is not limited by thermodynamic equilibrium and hence, it can be carried out at relatively low temperatures compared to that required for the direct dehydrogenation reactions. [1-3]

In the ODH of n-butane, butadiene is obtained through a successive dehydrogenation sequence (first step dehydrogenation to butenes and second step dehydrogenation to butadiene). A major challenge is the loss of selectivity as a result of deep oxidation to carbon oxides. This motivates our interest in understanding the reaction network and the associated kinetics to enable the design of highly selective catalysts and reactors for an improved result.

The reaction network for the ODH reaction is not fully understood. The major challenge is whether 1,3-butadiene is obtained only from 1-butene intermediate or from both 1-butene and 2-butenes. The formation of 1,3-butadiene from 1-butene only is supported by the work of Blasco et al.[4] who suggested two different mechanisms for ODH of n-butane depending upon the acid-base character of the catalyst. Catalysts with higher basic sites favor 1-butene formation and its subsequent dehydrogenation to butadiene, while catalysts with acidic character resulted in a high content of initial 2-butenes, which

further give carbon oxides through a series reactions. This also agree with the findings of Chaar et al.,[5] Harding et al.,[6] and Madeira et al.[7]

Similarly, recent reports by Tanimu et al.[8-9] using a Ni-BiO/supported catalyst suggested that the mechanistic route in the ODH also depends upon the acid-base nature of the catalyst and that 1,3-butadiene is formed only from 1-butene. Their proposed mechanism is shown in Figure 6.1. The butadiene selectivity was shown to depend upon the selective dehydrogenation to 1-butene and successively to butadiene. The basic character of catalyst withdraws a hydrogen atom as a proton at the α-methyl carbon of n-butane, while hydrogen is selectively withdrawn as a hydride by the acidic character of the catalyst from the β-methylene carbon of n-butane. The basicity of the catalyst ensured selective abstraction of hydrogen (from both butane and 1-butene), and the weak acidity played a role in the adsorption of the intermediate without desorption into the gas phase, isomerization to 2-butenes, and deep oxidation into CO_x products. Their proposal was that the reaction network starting with n-butane proceeds through 1-butene and then to 1,3-butadiene in series, while 2-butene either isomerizes to 1-butene or forms cracking and deep oxidation products.

CH$_3$-CH$_2$-CH$_2$-CH$_3$

CH$_3$-CH$_2$-CH$_2$-CH$_3$ → C$^-$*H$_2$-CH$_2$-CH$_2$-CH$_3$ → C$^-$*H$_2$-C$^+$*H-CH$_2$-CH$_3$ → CH$_2$=CH-CH$_2$-CH$_3$

B$^{\delta-}$*- A$^{\delta+}$* B$^{\delta-}$*- A$^{\delta+}$* H$^+$-B-* A$^+$* H$^+$-B-* A$^+$*-H$^-$ B$^{\delta-}$* A$^{\delta+}$*

CH$_2$=CH-CH=CH$_2$

→ CH$_2$=CH-CH$_2$-CH$_3$ → CH$_2$=CH-CH$_2$-C$^+$*H$_2$ → CH$_2$=CH-C$^-$*H-C$^+$*H$_2$ ↗

A$^{\delta+}$* B$^{\delta-}$* A$^{\delta+}$* B-*-H$^+$ H$^-$-A$^+$* B-*-H$^+$ A$^{\delta+}$* B$^{\delta-}$*
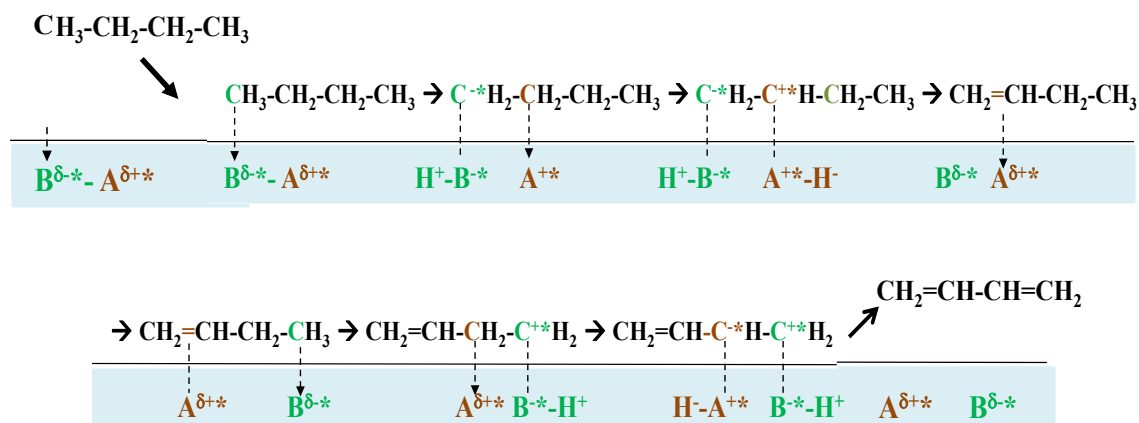
Figure 6.1 Schematic reaction mechanism for ODH of n-butane to butadiene.

In summary, all of the foregoing literature suggested that 1,3-butadiene is formed from n-butane through 1-butene only and that the formation of 2-butene did not produce butadiene, but rather led to CO$_x$. But the literature also contains information suggesting that 2-butene, also produces butadiene.

Lopez Nieto et al.[10,11] and Ramani et al.[12] showed the possibility of obtaining butadiene from both 1-butene and 2-butene (cis- and trans-) intermediates. Their mechanistic scenario is shown in Figure 6.2. They explained that the n-butane oxidation reaction is normally initiated by abstraction of hydrogen, thereby forming a butyl species. Subsequent hydrogen abstraction leads to the formation of intermediate mono-olefins, which, depending upon the reaction temperature and nature of catalysts, isomerize reversibly or form carbon oxides on acid catalysts. For the case of basic catalysts, the formed olefins were readsorbed and allylic species were formed, which eventually gave butadiene. Ramani et al.[12] suggested that, depending upon the metal oxides used in the

catalyst, a Bronsted-catalyzed mechanism or an allylic mechanism can be proposed for the successive dehydrogenation to butadiene. The nature of the oxygen species also plays a role in the product obtained because lattice oxygen leads to dehydrogenation (to olefins and diolefins), while adsorbed oxygen leads to deep oxidation to carbon oxides. The reaction system follows the Mars-van Krevelen mechanism.

$$CH_3\text{-}CH_2\text{-}CH_2\text{-}CH_3 \longrightarrow CO_x$$

$\downarrow$ -H·

alkyl species $\left[\overset{+}{CH_3CH}\text{-}CH_2\text{-}CH_3 \right]$

-H⁺ $\swarrow$　　$\searrow$ -H⁺

$$CH_2\text{=}CH\text{-}CH_2\text{-}CH_3 \rightleftarrows CH_3CH\text{=}CH\text{-}CH_3$$

-H· $\searrow$　　$\swarrow$ -H·

Allylic species $\left[\begin{array}{c} H_3C \quad\quad H \\ C \cdots C \\ H \quad + \quad CH_2 \end{array} \right] \longrightarrow CO_x$

$\downarrow$ -H⁺

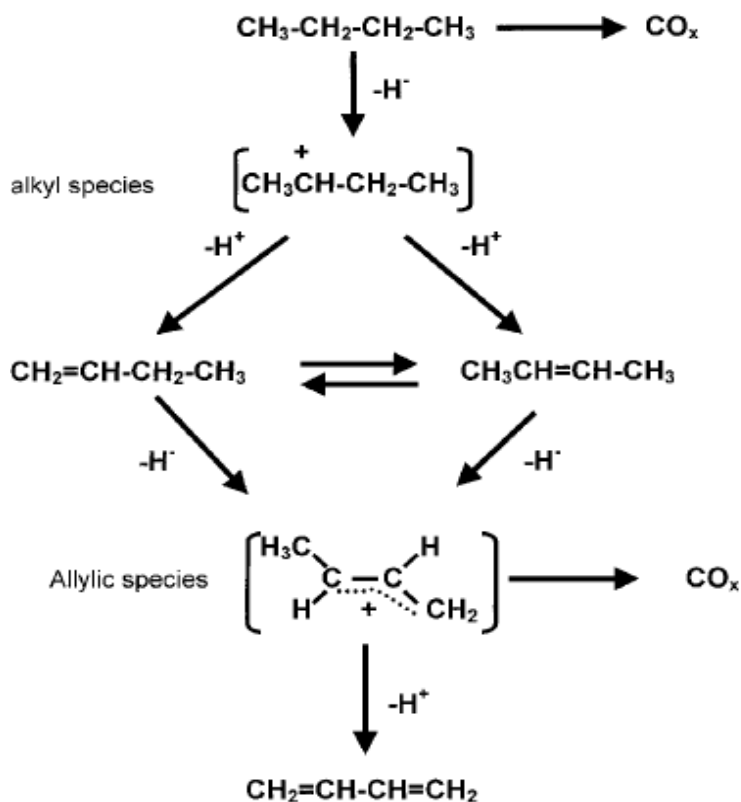$$CH_2\text{=}CH\text{-}CH\text{=}CH_2$$

Figure 6.2 Reaction network for ODH of n-butane and butenes.

The foregoing allows for the inference that the intermediate allylic species can be obtained from both 1-butene and 2-butene, because it affords a stabilized allylic bond between secondary carbons (methylene) in the compounds. The extent of isomerization (dependent

145

to a large extent upon the catalyst acidity) also plays a role as a competitive side reaction that can affect the butadiene formation.

The essential issue in these network scenarios is whether the formation of butadiene is from both 1-butene and 2-butene or 1-butene only. To this end, experiments were carried out in support of the Delplot method for reaction network elucidation to help resolve this conflict.

The Delplot method is used to determine the rank of the various products in the reaction sequence of observable species. It comprises a set of plots that enable the separation of products based on their ranks. A first-rank Delplot is a plot of yield/conversion (Y/X) for each observed product versus conversion (X) of the reactant. The ranks of the product are determined on the basis of the intercepts as $X \rightarrow 0$. Primary products will have a non-zero intercept, while higher-rank products will have zero intercepts. Higher-rank Delplots fill out the reaction network because the intercept $X \rightarrow 0$ of Y/X^n against X will either have a finite intercept for an nth rank product, a zero intercept for higher-rank products or a divergence for lower-rank products.[13-15]

6.2   Experimental Section

The ODH reaction was carried out in an automated fixed-bed reactor purchased from MicrotracBel, Corp, Japan. A total of 300 mg of the as-prepared catalyst [8-9] was loaded into the reactor and calcined under an air atmosphere. The detailed synthesis procedure, and chemical and textural properties of the catalyst have been discussed previously.[8] After calcination, the reaction started in a nitrogen atmosphere. The effects of six different temperatures (300-550 °C) and different feeds (n-butane, 1-butene, and 2-butene) were tested. The products were analyzed through an online gas chromatograph (GC) system,

146

(Agilent, 7890N). The details of the GC can be found in our previous studies.[8-9] The conversion $(1-N_A/N_{AO})$, product selectivities $(N_i-N_{io})/N_{AO}$, and yields (N_i/N_{AO}) were measured to probe the kinetics and reaction network.

6.3   Results and Discussion

The major products were 1-butene, trans-2-butene, cis-2-butene, 1,3-butadiene, cracking products (ethylene and propylene), and carbon oxides (CO and CO_2). Gases, such as CH_4, C_2H_6, and C_3H_8 were also detected but in negligible quantities.

Panel a and b of Figure 6.3 show the dependence of the product yields upon the temperature and contact time, respectively.
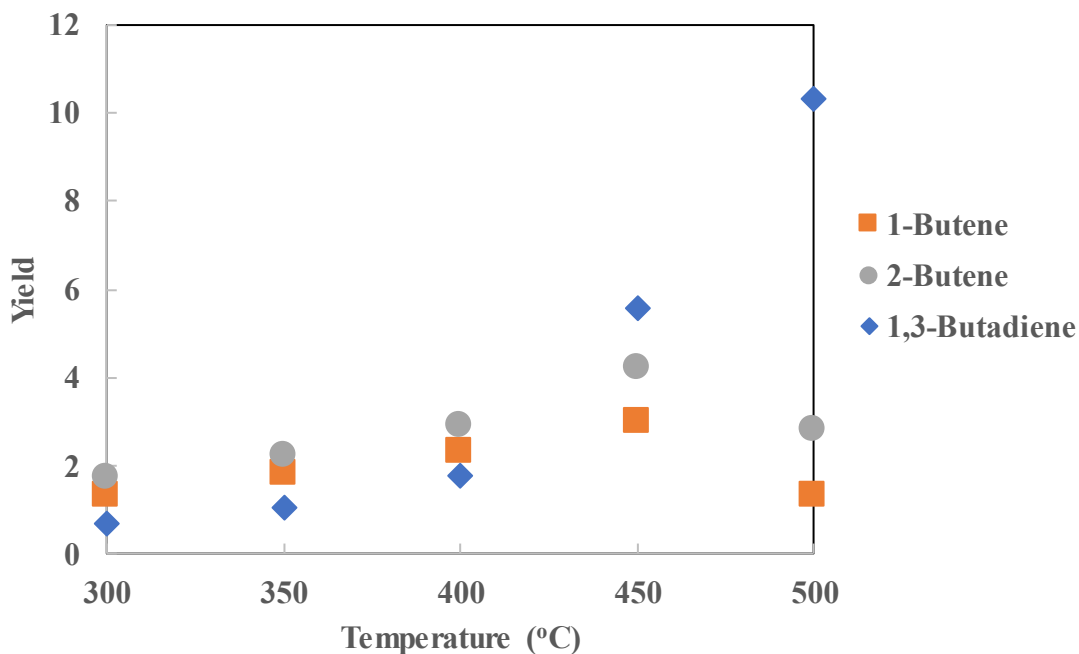

a)
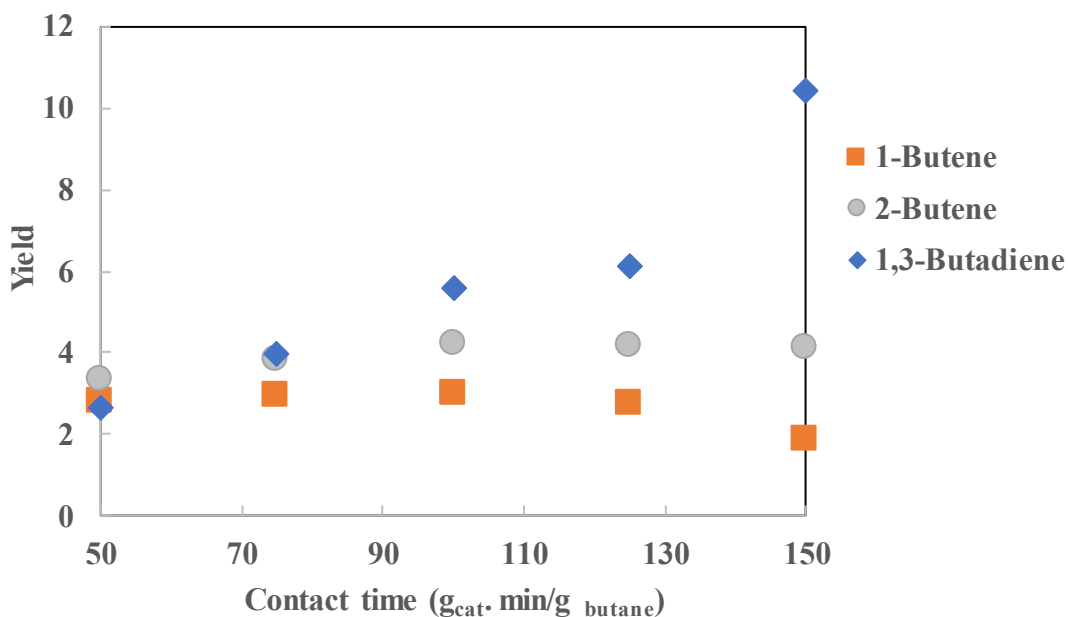
b)

Figure 6.3 Plots of the yield versus (a) reaction temperature at a contact time of 100 g_{cat}.min/g_{butane} and (b) contact times at 450 °C.

The plot of the main product yield against temperature is shown in Figure 6.3a. At lower reaction temperatures up to 400 °C and contact time of 100 g_{cat}.min/g_{butane}, the yields of both 1-butene and 2-butene were higher than that of 1,3-butadiene. The yield of 2-butene was higher than that of 1-butene over all of the reaction temperatures and they both increased up to 450 °C before decreasing at higher temperatures. This is an indication that, at higher temperatures, the rate of their consumption to secondary products is greater than the rate of their production from n-butane. 1,3-Butadiene increased at a lower rate up to 400 °C, after which the rate of production rapidly increased up to 500 °C.

148

The dependence of the main product yields against the contact time at 450 ºC is shown in Figure 6.3b. 2-Butene was produced in a higher yield than 1-butene at all contact times. At higher contact times, the yield of 2-butene remained constant, while that of 1-butene decreased. The yield of 1,3-butadiene increased continuously with an increase in contact time. This is an indication that, at the studied reaction temperature, an increased contact time favored both first and second step dehydrogenation to butadiene without further reaction. These results were examined further through the construction of Delplots.

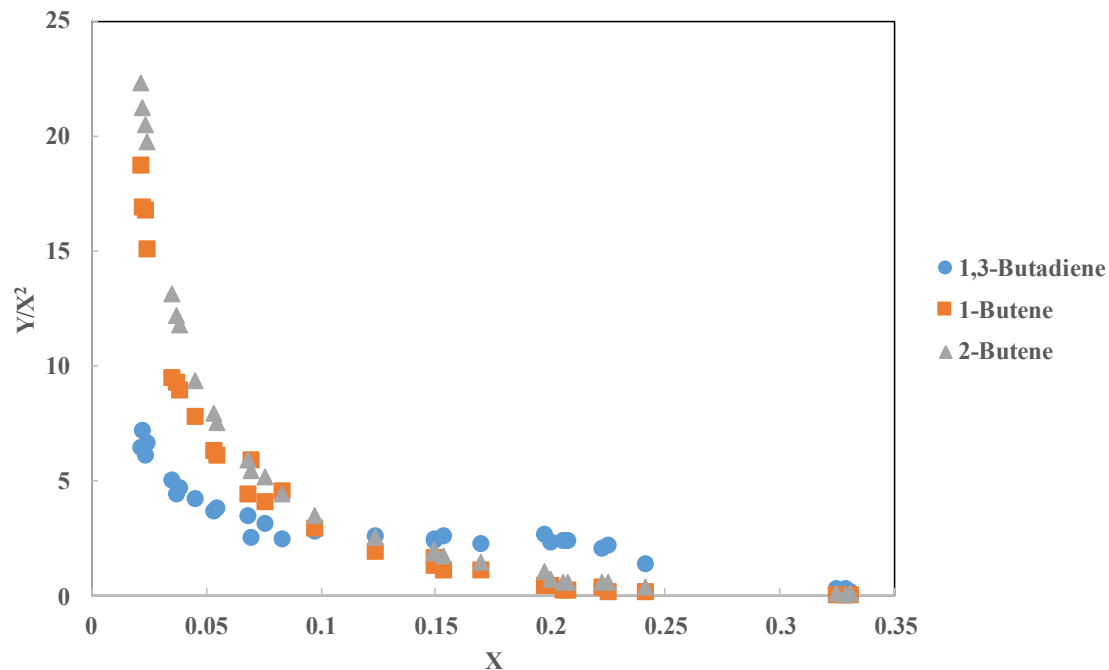## 6.3.1 Delplots from Experiments with Butane Feed

The first-rank Delplot with n-butane as feed is shown in Panel a and b of Figure 6.4, the former for the major products of interest and the latter for the minor side products. Inspection of Figure 6.4 shows that 1-butene and 2-butene have a finite intercept, which implies that they are primary products. Figure 6.4b shows that other products all have approximately zero intercepts, indicating that they are higher-rank products. Figure 6.4c presents the second-rank Delplot. Both 1-butene and 2-butene have diverging intercepts, indicating that they are lower-rank (i.e, primary) products. The finite intercept for butadiene indicates that it is a secondary product.

a)

b)

Y/X² axis, X axis

Legend: ● 1,3-Butadiene, ■ 1-Butene, ▲ 2-Butene
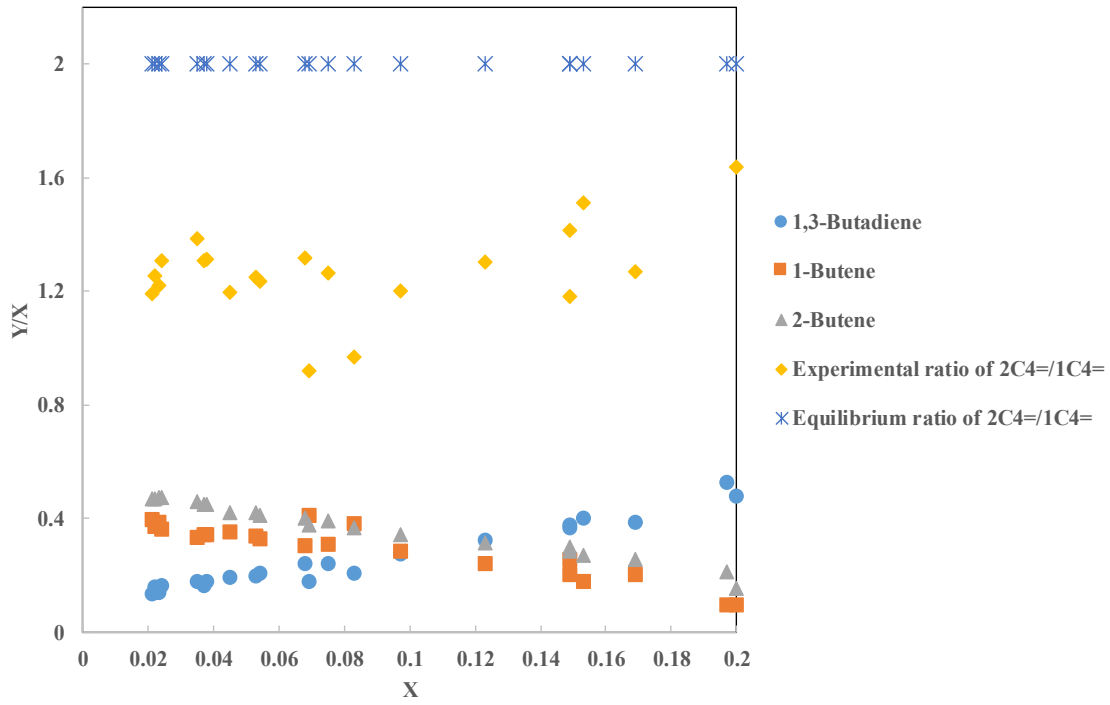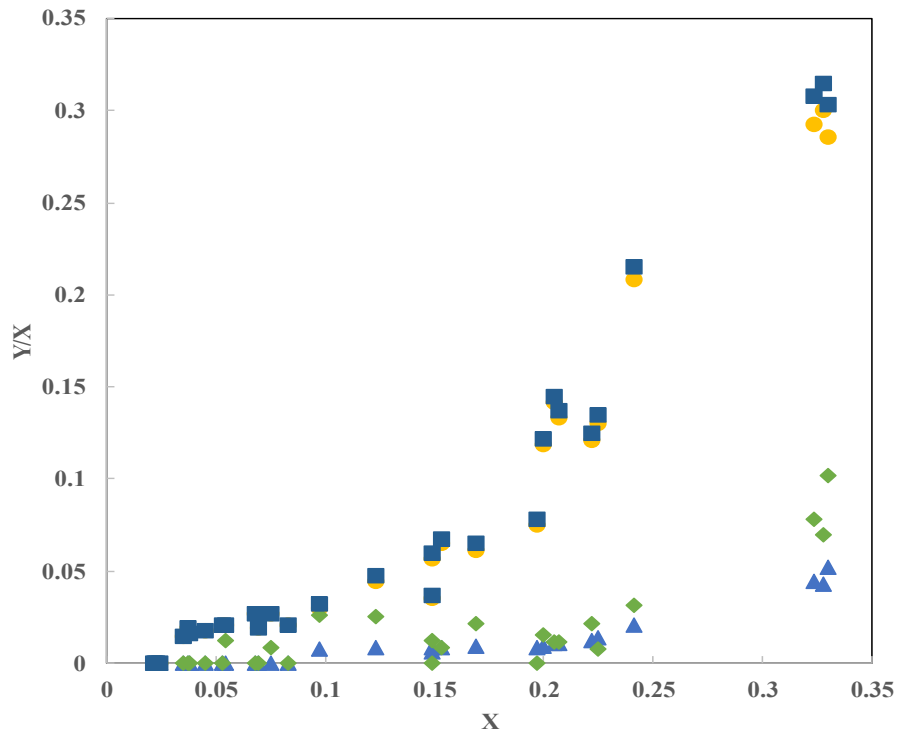
c)

Figure 6.4 First, and second-rank Delplots for experiments with n-butane feed.

6.3.2 Delplots from Experiments with 1-Butene and 2-Butene Feeds

The Delplots from experiments with 1-butene and 2-butene feeds are shown in Figures 6.5 and 6.6, respectively. In the first-rank Delplot from the experiments with 1-butene feed (Figure 6.5a), both 2-butene and butadiene have a finite intercept, indicating that they are both primary products. The second-rank Delplot (Figure 6.5b) shows that they both diverge, which further confirms that they are primary products.
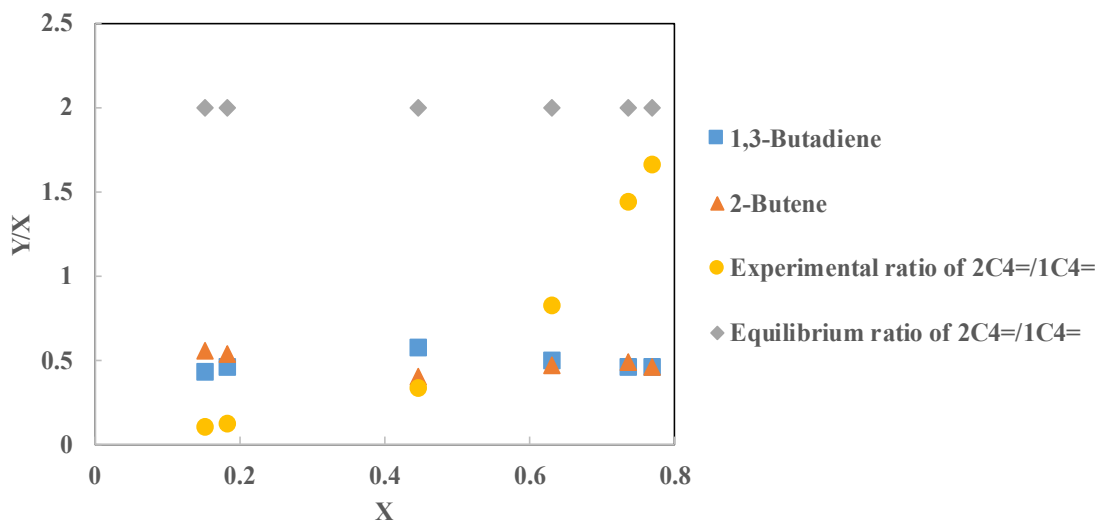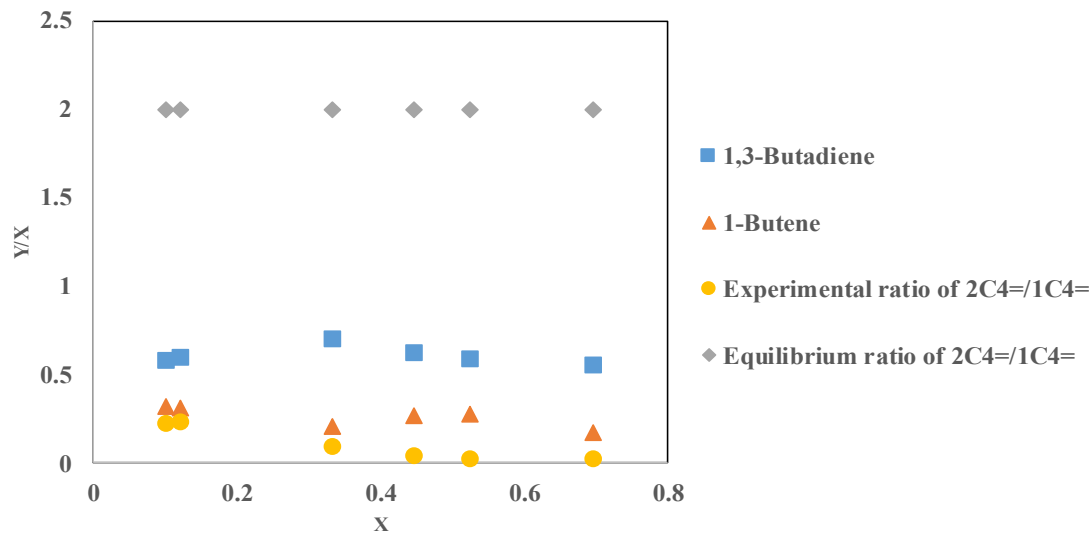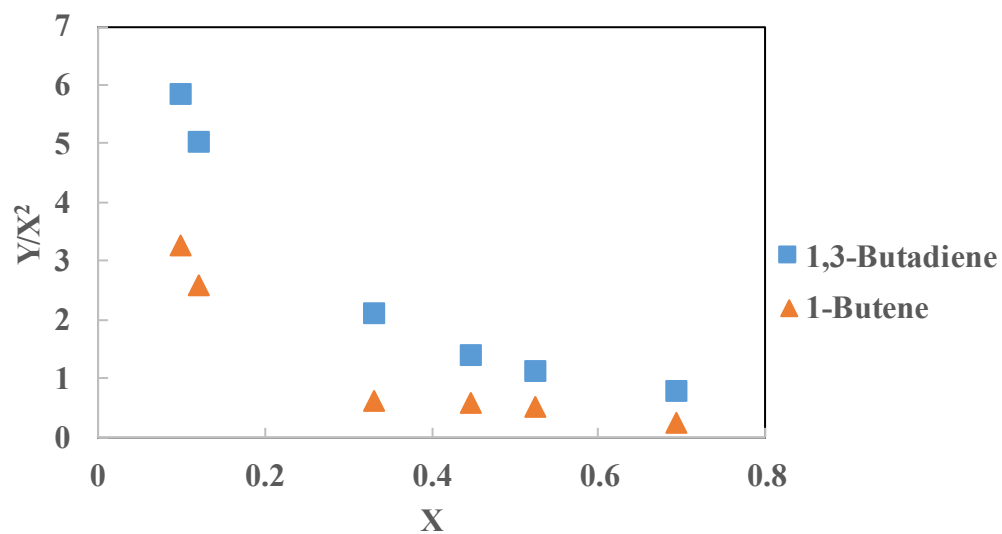
a)
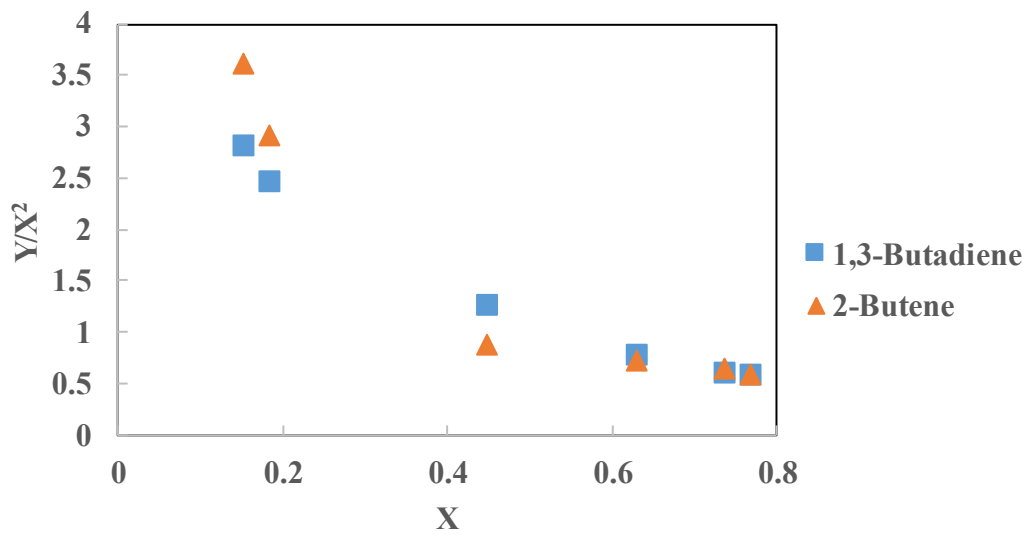
b)

Figure 6.5 First, and second-rank Delplots for experiments with 1-butene feed.

152

a)

b)

Figure 6.6 First and second-rank Delplots for experiments with 2-butene feed.
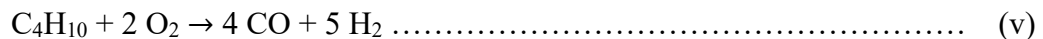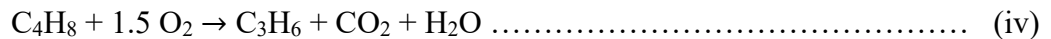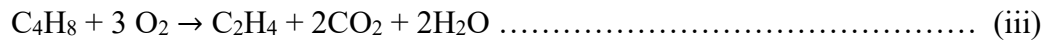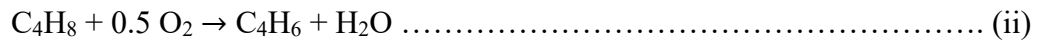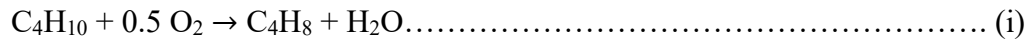
The Delplots for experiments with 2-butene feed are shown in Figure 6.6. The first-rank Delplots (Figure 6.6a) showed a finite intercept for 1-butene and butadiene, indicating that they are both primary products. The second-rank Delplots (Figure 6.6b) further showed that the products with finite intercepts in the first rank now diverge.

This Delplot analysis suggests that, during the ODH of n-butane, the desired product 1,3-butadiene forms from both 1-butene and 2-butene and also that a reversible isomerization reaction takes place between 1-butene to 2-butene. Collectively, the results of this analysis support the conclusions of Lopez Nieto et al.[11] and Ramani et al.[12] The network is consistent with a mechanism where both 1-butene and 2-butene formed an allylic species, which eventually dehydrogenates to 1,3-butadiene.

If the isomerization between 1-butene and 2-butene is very fast, there remains at least one possible kinetic scenario in support of the network where 1,3-butadiene forms from 1-butene only. In this case, the apparent reaction of 2-butene to 1,3-butadiene could take place through the rapid reaction of 2-butene to 1-butene, which then produces 1,3-butadiene in a rate determining step. This would require a virtual equilibrium between 1-butene and 2-butene, which was probed through the calculation of the equilibrium levels of 1-butene to 2-butene as a function of conversion. The results of this analysis which accounted for both cis- and trans- isomers of 2-butene, are shown in Figures 6.4a, 6.5a, and 6.6a as a plot of the calculated equilibrium ratio of 2-butene to 1-butene versus conversion (X) and the experimental ratio of 2-butene to 1-butene. This analysis suggests that the 2-butene to 1-butene equilibrium was not established, which further supports the direct reaction of 2-butene to 1,3-butadiene.

6.4   Kinetic Studies using Kinetic Model Editor (KME)

Kinetic studies is also a tool that is utilized for further characterization in order to confirm the performance of the catalysts. It can also be used in data prediction, reactor design and also in improving catalytic performance by tuning it properties. Based on the reaction network obtained for n-butane ODH using Delplots techniques, the following reactions (i-v) were proposed which also agreed with the product distribution. The main reaction products are butenes and butadiene while C_2H_4, C_3H_6, CO_2, CO and H_2 are minor products. The GC system utilized for this process does not identify water, hence water is not included in the product distribution.

$$C_4H_{10} + 0.5\ O_2 \rightarrow C_4H_8 + H_2O \dots\dots\dots\dots\dots\dots\dots\dots\dots\dots\dots\dots\dots\dots \text{(i)}$$

$$C_4H_8 + 0.5\ O_2 \rightarrow C_4H_6 + H_2O \dots\dots\dots\dots\dots\dots\dots\dots\dots\dots\dots\dots\dots\dots \text{(ii)}$$

$$C_4H_8 + 3\ O_2 \rightarrow C_2H_4 + 2CO_2 + 2H_2O \dots\dots\dots\dots\dots\dots\dots\dots\dots\dots\dots\dots \text{(iii)}$$

$$C_4H_8 + 1.5\ O_2 \rightarrow C_3H_6 + CO_2 + H_2O \dots\dots\dots\dots\dots\dots\dots\dots\dots\dots\dots\dots \text{(iv)}$$

$$C_4H_{10} + 2\ O_2 \rightarrow 4\ CO + 5\ H_2 \dots\dots\dots\dots\dots\dots\dots\dots\dots\dots\dots\dots\dots \text{(v)}$$

Kinetic model editor (KME) is a user friendly software that writes out the system of differential equations based on the reactions entered by the user. The user also specifies the rate law and reactor type and KME combines the system of equations. The solution proceeds as an initial value problem (IVP) with the provision of feed composition in molar flow. The INP, COND, RTK and OBS sheets representing input, conditions, reaction

parameters, observed, respectively, are all filled with the experimental values in mol/s and reactor/reaction conditions (temperature, pressure, outer radius etc).

6.4.1 Kinetic Parameters Optimization

For the ODH reaction, PFR and micro-kinetic were chosen as reactor type and rate law respectively. For optimizing the kinetic parameters, the objective function F, measures the fitting accuracy of the model. It determines how well the predicted molar flows matches with the experimental measurements. The expression for determining the objective function F, is given in equation vi.

$$\sum_{i,meas} \left(\frac{\text{measured } _i - \text{predicted } _i \text{ (rate parameters)}}{w_i} \right)^2 \quad \ldots\ldots\ldots\ldots\ldots\ldots\ldots\ldots\ldots \text{ (vi)}$$

KME utilizes a global optimization algorithm (Simulated Annealing) to optimize the model to experimental data. The results of the optimization are sets of log A and E_a tuned parameters. The results can be analyzed by comparing plots of model predictions and experimental measurements.

The values of the model parameters (log A and E_a) are presented in Table 1.0. The apparent activation energies revealed how effective the catalyst is in overcoming the activated complex barrier from reactants to products. The pre-exponential (frequency) factor A (log A) describes the amount and the ease of accessibility to the active sites of the catalyst. The second step dehydrogenation has the largest pre-exponential factor which explains why the catalyst is more selective towards butadiene compared to the other reaction products.

Table 6.1 Kinetic parameters for ODH reaction.

Reactions	A (mol/g_{cat}.s	E_a (kJ/mol)
I	2.34	41.90
II	10.21	52.45
III	1.46	41.97
IV	0.74	44.67
V	0.12	55.05

The plots of the model predicted and experimental molar flows against reaction temperature for n-butane (main reactant) and butenes/butadiene (main products) are shown in Figures 6.7, 6.8 and 6.9 respectively. Good fittings were observed especially for the reactant. The deviations in the products fittings can be attributed to other possible series reactions that were not captured in the model and possibly due to unavoidable experimental errors.

Figure 6.7 n-butane molar flows at different reaction temperatures. B: butane, 1, 2 and 3 represents 0.15 g, 0.30g and 0.45 g catalyst weights respectively.
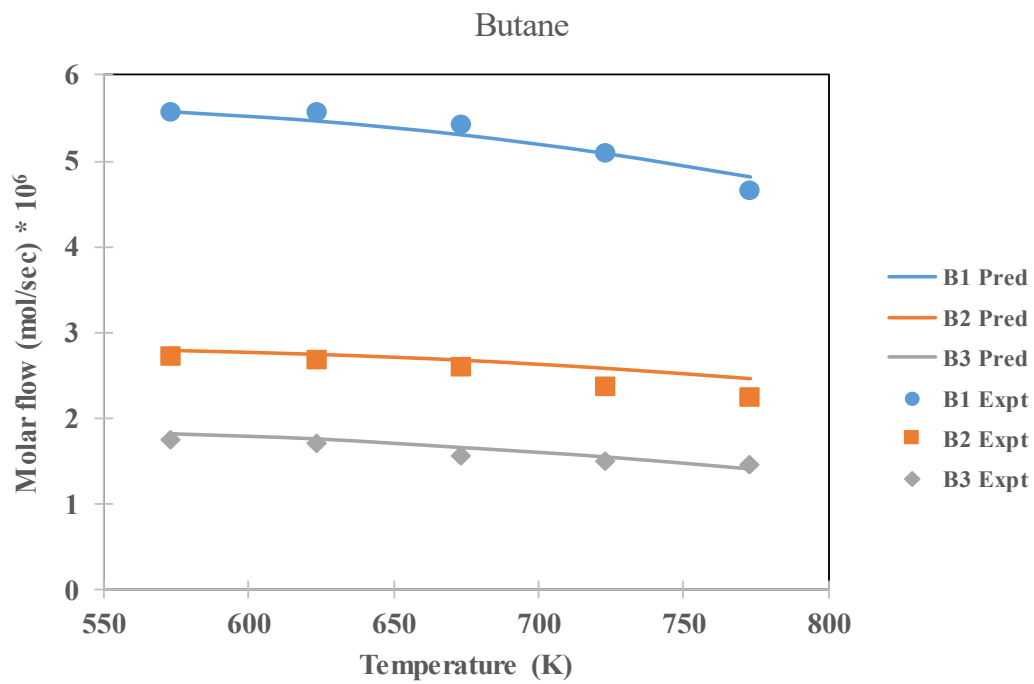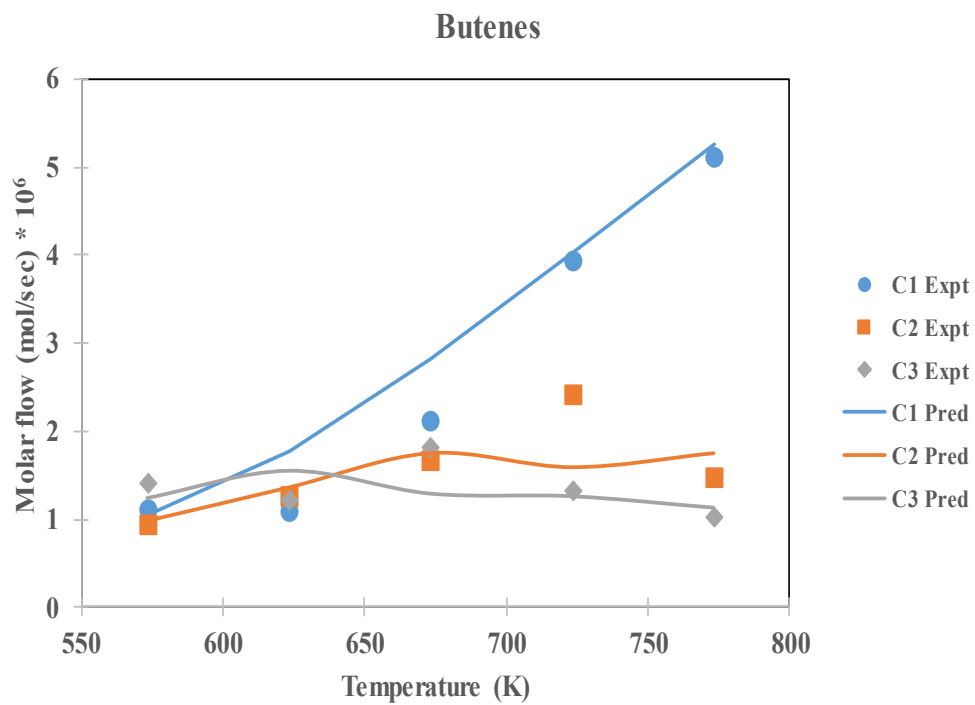
Figure 6.8 Butenes molar flows at different reaction temperatures. C: butenes, 1, 2 and 3 represents 0.15 g, 0.30g and 0.45 g catalyst weights respectively.
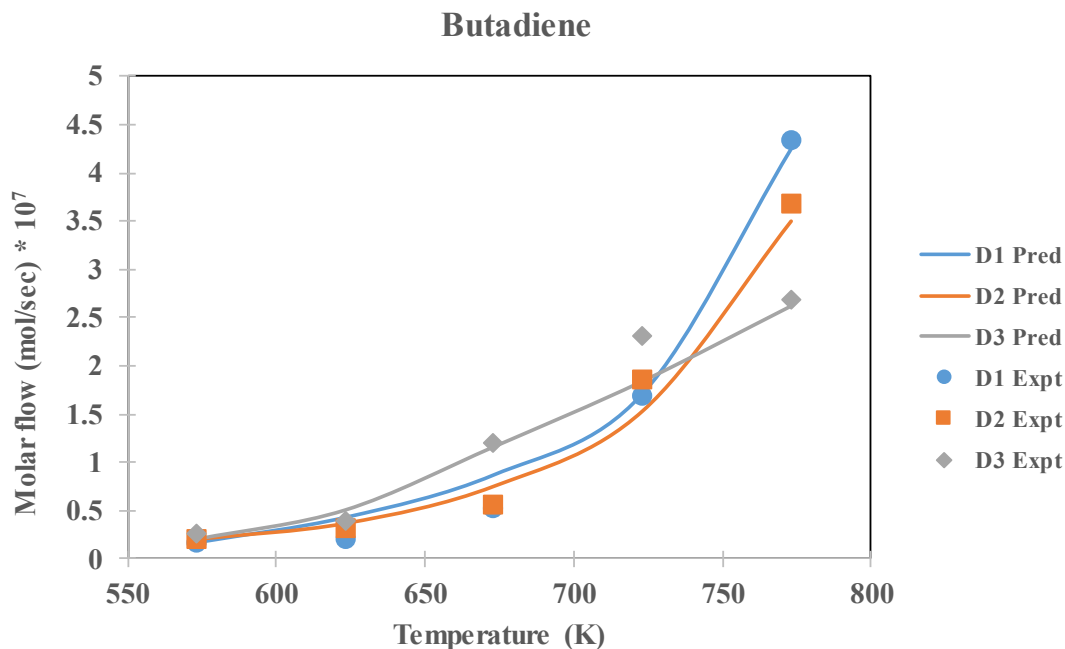
Figure 6.9 Butadiene molar flows at different reaction temperatures. D: butadiene, 1, 2 and 3 represents 0.15 g, 0.30g and 0.45 g catalyst weights respectively.

Conclusion

The ODH of n-butane to 1,3-butadiene reaction network was investigated using the Delplot method. Delplots were constructed for experiments with n-butane, 1-butene, and 2-butene feeds. On the basis of the results, the conclusions that can be drawn are that 1,3-butadiene is formed from both 1-butene and 2-butene and that 2-butene to 1-butene equilibrium was not established. Hence, the reaction network can be visualized as n-butane forming both 1-butene and 2-butene as intermediates that both undergo dehydrogenation in a series reaction to give 1,3-butadiene. The developed reaction network will allow for the determination of ODH reaction kinetic parameters. The reaction network was used in kinetic model editor and the apparent activation energies estimated for 1st and 2nd step dehydrogenations are 41.90 and 52.45 kJ/mol, respectively.

160

Acknowledgment

References

[1] Cherian, M., Rao, M. S., Hirt, A. M., Wachs, I. E., Deo, G. Oxidative dehydrogenation of propane over supported chromia catalysts: Influence of oxide supports and chromia loading. *J. Catal.* **2002,** 211, 482-495.

[2] Marcu, I., Sandulescu, I., Millet, J. M. Effects of the method of preparing titanium pyrophosphate catalyst on the structure and catalytic activity in oxidative dehydrogenation of n-butane. *J. Mol. Catal. A:Chem* **2003,** 203, 241-250.

[3] Gottifredi, J. C., Sham, E. L., Murgia, V., Farfa, E. M. Sol-gel synthesis of V_2O_5-SiO_2 catalyst in the oxidative dehydrogenation of n-butane. *Appl. Catal. A: Gen.* **2006,** 312, 134-143.

[4] Blasco, T., Lopez Nieto, J. M., Dejoz, A., Vazquez, M. I. Influence of the acid-base character of supported vanadium catalysts on their catalytic properties for the oxidative dehydrogenation of n-butane. *J. Catal.* **1995,** 157, 271-282.

[5] Chaar, M. A., Patel, D., Kung, M. C., Kung, H. H., Selective oxidative dehydrogenation of butane over VMgO catalysts. *J. Catal.* **1987,** 105, 483-498.

[6] Harding, W. D., Kung, H. H., Kozhevnikov, V. L., Poeppelmeier, K. R. Phase equilibria and butane oxidation studies of the MgO-V_2O_5-MoO_3 system. *J. Catal.* **1993,** 144, 597-610.

[7]   Madeira, L. M., Portela, M. F., Mazzocchia, C., Kaddouri, A., Anouchinsky, R., Reducibility of undoped and Cs-doped α-NiMoO$_4$ catalysts: kinetic effects in the oxidative dehydrogenation of n-butane. *Catal. Today* **1998,** 40, 229-243.

[8]   Tanimu, G., Jermy, B. R., Asaoka, S., Al-Khattaf, S., Composition effect of metal species in (Ni, Fe, Co)-Bi-O/gamma-Al$_2$O$_3$ catalyst on oxidative dehydrogenation of n-butane to butadiene. *J. Ind. Eng. Chem.* **2017,** 45, 111-120.

[9]   Tanimu, G., Asaoka, S., Al-Khattaf, S., Effect of Support in Ni-Bi-O/support catalyst on oxidative dehydrogenation of n-butane to butadiene. *Mol. Catal.* **2017,** 438, 245-255.

[10]   Lopez Nieto, J. M., Concepcion, P., Dejoz, A., Knozinger, H., Melo, F., Vazquez, M. I. Selective oxidation of n-butane and butenes over vanadium-containing catalysts. *J. Catal* **2000,** 189, 147-157.

[11]   Lopez Nieto, J. M., Concepcion, P., Dejoz, A., Melo, F., Knozinger, H., Vazquez, M. I. Oxidative dehydrogenation of n-butane and 1–butene on undoped and K-doped VO$_x$/Al$_2$O$_3$ catalysts. *Catal. Today* **2000,** 61, 361-367.

[12]   Ramani, N. C., Sullivan, D. L., Ekerdt, J. G., Jehng, J. M., Wachs, I. E. Selective oxidation of 1-butene over silica supported Cr (VI), Mo (VI), and W (VI) oxides. *J. Catal* **1998,** 176, 143-154.

[13]   Agarwal, P., Evenepoel, N., Al-Khattaf, S. S., Klein, M. T. Molecular-Level Kinetic Modelling of Methyl Laurate: The Intrinsic Kinetics of Triglyceride Hydroprocessing. *Energy Fuels* **2018,** 32, 5264-5270.

[14]   Bhore, N. A., Klein, M. T., Bischoff, K. B. The Delplot technique: A new method for reaction pathway analysis. *Ind. Eng. Chem. Res*. **1990**, 29 (2), 313-316.

[15]   Klein, M. T., Hou, Z., Bennett, C. Reaction network elucidation: Interpreting delplots for mixed generation products. *Energy Fuels* **2012,** 26, 52-54.

CHAPTER 7

Conclusions and Recommendations

7.1   Conclusions

This thesis investigated the oxidative dehydrogenation process for converting n-butane to mainly butadiene using metal oxides supported catalysts. The main findings of the work can be summarized as:

- The thermodynamic analyses revealed that the ODH pathway is not thermodynamically favorable, hence the need to design a catalyst that kinetically promote that pathway

- Metal oxides supported catalysts comprising of commercially available active species and supports were successfully synthesized using co-impregnation technique

- The role of different supports (Al_2O_3, SiO_2, and ZrO_2) in dispersing the active species of Ni and Bi was investigated. SiO_2 supported catalyst gave the best dehydrogenation selectivity resulting from it balanced acid and basic sites

- SiO_2 sol supported catalyst resulted in an impressive catalytic performance (n-butane conversion: 35.6 %, DH selectivity: 78.3 % and BD selectivity: 41.6 %) due to its interaction ability with the active species

- Mesoporous silica (SBA-15, SiO_2 foam, MCM-41) supported catalyst were studied. They were considered due to their ordered structure, stability and well defined pore-sizes suitable for stabilizing the performance of the active species

- The order of butadiene yield among the mesoporous silica supported catalysts is SBA-15 > SiO$_2$ foam > MCM-41 > Conventional SiO$_2$. BD selectivity of 47.5 % at n-butane conversion of 28.9 % was achieved with SBA-15 supported catalyst.

- An optimum loading of Ni and Bi species on SBA-15 supported improved BD selectivity up to 53.2 % due to an improved NiO species dispersion and stabilization by beta-Bi$_2$O$_3$/Bi$_2$SiO$_5$ species.

- The catalytic performance of all the catalysts agreed with their physical and chemical properties as supported by the various characterization techniques including XRD, BET, TPD, TPR, XPS and TEM.

- Delplots were constructed for experiments with n-butane, 1-butene and 2-butene feeds for the elucidation of the reaction network from n-butane to butadiene. It was confirmed that butadiene is formed from both 1-butene and 2-butene intermediates.

- Kinetic model editor (KME) was utilized to determine the ODH reaction kinetic parameters based on the developed reaction network. Activation energies of 41.90 kJ/mol and 52.45 kJ/mol were obtained for 1st and 2nd dehydrogenation steps, respectively.

7.2 Recommendations

The following points are recommended for further research work on ODH of n-butane to olefins:

- Other group of catalysts like silicalites, hybrid catalyst (consisting of micro and mesoporous materials), support modification using promoters (K, Mg, Ce etc) should be investigated.

- Other preparation methods like precipitation, sol-gel synthesis, and hydrothermal synthesis should be investigated and compared with the impregnation method.

- Different configurations of reactors like circulating bed reactors, membrane reactors, and two-zone fluidized bed reactors can be used and the performance compared with fixed bed reactor.

- In-situ characterization techniques that will reveal the changes in catalyst activity during operation should be explored.

Appendix

A.1 BET Surface Area

Table A1 Physical properties of Ni-Bi-O/SBA-15 catalysts.

Ni-Bi-O/SBA-15	BET surface area		Pore surface area		Pore volume		Average pore diameter
	$[m^2/g\text{-}catalyst]$	$[m^2/g\text{-}support]$	$[m^2/g\text{-}catalyst]$	$[m^2/g\text{-}support]$	$[cm^3/g\text{-}catalyst]$	$[cm^3/g\text{-}support]$	[nm]
5 Ni-10 Bi	426	501	505	594	0.51	0.60	4.1
(SBA-15: SB)		(657)		(1080)		(1.08)	(4.1)
10Ni-10 Bi	360	446	443	548	0.46	0.56	4.1
(SBA-15: SB)		(657)		(1080)		(1.08)	(4.1)
14Ni-10Bi	334	431	419	540	0.44	0.56	4.2
(SBA-15: SB)		(657)		(1080)		(1.08)	(4.1)
20Ni-10Bi	351	479	421	575	0.43	0.59	4.1
(SBA-15:SB		(657)		(1080)		(1.08)	(4.1)

A.2 Temperature Programmed Reduction
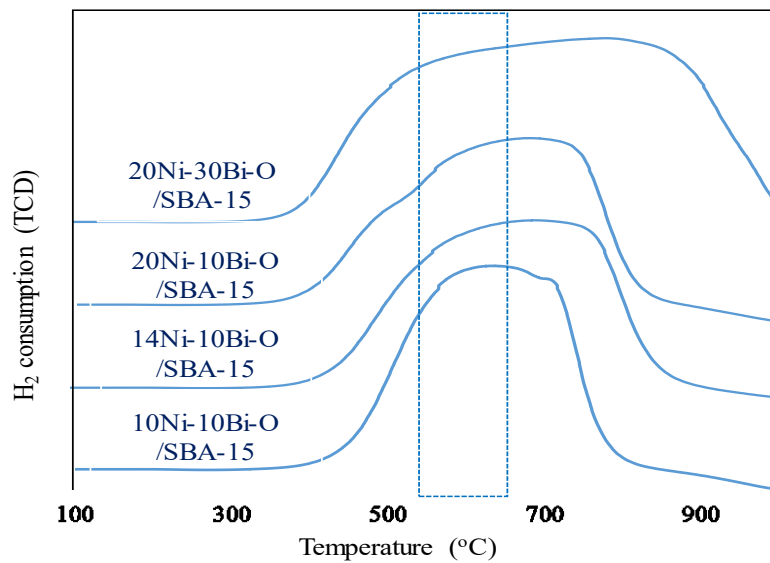

Figure A1 TPR profile for various metal oxide loaded in Ni-Bi-O/SBA-15 catalyst

Vitae

Name   : GAZALI TANIMU

Nationality   : NIGERIAN

Date of Birth   : 9/5/1991

Email   : gtu4ever@yahoo.coml

Address   : Kaduna, Nigeria

Academic Background   : Bachelor of Engineering, Ahmadu Bello University, Zaria

Master of Science (MSc in Chemical Engineering), King

Fahd University of Petroleum and Minerals, Kingdom of

Saudi Arabia

Publications

1. Elucidation of the reaction network for oxidative dehydrogenation of butane to butadiene, **Gazali Tanimu,** Sulaiman S. Al-Khattaf, Michael T. Klein, Energy Fuels 2019, 33, 2, 1473-1478 (IF 3.091)

2. Pore structure effect of support in Ni-Bi-O/mesoporous silica catalyst on oxidative dehydrogenation of n-butane to butadiene, **G. Tanimu**, A. Palani, S. Asaoka, S. Al-Khattaf, Catalysis Today 324, 2019, 97-105 (I.F 4.667).

3. Bimetallic Bi-Ni oxides over Carbide supports for oxidative dehydrogenation of *n*-butane: Experimental and kinetic modeling, Omer Elmutasim**, G. Tanimu**, Isam H. Aljundi, S. Al-Khattaf, Canadian Journal of Chemical Engineering, 2018, 1-10 (I.F 1.265).

4. Effect of support in Ni-Bi-O/support catalyst on oxidative dehydrogenation of n-butane to butadiene, **G. Tanimu**, S. Asaoka, S. Al-Khattaf, Molecular Catalysis 438, 2017, 245-255 (I.F 4.36).

5. Composition effect of metal species in (Ni, Fe, Co)-Bi-O/gamma-Al$_2$O$_3$ catalyst on oxidative dehydrogenation of n-butane to butadiene, **G. Tanimu**, B.R. Jermy , S. Asaoka , S. Al-Khattaf, Journal of Industrial and Engineering Chemistry 45, 2017, 111-120 (I.F 4.841).

Publications under Review/Preparation

1. New mesoporous catalyst system containing Bi$_2$SiO$_5$ for oxidative dehydrogenation of n-butane to butadiene, **G. Tanimu,** S. Asaoka, Microporous and Mesoporous Materials (under review)

2. Kinetic study on n-butane oxidative dehydrogenation over (Ni, Fe, Co)-Bi-O/gamma-Al$_2$O$_3$ catalyst, **G. Tanimu,** B. A. Abussaud, S. Asaoka, Chemical Engineering Research and Design (under review)

3. Oxidative dehydrogenation of lower alkanes to olefins: A short review, **G. Tanimu.**

4. CO$_2$ reforming of n-butane to ethylene/propylene and syngas over La-Co oxide/alumina catalyst, **G. Tanimu,** Z. S. Qureshi, S. Asaoka.

Contributions to Symposia

- Oxidative reforming of n-butane to ethylene, propylene and syngas on acid/base nano-hybrid catalyst; **G. Tanimu,** Z. S. Qureshi, H. S. Alasiri, S. Asaoka, S. Al-Khattaf; presented at 28th Annual Saudi-Japan Symposium, Saudi Arabia, November 12th -13th, 2018.

- Hierarchical nano-consortium catalyst of (Ni, Fe, Co)-Bi-O/support for oxidative dehydrogenation of butane to butadiene; **G. Tanimu**, B.R. Jermy, S. Asaoka , S. Al-Khattaf; presented at 26th Annual Saudi-Japan Symposium, Saudi Arabia, November 7th -8th, 2016.